CRYSTAL ENGINEERING ACROSS TETREL BONDS IN DONOR-ACCEPTOR COMPLEXES WITH TRIPHENYLTIN CHLORIDE AND VARIOUS PHOSPHORUS COMPOUNDS

Sachin Liyanage

Thesis submitted to the Department of Chemistry & Biomolecular Sciences,

University of Ottawa

in partial fulfilment of the requirements for the degree of

Masters in chemistry

Supervisor: Prof. David L. Bryce

© Sachin Liyanage, Ottawa, Canada, 2024

ABSTRACT

Supramolecular chemistry is a field of study that focuses on the design, synthesis, and characterization of large molecular assemblies held together by non-covalent interactions. One of the latest developments in this field is the concept of tetrel bonding, which is a type of non-covalent interaction between an electron-deficient atom from the group of 14 elements (carbon, silicon, germanium, tin, and lead) and a Lewis base. The nature of tetrel bonding is electrostatic, and it can lead to the formation of supramolecular assemblies with unique properties and functions. The use of tetrel bonding as an alternative to traditional hydrogen bonding in supramolecular chemistry has recently gained significant attention, given its potential applications in materials science, catalysis, and drug delivery. Thus, the primary objective of this project is to prepare novel tetrel-bonded cocrystals using heavier pnictogens such as phosphorus as electron donors. Multiple attempts were made to achieve the intended objective. One of the initial experiments involved the slow evaporation process of triphenyltin chloride and triphenylphosphine, resulting in the formation of our first novel cocrystal. Subsequently, a second experiment utilized triphenyltin chloride and cyclohexyldiphenylphosphane, leading to the creation of our second novel cocrystal. To further investigate, cocrystal 1 underwent analysis through powder X-ray diffraction (PXRD) and Nuclear Magnetic Resonance (NMR) techniques. These analyses confirmed the presence of the first-ever purposely engineered cocrystal featuring a tetrel bond between tin and phosphorus, marking a noteworthy development in our exploration of molecular interactions.

ACKNOWLEDGEMENTS

I would like to take this opportunity to express my profound gratitude to all those who have contributed to this project.

Nuclear Magnetic Resonance (NMR) is known for its ability to provide detailed structural and molecular information about compounds through the analysis of nuclear spins and their interactions in a magnetic field. I had the privilege of joining Dr. David Bryce's team, where I had the chance to enhance my understanding of this technique in an optimal setting. My time spent in the laboratory has proven to be a profoundly enriching experience, and I am thankful for the opportunity to pursue my master's degree in chemistry under his supervision. I wish to express my profound gratitude to Dr. Bryce for enabling all of this. Your patience, expertise, and motivation will help me in guiding towards achieving my full potential.

I would also like to thank my colleagues and collaborators, who have been an invaluable source of idea and help throughout this research journey. Their helpful discussions, feedback, and assistance in various aspects of this research enriched the quality of the work.

In addition, I would like to extend my appreciation to the funding programs that supported this project. Without their financial support, this research would not have been possible. I would also like to acknowledge the technical staff who provided their assistance and expertise throughout the experimental work.

Furthermore, I would like to express my heartfelt appreciation to Shubha Gunaga and Tamali Nag for their generous assistance and for addressing my questions during

this research project. Vincent Morin and Patrick Szell special recognition for their guidance on the usage of the 200/400 NMR apparatus and their consistent support throughout the year. My time in the lab has been amazing because of you guys; you are all friendly and cheerful, and I am grateful to be able to call you, my friends. Everyone has been a huge inspiration, and you all, in my opinion, are examples of how hard work and dedication can lead to excellent scientific research. I hope everything you do goes well for you all.

The Bryce Lab has been an invaluable source of advice and support. Their collective expertise and willingness to help have been critical to the successful completion of this project.

Finally, I would like to acknowledge my family and friends for their encouragement and support throughout my academic journey. Their faith in me has been a constant source of motivation and inspiration. I am profoundly thankful for their understanding and patience during the challenging times of stress and uncertainty. This project's success is, in no small part, a testament to their unwavering support.

TABLE OF CONTENTS

LIST OF FIGURES

Chapter 1.

Chapter 2.

Chapter 3.

Chapter 4.

Paper #1

Paper #2

Synthesis and Results

Appendix

LIST OF TABLES

Chapter 1.

Chapter 4.

Paper #1

Paper #2

Synthesis and Results

Chapter 1. Introduction and Objectives

a. Non-covalent Interactions

Non-covalent interactions are weak interactions that occur between atoms or molecules, and they play a part in many chemical and biological processes. Unlike strong covalent bonds, which involve the sharing of electrons, non-covalent interactions do not require such electron exchange. Instead, they encompass a wider range of electrostatic interactions, occurring either between molecules or within a single molecule. Typically, the chemical energy involved in the formation of non-covalent interactions ranges from 1-5 kcal/mol. These interactions are essential for maintaining the tertiary structure of macromolecules like proteins and nucleic acids. They also play a crucial function in several biological processes requiring precise yet transient interactions among molecules [1,2].

Furthermore, these interactions have a profound impact on drug design, crystallinity, and material design. Their impact is especially noticeable in the context of self-assembly, crystal engineering, and the total synthesis of numerous organic compounds.

In the following sections, I will focus on specific categories of non-covalent interactions. In Section ***b***, we will examine electrostatic interactions and ionic bonding, with a focus on van der Waals interactions including London dispersion forces, Debye forces, and Keesom forces (subsection ***b.i***). Following this, Section ***c*** will discuss σ-hole interactions, highlighting their role in molecular recognition and self-assembly. Subsequently, we will explore the unique characteristics and biological significance of hydrogen bonds in

Section ***d*** and halogen bonds in Section ***e***. Finally, Section ***f*** will elucidate the intriguing properties and applications of tetrel bonds. By examining these distinct types of non-covalent interactions, we can develop a comprehensive understanding of their diverse roles in chemistry, biology, and materials science.

b. Electrostatic Interactions and Ionic Bonds

Electrostatic interactions occur from the attractive Coulombic force between ions or molecules bearing opposite charges. This force, described by Coulomb's law, quantifies the strength of the interaction between charged particles[3]:

$$F = \frac{k \cdot |q_1 \cdot q_2|}{r^2}$$

Where:

- F is the magnitude of the electrostatic force between the charges.
- k is Coulomb's constant (8.9875 x 10^9N m^2/C^2).
- q_1 and $q_2$are the magnitude of the charges.
- r is the distance between the charges.

These electrostatic interactions, which are significantly stronger than other non-covalent forces, play an important role in determining molecular structures and influencing a wide range of chemical phenomena.

Moreover, charged objects can induce a partial opposing charge on nearby uncharged objects, leading to mutual attraction between them. This phenomenon highlights the widespread influence and significance of electrostatic interactions in everyday scenarios[4].

With our understanding of electrostatic interactions, particularly their role in creating attractions and repulsions between charged particles, we can now focus on a specific application of these forces: the formation of ionic bonds.

When an atom undergoes electron loss, it becomes a positively charged cation, while gaining electrons results in a negatively charged anion. The attraction between ions of opposite charges leads to the formation of an ionic bond. This interaction extends to ions or molecules with full, permanent charges of opposing signs, resulting in an ionic interaction. For example, in NaF, the sodium ion (Na^+) is attracted to the fluoride ion (F^-) due to their opposite charges, although this interaction is weakened in the presence of highly polar solvents like water. Entropy influences which ions associate in water, with attractive forces across a single salt bridge approximately at 1.2 kcal/mol in moderate ionic strengths and around 1.9 kcal/mol at weak ionic strengths. The G values are additive and often independent of the types of ions present, with the exception of transition metal ions[5].

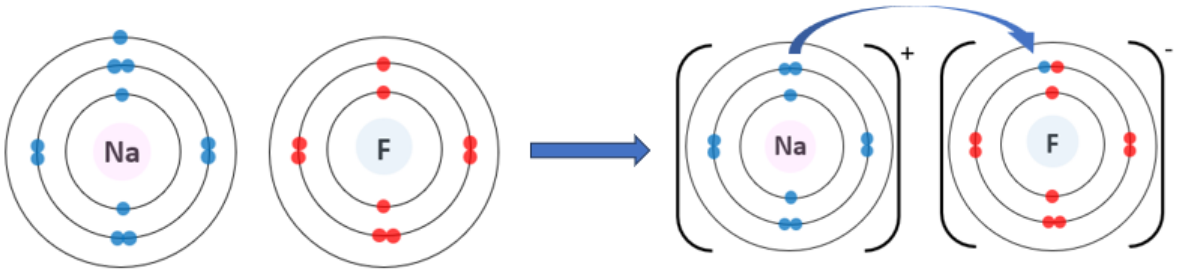

***Figure 1**. Ionic Bond (formation of sodium fluoride. Left: Prior to them bonding. Right: They have bonded).*

Additionally, Ion-dipole interactions occur when a charged species, typically an ion, forms a stable complex with a polar molecule or functional group. In biological organic chemistry, the most common instance of an ion-dipole interaction is between a metal cation, often Mg^{2+} or $Zn^{2+,}$ interacting with the partially negative oxygen of a carbonyl group[6]. This interaction causes an increase in the partial positive charge on carbon due to the high electronegativity of the metal cation[7].

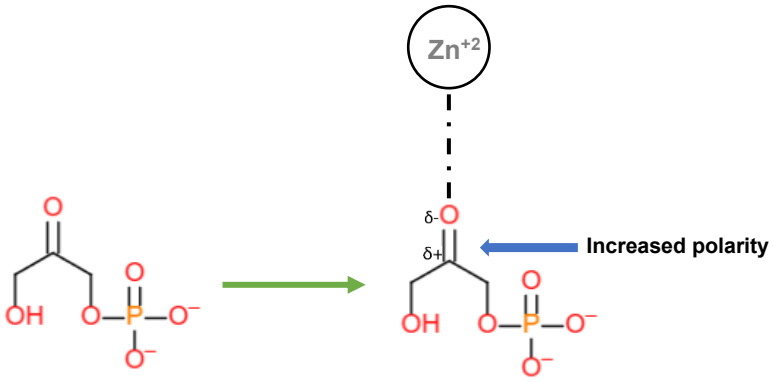

Figure 2. *Example of an ion-dipole interaction*

Thus, electrostatic interactions involving ions are very important in chemistry as they are essential to the formation and stability of compounds. Their unique nature, characterized by electron movement among atoms, greatly influence the properties of various substances. These bonds are important components of chemistry, as seen by their widespread occurrence in biological systems, such as DNA and proteins, as well as in a variety of industrial processes.

Now having discussed electrostatic interactions and their role in ionic bonding, we will delve into a related but distinct area: van der Waals forces. Subsection ***b.i*** will provide a detailed examination of these forces, including London dispersion forces, Debye forces,

and Keesom forces. While not as strong as ionic bonds, van der Waals forces are fundamental in shaping molecular structures and interactions, particularly in nonpolar environments. Understanding these interactions is essential for gaining insight into various chemical and biological processes.

b.i Van der Waals forces

These forces result from the formation of spontaneous dipoles and the resulting attraction between them. Van der Waals forces, despite their low strength in comparison to other types of interactions, can occur between almost any type of atom, making them important on a larger molecular scale. They are the primary forces behind hydrophobic interactions connecting hydrophobic molecules and domains. Nonpolar molecules, like hydrocarbons, also experience relatively small yet significant non-covalent attraction forces. Van der Waals forces arise due to the constantly shifting electron density within molecules. Even a molecule that lacks polarity will, at any given instant, exhibit a weak and transient dipole. With the formation of a temporary dipole-dipole interaction, this transient dipole will cause a nearby nonpolar molecule to also produce a transient dipole. The van der Waals forces, while weak, continuously produce and dissipate between closely packed nonpolar molecules. When these forces build up, their combined influence may become significant[8]. Van de Waals forces encompass various types of non-covalent interactions, including:

- London dispersion forces (induced dipole-induced dipole interactions)
- Debye forces (dipole-induced dipole interactions)
- Keesom forces (Permanent dipole-dipole interactions)

London dispersion forces

The London dispersion force represents the weakest type of van der Waals interaction, arising from transient changes in electron distributions around atoms and molecules. Even in nonpolar molecules, these changes lead to the formation of induced dipoles. Noble gases, such as helium (He) and neon (Ne), are examples of nonpolar substances consisting of individual atoms. In noble gases, the primary van der Waals interaction observed is the London dispersion force, which occur between noble gas atoms due to temporary fluctuations in electron density. Despite their weakness, these interactions play a crucial role in the process of noble gases condensing into liquids and solids at low temperatures[9].

In organic compounds, interactions between molecules, especially in the presence of heteroatoms, can have significant effects. These interactions, also known as "induced dipole-induced dipole interactions," occur between all molecules, particularly ones with no permanent dipoles. The strength of these dispersive interactions is influenced by the polarizability of the groups involved, with solvents possessing higher polarizabilities decreases their effectiveness[10].

For example, hexane, a highly nonpolar hydrocarbon, predominantly exists as a liquid at room temperature due to London dispersion forces. In this scenario, the electron cloud of one hexane molecule may experience temporary distortion induced by the transient, weak, partly negative dipole of another hexane molecule, resulting in the formation of a partially positive dipole. Consequently, hexane molecules crystallize in the absence of solvents due to dispersive forces. The temperature at which these crystals sublimate serves as a potential metric for evaluating the strength of dispersive interactions. Despite

being transient and weak, these interactions are adequate to maintain certain non-polar substances in a liquid state at ambient temperatures[10].

Debye forces

When a polar molecule with a permanent dipole approaches a non-polar molecule without a permanent dipole, they experience an interaction known as a dipole-induced dipole interaction, commonly referred to as Debye force. The dipole of the approaching molecule induces a temporary dipole in the nonpolar molecule, resulting in the polarization of its electron cloud. This polarization causes the electrons to redistribute, either towards or away from the induced dipole, depending on the direction of the permanent dipole. Consequently, the induced dipole in the nonpolar molecule experiences an attractive or repulsive to the permanent dipole. Atoms with larger atomic radii exhibit higher "polarizability," leading to stronger attractions due to the Debye force [11].

For example, when HCl, a polar molecule, interacts with Argon (Ar), a nonpolar atom, the permanent dipole of HCl induces a temporary dipole in Ar. As Ar approaches HCl, its electrons are drawn towards the hydrogen (H) side of HCl and simultaneously repelled from the chlorine (Cl) side. This interaction, known as the Debye force, arises due to the polarization of Ar by the permanent dipole of HCl. Despite Ar's nonpolar nature, these subtle interactions significantly contribute to the overall stability of matter[12,13].

Keesom forces

Keesom forces, also known as dipole-dipole interactions, occur when polar molecules with permanent dipoles interact with one another. These interactions, characterized by the attraction between the partial positive and negative charges of

adjacent molecules, are stronger than London dispersion forces. For example, hydrogen fluoride (HF) exhibits a polar nature due to the difference in electronegativity between hydrogen and fluorine. The partial positive charge (δ+) on hydrogen and the partial negative charge (δ−) on fluorine attract one another, leading to dipole-dipole interactions between neighbouring HF molecules. As a result of these interactions, molecules tend to arrange themselves in a manner that increases their attraction, minimizing potential energy. Elements with high electronegativity, such as oxygen, nitrogen, sulphur, and fluorine, are commonly associated with the presence of dipoles[10].

Another example of a dipole-dipole interaction is the acetone in nail polish removers. Acetone contains a carbonyl group, resulting in a net dipole. Oxygen's higher electronegativity than carbon leads to a partial negative charge (δ−) on oxygen and a partial positive charge (δ+) on carbon. While electrons are shared covalently between oxygen and carbon, creating partial charges, complete charge transfer would yield electrostatic interaction (Figure 3)[14].

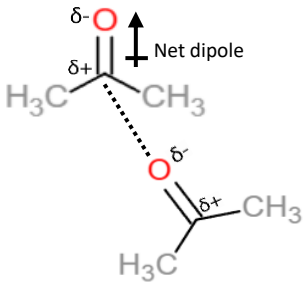

Figure 3. *Example of a dipole-dipole interaction*

It is important to note that while many molecules contain dipolar groups, some may lack a net dipole moment due to molecular symmetry, leading to the cancellation of dipoles. This phenomenon is seen in compounds such as tetrachloromethane. Additionally, it is

worth mentioning that dipole-dipole interactions between two separate atoms are often small, as individual atoms lack a permanent dipole[15].

c. Hydrogen Bonds

Hydrogen bonds are essential non-covalent interactions formed when a lone pair of electrons, often associated with slightly electronegative atoms like oxygen or nitrogen, interacts with a hydrogen atom covalently bonded to a more electronegative atom, such as a hydroxyl, amino, or protonated carboxyl group. These bonds are essential in proteins, regulating the formation of α-helix and β-strand structures. Despite water's low molecular weight, its liquid state at ambient temperature is maintained due to hydrogen bonding. While hydrogen bond typically ranges in strength from 0 to 4 kcal/mol, hydrogen bonds can reach up to 40 kcal/mol under extreme conditions[16].

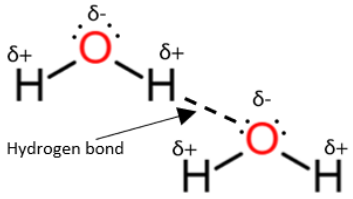

Figure 4. *Formation of hydrogen bond between two water molecules*

In chemical structures, hydrogen bonds are often represented using dotted lines. These bonds involve two key concepts: hydrogen bond donors and acceptors. A hydrogen bond donor is an entity that donates a proton to a hydrogen bond, typically involving a hydrogen atom bonded to a strongly electronegative atom like nitrogen, oxygen, or fluorine. In contrast, a hydrogen bond acceptor provides a lone pair of electrons from an atom, usually oxygen or nitrogen, to participate in the bond. Notably, many organic functional groups may act as hydrogen bond donors, acceptors, or both during hydrogen bond formation. For instance, water and alcohol can act as both donors and acceptors due to

their polar nature. However, certain groups, such as ethers, aldehydes, ketones, and esters, exclusively function as acceptors. A notable exception is the carbonyl group found in compounds like aldehyde and ketones. Due to the absence of a hydrogen atom bonded to an oxygen or nitrogen atom, the carbonyl group is limited to functioning solely as a hydrogen bond acceptor[17].

Hydrogen bonding between a ketone (acceptor) and water (donor)

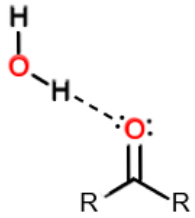

Hydrogen bonding between a ketone (acceptor) and an amide (donor)

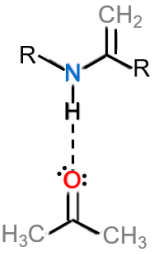

***Figure 5**. Hydrogen bonding between a ketone (acceptor) and R (donor).*

Hydrogen bonds, generally stronger than dipole-dipole interactions but weaker than covalent bonds, are important in biology. Within the cell, the process of DNA replication relies on precise hydrogen bonding interactions between complementary DNA strands, with adenine pairing with thymine and guanine with cytosine. Beyond biology, hydrogen bonds, together with other non-covalent interactions, are essential for ligand-protein binding. Moreover, hydrogen bonding serves as a strong tool in crystal engineering. This area of study focuses on deliberately designing and assembling molecular components through non-covalent interactions, particularly hydrogen bonds, to create functional crystalline materials. One can manipulate the structure, stability, and characteristics of molecules within crystals by selectively using hydrogen bonds, leading to the creation of novel materials with diverse applications[18].

In summary, hydrogen bonding is fundamental in natural phenomena, significantly influencing water properties, shaping biological molecules, and facilitating important interactions. Its importance extends to scientific knowledge, contributing to molecular recognition intricacies, macromolecular stability, and crystal engineering. This versatile approach enables the intentional manipulation of molecular structures within crystals, leading to the development of materials with diverse applications.

d. The Sigma Hole

Certain types of non-covalent interactions between Groups IV–VII atoms and negatively charged sites, such as lone pairs of Lewis bases or anions, are known as sigma–hole bonds. A σ-hole refers to a region of elevated electrostatic potential at the atomic end of a covalent bond. This phenomenon arises from anisotropic charge distribution within the atom, leading to the development of electron-deficient region, or sigma-holes, in elements of Groups 14 to 17 in the periodic table. These σ-holes represent a region of decreased electron density on the atom's surface, often along the bond axis's extension[19].

Sigma-hole interactions can occur when halogen atoms (F, Cl, Br, or I) interact with non-polar molecules containing a lone pair of electrons. These interactions are considered weak. During sigma-hole interactions, a halogen bond forms between the halogen atom and the lone pair of electrons in the non-polar molecule. This bond weakens the original bond and creates an empty orbital, or "hole," in the non-polar molecule by transferring electron density to the lone pair. This newly formed empty orbital holds the potential to engage in further interactions when it interacts with another molecule[23].

For example, consider the interaction between ICF_3 and H_2O (water) molecules shown in Figure 6. Here, water acts as the electron donor, contributing its unshared pair of electrons to the empty orbital on the iodine atom of ICF_3. Conversely, ICF_3 acts as the electron acceptor, receiving the unshared pair from water and forming a halogen bond. This breaks the water molecule's hydrogen bond and weakens the fluorine-carbon connection. This positive region may then form a new hydrogen bond by interacting with another molecule, such as another water molecule. This demonstrates the dynamic nature of sigma-hole interactions in altering molecular structures and facilitating bond formation[23,24].

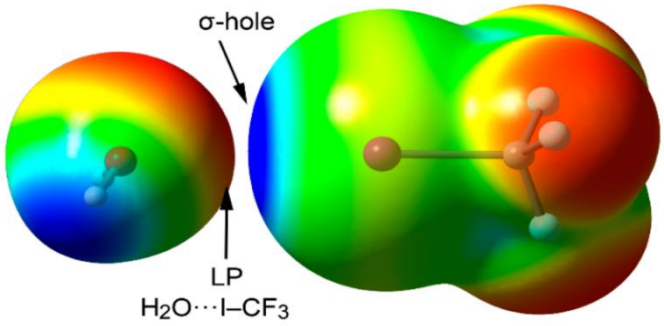

Figure 6. *A schematic of an electron donor and acceptor moiety, H_2O and ICF_3, forming a prototypical halogen-bonded σ-hole complex. Electronegative zones are shown in red, while electropositive regions are shown in blue.*[34] *(All articles published by MDPI are made immediately available worldwide under an open access license; Permission to reuse the figures granted)*

The current surge in interest and rise in studies in non-covalent interactions containing elements from groups 14 to 17 has prompted the development and use of novel research methodologies. Exploring the distribution and dynamics of sigma-holes among different elements reveals important information about the broad implications of sigma-hole interactions. Researchers are interested by the coexistence of lone pairs and σ-holes on the same element, a phenomenon that has attracted attention and prompted theoretical

investigations revealing highly anisotropic electron density distribution in elements Ha (halogens), Ch (chalcogens), Pn (pnictogens), and Tt (tetrels)[25-29].

The behaviour of elements within specific groups on the periodic table reveals interesting patterns influenced by their valency and bonding tendencies. Notably, elements with monovalent (Ha), divalent (Ch), trivalent (Pn), and tetravalent (Tt) tendencies exhibit varying numbers of lone pairs (LPs) from three to none, and the number of σ-holes ranges from one to four (Figure 7).

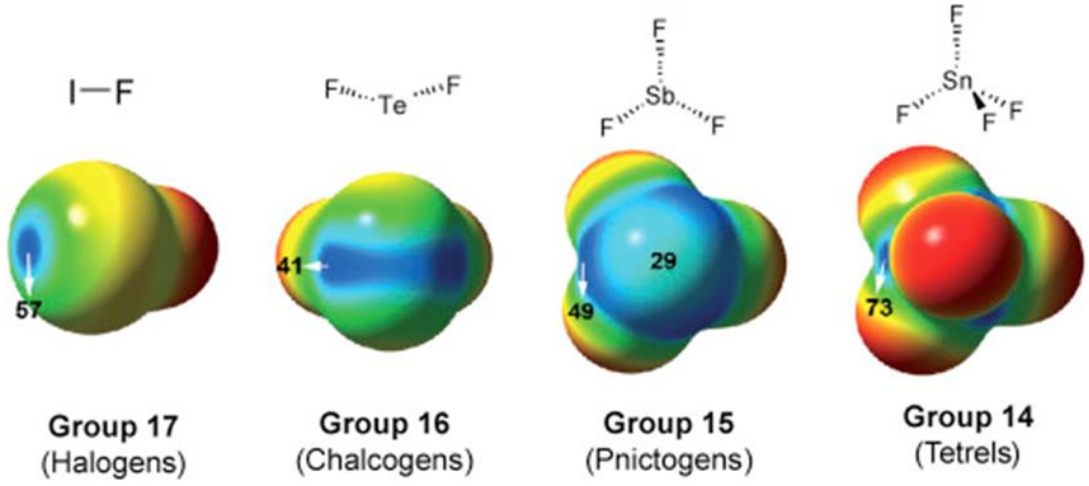

Figure 7. MEP showing the locations of the σ-holes on Group 14–17 elements of the same period bonded to fluorine (*Lim, J.Y., & Beer, P.D. (2018). Sigma-Hole Interactions in Anion Recognition. Chem, 4, 731-783.)*[30]

- Monovalent Ha: 7 valence electrons, 3 lone pairs, 1 sigma-hole.
- Divalent Ch: 6 valence electrons, 2 lone pairs, 2 sigma-holes.
- Trivalent Pn: 5 valence electrons, 1 lone pair, 3 sigma-holes.
- Tetravalent Tt: 4 valence electrons, zero lone pairs, 4 sigma-holes.

These findings are based on fundamental principles of chemical bonding, molecular geometry, and structural properties found in compounds containing these components.

While differences may arise in unique compounds and molecular settings, these patterns provide a basic framework for understanding the behaviour of each group of elements[31].

Furthermore, Figure 7 reveals several important differences in the nature of each σ-hole interaction. These regions arise due to the asymmetrical distribution of electron density around the atom, typically occurring in Group 14 to Group 17 elements of the periodic table. The number of σ-holes exhibited by an element correlates with its valence electron configuration and bonding behaviour. For instance, halogens in Group 17, with one valence electron short of a complete octet, possess one sigma hole. Chalcogens in Group 16, having two unpaired electrons available for bonding, display two sigma holes. Similarly, pnictogens in Group 15, with five valence electrons, demonstrate three sigma holes, while tetrels in Group 14, with four valence electrons, exhibit four sigma holes[32]. These sigma holes play a pivotal role in facilitating directional non-covalent interactions such as halogen bonding, chalcogen bonding, pnictogen bonding, and tetrel bonding, which are essential in various chemical processes including molecular recognition, crystal engineering, and materials science research.

e. Halogen Bonds

The concept of halogen bonding (HaB) has evolved significantly since its introduction in the 20th century. Initially introduced by Zingaro and Hedges in 1973 to describe halogens behaving as electrophilic entities, the study of halogen bonds has seen substantial progress. It is now acknowledged that HaB have a significant impact on several chemical processes, such as protein folding, catalysis, and drug design [27]. They used this idea to explain why halogens and interhalogens react to form complexes in solution with

phosphine oxides and sulphides[33]. Adducts were first observed to develop between haloforms, ethers, and amines in the gas phase in 1976 by Martire et al[34]. But Dumas et al. in 1983 labelled these bonds as halogen adducts[35]. After the review by Metrangolo and Resnati, which gave efficient techniques for determining a connection between the structure of the donor and acceptor components engaged in the halogen bond and the strength of the interaction, the term "halogen bond" became widely used[36].

Additionally, non-covalent interactions, such as halogen bonding, share similarities with the dipole-dipole interaction of hydrogen bonding, as they do not require the formation or breaking of chemical bonds. Halogen bonding occurs when a halogen atom forms a weak electrostatic connection with an electron-rich nucleophilic atom, often anionic molecules or highly electronegative atoms like oxygen, nitrogen, or sulphur. Notably, halogen bonding is characterized by the presence of a sigma hole on the halogen atom, which acts as an electrophilic site, attracting electron-rich nucleophiles and influencing the interaction's direction and strength[37].

In recent years, there has been a surge of interest in HaB among scientists, leading to a growing number of experimental and theoretical studies. In 2009, the International Union of Pure and Applied Chemistry (IUPAC) project 2009-032-1-100 was initiated to comprehensibly explore interactions involving halogens as electrophilic species. This study has developed to include more interactions within the σ-hole family[41]. According to the IUPAC definition, a HaB is represented as R···HaY, where the halogen atom, Ha, form a covalent bond with the R-group, exhibiting a region of positive electrostatic potential known as the σ-hole. The nucleophile, or HaB acceptor, denoted as Y, can exist as a lone pair, anion, or other electron-rich system[38-40].

Also, the strength of halogen bonding and other σ-hole interactions is influenced by two primary factors. Firstly, as atoms progress down the periodic table, their polarizability increases, causing the positive charge region on the σ-hole to expand due to enhanced polarization along the electron-withdrawing group (EWG)-X bond. This results in an enhancement of the non-covalent interaction (NCI). Secondly, increasing the EWG's electron-withdrawing capacity is another option for producing polarization in the EWG-X bond. Therefore, the positive potential and size of the σ-hole are enhanced when heavy elements are associated with strong electron-withdrawing groups, leading to the enhancement of non-covalent interaction via an increase in the electrostatic term[41, 42].

f. Tetrel Bonds

Tetrel bonding refers to a specific kind of non-covalent interaction that occurs between atoms belonging to group 14 of the periodic table. This group includes carbon (C), silicon (Si), germanium (Ge), tin (Sn), and lead (Pb). The formation of a tetrel bond occurs when an electrophilic region associated with a tetrel atom interacts favourably with a nucleophilic region on another molecule or within the same molecule. Conceptually, tetrel bonding shares similarities with well-established non-covalent interactions such as hydrogen bonding and halogen bonding. Tetrel bonding has been detected in several chemical and biological systems, holding interest in the fields of crystal engineering, supramolecular chemistry, and materials research[43]. It has the potential to affect crystal packing and molecular complex stability. To investigate and assess tetrel bonding interactions across diverse chemical systems, scientists often employ computational methods like density functional theory (DFT) simulations[43].

The concept of tetrel bonding is a relatively recent concept in the study of non-covalent interactions. Table 1 shows the polarizability and van der Waals radii of tetrel elements from periods 2 through 5 provide insights into their bonding behavior. Silicon (Si) exhibits a polarizability approximately three times greater than carbon (C), while there is minimal difference between the polarizability of Si and Ge, as well as between Ge and Sn. Additionally, Table 1 presents the molecular electrostatic potential (MEP) values for the Tt-holes across the four fluoride derivatives. For example, Figure 8 illustrates the MEP surface of SnF_4. Small, well-defined holes suggest that the TtB interaction is very directed. Among the Tt series, the biggest MEP value is found at the Sn sigma-hole. Finally, the large and negative MEP values obtained at the fluorine (F) atoms support the high polarity of the Sn-F bonds[43]. MEP values increase as one moves down the group, which agrees with the trend observed in atomic polarizability[43].

Table 1. *The polarizability (α, a.u.), van der Waals radius (in Å), and π-hole MEP (in kcal/mol) of the tetrafluoride forms. Values are derived from the ref [44].*

Tt	α	R_{vdW}	MEP (TtF_4)
C	9.0	1.70	18.6
Si	26.1	2.10	39.0
Ge	28.4	2.11	50.2
Sn	37.3	2.17	66.5

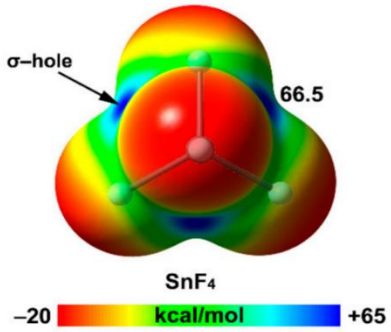

Figure 8. *The MEP surface of SnF_4 (energy in kcal/mol) was modelled using the 0.001 a.u. isosurface and the MP2/def2-TZVP level of theory.*[34]*(All articles published by MDPI are made immediately available worldwide under an open access license; Permission to reuse the figures granted)*

Tetrel-bonding interactions exhibit distinct behaviour in terms of steric requirements, as opposed to other σ-hole interactions. In a typical halogen bonding (HaB) complex, the Lewis base, and the electron-withdrawing group (EWG) attached to the Ha atom are typically oriented 180 degrees apart. Unlike in HaB interactions, the magnitude of the EWG interaction with tetrel-bonding (TtB) is not influenced by the size of the EWG. The transition from ChBs (chalcogen bonding) to TtBs highlights the steric effects, with the former exhibiting steric properties analogous to HaBs. While in most cases, the atom with an electron surplus can approach the PnB (pnictogen bonding) or NgB (noble gas bonding) without experiencing significant steric repulsion. Tt atoms, on the other hand, have a quite different situation since the tetrahedral configuration of its four substituents increases both steric repulsion and steric crowding with the electron-rich atom. This characteristic, crucial in TtBs, has been extensively investigated[44]. Researchers have explored the impact of altering the Tt atom's size (ranging from Si to Pb), the size and electron-withdrawing capability of the substituents, and the nature of the electron-rich atom (neutral or charged)[45].

The term "tetrel bonding" was introduced in 2013 to describe σ-hole interactions where atoms from group IV function as Lewis acids[37]. However, before that, scientists had extensively studied this interaction. Anion or lone pair “p” interactions are examples of "p-hole" interactions utilized by tetrel atoms in a sp^2-hybridized state to interact with electron-rich compounds. While most tetrel atoms are well-suited for tetrel bonding, other elements may easily enhance their valence and take part in conventional chemical processes. The wide variety of coordination chemistry shown by lead (Pb) and tin (Sn) leads to their classification as metals. Metalloids are hypervalent species consisting of germanium (Ge) and silicon (Si) that are both rare and widely known. It is conceivable that these larger tetrel atoms (Si-Pb) may participate in non-covalent interactions under specific chemical circumstances that prevent hyper valency. Numerous studies have explored such interactions involving Si, Ge, and Sn. For instance, Alkorta et al., (2001) conducted a study on molecular complexes involving silicon derivatives (SiX_4, where X represents a halogen) and electron-rich groups (such as NH_3, H_2O, etc.), along with examining this interaction in aminopropylsilanes[46].

In summary, tetrel bonds represent an important category of non-covalent interactions with potential applications across materials science and supramolecular chemistry. Serving as a valuable asset for researchers across diverse domains, from drug design to crystal engineering, tetrel bonds offer a means to create novel molecular structures and materials. Moreover, investigations into tetrel bonding contribute to our comprehension of intermolecular forces and their impact on molecular structure and characteristics.

g. Supramolecular Chemistry and Crystal Engineering

g.i. Supramolecular Chemistry

Supramolecular chemistry, often referred to as "chemistry beyond the molecule," is a dynamic and interdisciplinary field that investigates molecular recognition and the formation of complex assemblies via non-covalent interactions. It emphasizes on the study of molecular ensembles and intermolecular interactions, diving into complex chemical systems from disciplines such as chemistry, biology, physics, and material science. Understanding these weak yet reversible forces is essential for understanding biological processes, self-assembling systems, and advancing the development of complex materials and molecular machinery. The Nobel Prize in Chemistry was jointly awarded in 1987 to Donald J. Cram, Jean-Marie Lehn, and Charles J. Pedersen for their pioneering contributions to this field, solidifying supramolecular chemistry as a distinct branch of chemistry[47,48].

Supramolecular chemistry may be classified into two distinct disciplines: Host-Guest Recognition and Self-Assembly (as illustrated in Figure 9). In Host-Guest Recognition, a receptor (host) interacts with a substrate (guest), resulting in the formation of a complex. On the other hand, Self-Assembly includes the assembly of several components to produce more complex structures[49].

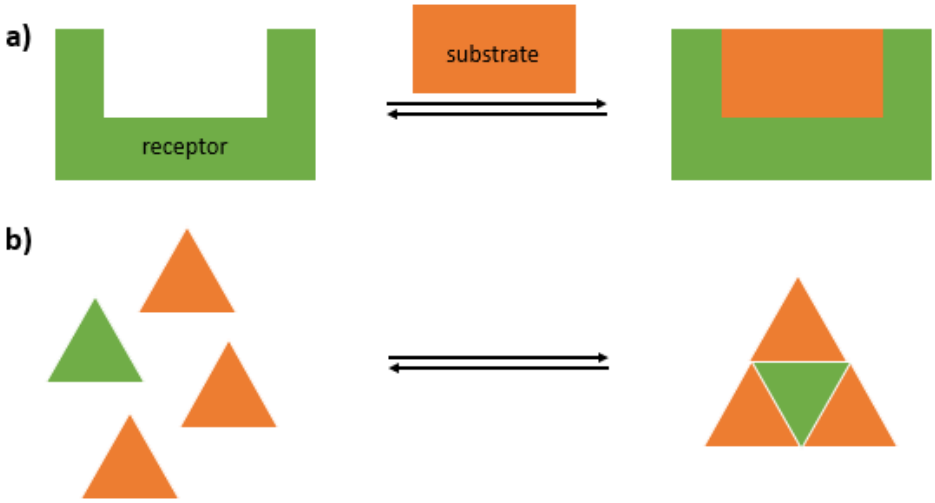

Figure 9. *Supramolecular chemistry: (a) host-guest recognition and (b) self-assembly.*

Additionally, natural receptors, like enzyme active sites, and self-assembled structures such as the DNA double helix, serve as valuable sources of inspiration for supramolecular chemists. These receptors frequently exhibit molecular recognition and interactions akin to the host-guest interactions studied in supramolecular chemistry. In a solution, the host H, guest G, and complexes HpGq exist in a state of equilibrium. For the most basic scenario when p and q both equal 1 (p = q =1), the equilibrium may be expressed as:

$$H + G \rightleftharpoons HG$$

The Gibbs free energy change, ΔG, for this reaction can be calculated by the addition of an enthalpy component, ΔH, to the product of the temperature, T, and the entropy term, ΔS.

$$\Delta G = \Delta H - T\Delta S$$

The values of both ΔG and ΔS may be calculated at a certain temperature, T, using isothermal titration calorimetry. The molecular surroundings of a supramolecular system are crucial for its functioning and lifespan. Several solvents have robust hydrogen

bonding, electrostatic, and charge-transfer capacities, enabling them to engage in intricate equilibria with the system, perhaps even disrupting complexes entirely. Hence, the selection of solvent might be crucial[50].

Furthermore, double-stranded DNA is a famous example of two linear strands that may link to one another via stabilizing interactions such as hydrogen bonding. In this case, the system stores and replicates a lot of information, and it also processes it. When compared to the basic model systems created by humans, supramolecular examples found in nature are much more complex. However, artificial models aid in the development of increasingly complex systems and an understanding of fundamental processes. Over the course of the past four decades, supramolecular chemistry has developed into a vivid, highly important multidisciplinary yet self-sufficient area of study[51].

In summary, supramolecular chemistry emerges as dynamic and interdisciplinary field, focusing on the exploration of non-covalent interactions and the assembly of molecular structures that surpass individual molecules. By strategically harnessing forces like hydrogen bonding and van der Waals interactions, researchers can strategically design and synthesize complex, functional systems. The impact of supramolecular chemistry has far-reaching effects in fields such as materials science, medicine delivery, catalysis, and nanotechnology, among others. The ability to design complex and programmable supramolecular structures provides scientists with a powerful toolkit for developing new materials and functional systems, stimulating creativity in a variety of scientific fields [47,48,52].

g.ii. Crystal Engineering

Crystal engineering is an interdisciplinary field that intentionally manipulates intermolecular interactions to design and synthesize solid-state structures with specific properties. By employing techniques like hydrogen bonding, halogen bonding, and coordination bonding, crystal engineers create materials tailored for various applications. Over the last five decades, the field has grown significantly due to the synergy between solid-state and supramolecular chemistry[53].

The relationship between crystallography and chemistry is important. While crystallography studies the arrangement and bonding of atoms in crystalline materials, chemistry focuses on understanding molecules. Together, these disciplines contribute to the advancement of crystal engineering.

Notably, in 1921, W. H. Bragg, was the first to examine the relationship between molecules and crystals. He observed that specific structural components, such as a benzene ring, maintain their size and shape across different crystal structures (Figure 10). This insight provided fundamental understanding of how molecules organize in crystals, shaping subsequent advancements in crystallography and crystal engineering[53].

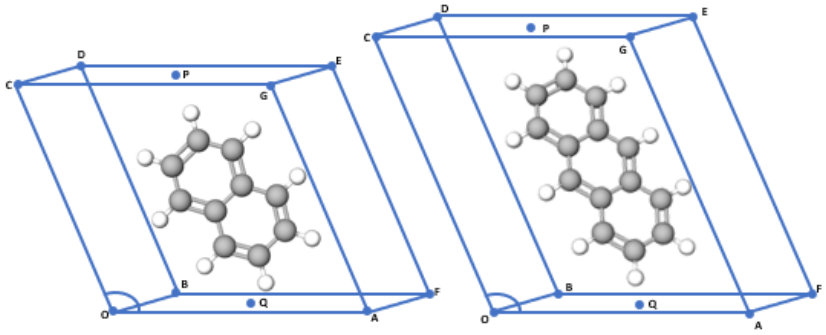

Figure 10. *The correlation between the crystal unit cells of naphthalene and anthracene could be used to determine the dimensions of a benzene ring. Adapted from ref [54].*

Crystal engineering encompasses a range of fundamental concepts and techniques essential for the design and synthesis of solid-state structures with tailored properties. Among these, several key concepts are important in shaping the organization and characteristics of crystalline materials. Next, we will take a closer look at some of the essential principles in crystal engineering.

Key Concepts in Crystal Engineering

- **Non-covalent interactions:** The arrangement of molecules and ions in the solid state in crystal engineering is achieved using non-covalent interactions, including hydrogen bonding, halogen bonding, and coordination bonding. Hydrogen bonds were a major focus of early research on just organic systems, but coordination and halogen bonds allow for even more precise control in crystal formation.
- **Supramolecular synthons:** In the solid state, some groups may be ordered by using supramolecular synthons, which are building blocks shared by numerous structures. In most cases, they are engineered to have complementary interactions that will cause them to self-assemble into a certain crystal structure. In contrast to an intermolecular interaction, a supramolecular synthon may be easily identified as a component of the design. It is important to note that synthons are not the same as the interactions themselves, but rather the result of carefully designed combinations of them. Crystal engineering relies heavily on supramolecular synthons, which provide a robust strategy for designing and synthesizing novel materials with broad potential uses.

- **Crystal packing:** Crystal packing describes how molecules are arranged inside a crystal. Non-covalent interactions between molecules are what ultimately decide how they pack together in a crystal.
- **Supramolecular architecture:** The supramolecular arrangement of a crystal refers to the overall organization of its constituent molecules, including factors such as their interactions, topological characteristics, and dimensional properties.

Polymorphism and Isomorphism

In material design, polymorphism and isomorphism influence material qualities and applications. Isomorphism refers to the structural resemblance observed in the crystalline arrangements of two different substances, indicating an identical atomic configuration. For crystals to be isomorphous, they must share the same space group and unit-cell dimensions, while their atom types and positions remain nearly identical. One common example of isomorphism in crystal engineering involves the substitution of ions within a crystal lattice. For instance, consider the mineral olivine, which has a chemical formula represented as $(Mg,Fe)_2SiO_4$. In olivine, magnesium (Mg) and iron (Fe) ions can substitute for each other within the crystal lattice without significantly altering the overall structure. As iron content increases, the colour of olivine shifts from green to brown. This change in colour occurs because iron ions absorb different wavelengths of light compared to magnesium ions, affecting the mineral's optical properties. Despite the substitution of iron for magnesium, the crystal lattice of olivine remains essentially unchanged, demonstrating isomorphism[55].

On the other hand, polymorphism, also known as allotropy among chemical elements, refers to the phenomenon where a substance can exist in multiple crystalline forms with different atomic arrangements. This may occur due to variations in the molecular arrangement inside the substance. For example, carbon exhibits polymorphism in two distinct crystalline structures, diamond, and graphite (Figure 11). Diamond has a rigid and brittle crystalline structure due to each carbon atom being covalently bonded to four others, making it exceptionally hard. On the other hand, graphite is flexible and elastic because each carbon atom is linked to three others, forming layers with relatively weak intermolecular forces. These difference in molecular arrangements explains the distinct properties seen in diamond and graphite[56,57].

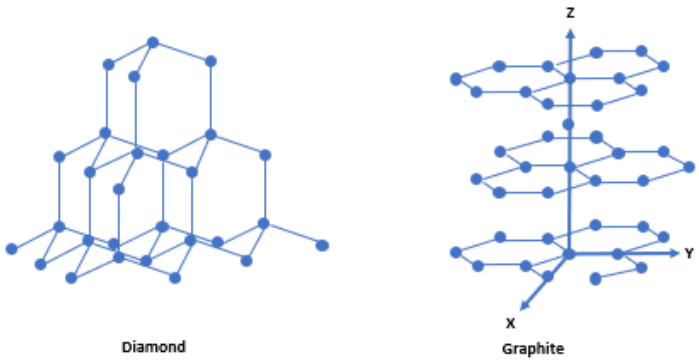

Figure 11. *Different forms of carbon[57].*

Both polymorphism and isomorphism hold significant roles in crystal engineering, as they have potential to influence the characteristics of materials. A notable example involves the presence of distinct polymorphs of a substance, each exhibiting unique physical characteristics like melting point, density, and hardness. The concept of isomorphism may also be used in the development of novel materials that possess certain desirable features. Polymorphism, as an inherent property of chemical materials, allows them to exhibit multiple crystalline states, each with unique characteristics in terms of solubility,

colour, and melting point. This behaviour is observed in both inorganic and organic compounds. Different polymorphs may be easily distinguished using X-ray powder diffraction. The strong transmission of the X-rays makes it possible to investigate medicinal tablets (in blisters) and to utilize them to detect counterfeits[58].

Challenges

Crystal engineering faces challenges in regulating crystal growth to achieve desired shapes, sizes, and characteristics. Controlling intermolecular interactions and ensuring uniform growth pose significant obstacles. The presence of different polymorphs adds complexity, as each may exhibit distinct characteristics, making the regulation of specific polymorphs challenging. Crystal growth is a complex and time-consuming process, making industrial scaling a challenge. Developing effective crystal growth techniques requires innovation in supramolecular synthons and advanced computational methods like density functional theory and Monte Carlo simulations. These methods are essential for controlling crystal packing and designing materials with tailored properties[59].

h. Objectives

In our research, we introduce crystal engineering with phosphine acceptors as a novel approach to investigate tetrel bonds and to investigate it through NMR techniques. The primary goal of our research extends beyond the synthesis of a cocrystal, specifically a TtB (tetrel bond) complex. The overarching goal of this study is to look at tetrel bonds, particularly those that use heavier pnictogens as electron donors. Our goal with the cocrystal synthesis is to dig into the realm of tetrel bonds, examining their strength and properties, with a particular emphasis on interactions with significant pnictogenic elements. Subsequent to confirming the cocrystal structure, our approach involves quantum chemical calculations, such as density functional theory (DFT), to meticulously compute and validate the bond strength of these tetrel bonds.

References Chapter 1

1. Hobza, P., Zahradník, R., & Müller-Dethlefs, K. (2006). The World of Non-Covalent Interactions: 2006. Collection of Czechoslovak Chemical Communications, 71, 443-531.
2. Singh, S. K., & Das, A. (2015). The n → π* interaction: a rapidly emerging non-covalent interaction. Physical Chemistry Chemical Physics, 17(15), 9596–9612.
3. Serway, R. A., Jewett, J. W., & Wilson, J. (2013). Physics for Scientists and Engineers with Modern Physics. Cengage Learning.
4. Karshikoff, A. (2006). Non-Covalent interactions in proteins. In Published by imperial college press and distributed by world scientific publishing co. eBooks.
5. Bickelhaupt, F. M., Solà, M., & Guerra, C. F. (2006). Covalent versus ionic bonding in alkalimetal fluoride oligomers. Journal of Computational Chemistry, 28(1), 238–250.
6. Minkin, V.I., Osipov, O.A., & Zhdanov, I.A. (1970). Dipole moments in organic chemistry. In Springer eBooks.
7. Mahadevi, A. S., & Sastry, G. N. (2012). Cation−π Interaction: Its Role and Relevance in Chemistry, Biology, and Material Science. Coordination Chemical Reviews, 113(3), 2100–2138.
8. Corminbœuf, C. (2014). Minimizing Density Functional Failures for Non-Covalent Interactions Beyond van der Waals Complexes. Accounts of Chemical Research, 47(11), 3217–3224.
9. Lin, I., von Lilienfeld, O.A., Coutinho-Neto, M.D., Tavernelli, I., & Rothlisberger, U. (2007). Predicting noncovalent interactions between aromatic biomolecules with London-dispersion-corrected DFT. The journal of physical chemistry. B, 111 51, 14346-54.
10. Riley, K. E. & Hobza. (2011). Non-covalent interactions in biochemistry. 1, 3-17
11. Avila-Montiel, C., Tapia-Benavides, A. R., Islas-Trejo, E., Ariza, A., & Tlahuext, H. (2020). Non-covalent interactions in organic-inorganic hybrid compounds derived from amino amides. Journal of Molecular Structure, 1202, 127258

12. George, W.O., Williams, D.A. (1996). Association Between Electron Donor Molecules and HCl in Argon Matrices. In: Fausto, R. (eds) Low Temperature Molecular Spectroscopy. NATO ASI Series, vol 483. Springer.
13. Dunaev, A.V. (2015). Survey of emission spectra of the plasma of chlorine, hydrogen chloride, argon, and hydrogen. Russ Microelectron 44, 173–177.
14. Kollman, P. A. (2008). Non-covalent interactions. 10, 365-371.
15. Axilrod, B.M. (1951). Triple-Dipole Interaction. I. Theory. Journal of Chemical Physics, 19, 719-724.
16. Juanes, M., Saragi, R. T., Caminati, W., & Lesarri, A. (2019). The Hydrogen Bond and Beyond: Perspectives for Rotational Investigations of Non-Covalent Interactions. Chemistry (Weinheim an der Bergstrasse, Germany), 25(49), 11402–11411.
17. Böhm, H., Brode, S., Hesse, U., & Klebe, G. (1996). Oxygen and Nitrogen in Competitive Situations: Which is the Hydrogen-Bond Acceptor? Chemistry - a European Journal, 2(12), 1509–1513
18. Voet, D., Voet, J. G., & Pratt, C. W. (2016). Fundamentals of Biochemistry: Life at the Molecular Level. Wiley.
19. Bauzá, A., Mooibroek, T. J., & Frontera, A. (2015). The bright future of unconventional σ/π-hole interactions. Chemphyschem : a European journal of chemical physics and physical chemistry, 16(12), 2496–2517.
20. Lim, J. Y. C., & Beer, P. D. (2018). Sigma-Hole interactions in anion recognition. Chem, 4(4), 731–783.
21. Zierkiewicz, W., Michalczyk, M., & Scheiner, S. (2021). Noncovalent Bonds through Sigma and Pi-Hole Located on the Same Molecule. Guiding Principles and Comparisons. Molecules (Basel, Switzerland), 26(6), 1740.
22. Jena, S., Dutta, J., Tulsiyan, K. D., Sahu, A. K., Choudhury, S. S., & Biswal, H. S. (2022). Noncovalent interactions in proteins and nucleic acids: beyond hydrogen bonding and π-stacking. Chemical Society Reviews, 51(11), 4261–4286.
23. Metrangolo, P., Neukirch, H., Pilati, T., & Resnati, G. (2005). Halogen bonding based recognition processes: a world parallel to hydrogen bonding. Accounts of chemical research, 38(5), 386–395.

24. Zingaro, R. A., & Hedges, R. M. (1961). Phosphine oxide – halogen complexes: effect on P–O and P–S stretching frequencies. The Journal of Physical Chemistry, 65(7), 1132–1138.
25. Frontera, A., & Bauzá, A. (2021). On the Importance of σ–Hole Interactions in Crystal Structures. Crystals.
26. Bleiholder, C., Gleiter, R., Werz, D. B., & Köppel, H. (2007). Theoretical investigations on heteronuclear chalcogen-chalcogen interactions: on the nature of weak bonds between chalcogen centers. Inorganic chemistry, 46(6), 2249–2260.
27. Franconetti, A., Quiñonero, D., Frontera, A., & Resnati, G. (2019). Unexpected chalcogen bonds in tetravalent sulfur compounds. Physical Chemistry Chemical Physics, 21(21), 11313–11319.
28. de Azevedo Santos, L., van der Lubbe, S. C. C., Hamlin, T. A., Ramalho, T. C., & Matthias Bickelhaupt, F. (2021). A Quantitative Molecular Orbital Perspective of the Chalcogen Bond. ChemistryOpen, 10(4), 391–401.
29. De Vleeschouwer, F., Denayer, M., Pintér, B., Geerlings, P., & De Proft, F. (2017). Characterization of chalcogen bonding interactions via an in-depth conceptual quantum chemical analysis. Journal of Computational Chemistry, 39(10), 557–572.
30. Lim, J.Y., & Beer, P.D. (2018). Sigma-Hole Interactions in Anion Recognition. Chem, 4, 731-783.).
31. Frontera, A., & Bauzá, A. (2021). On the Importance of σ–Hole Interactions in Crystal Structures. Crystals.
32. Miessler, G. L., Fischer, P. J., & Tarr, D. A. (2017). Inorganic Chemistry (6th Edition). Pearson.
33. Zingaro, R. A., & Hedges, R. M. (1961). Phosphine oxide – halogen complexes: effect on P–O and P–S stretching frequencies. The Journal of Physical Chemistry, 65(7), 1132–1138.
34. D. E. Martire, J. P. Sheridan, J. W. King, and S. E. O'Donnell. (1976) Thermodynamics of molecular association. 9. An NMR study of hydrogen bonding of chloroform and bromoform to di-n-octyl ether, di-n-octyl thioether, and

di-n-octylmethylamine. *Journal of the American Chemical Society*. **98**, 3101-3106.

35. Dumas, J., Gomel, M., & Guérin, M. (2010). Molecular interactions involving organic halides. In John Wiley & Sons, Ltd eBooks (pp. 985–1020)
36. Metrangolo, P., Neukirch, H., Pilati, T., & Resnati, G. (2005). Halogen bonding based recognition processes: a world parallel to hydrogen bonding. Accounts of chemical research, 38(5), 386–395.
37. Alkorta I, Elguero J, Frontera A. (2020). Not Only Hydrogen Bonds: Other Noncovalent Interactions. Crystals; 10(3):180.
38. Pancholi, J., & Beer, P. D. (2020). Halogen bonding motifs for anion recognition. Coordination Chemistry Reviews, 416, 213281.
39. Sarwar, M. G., Dragisić, B., Sagoo, S., & Taylor, M. S. (2010). A tridentate Halogen-Bonding receptor for tight binding of halide anions. Angewandte Chemie International Edition, 49(9), 1674–1677.
40. Robinson, S. K., Mustoe, C. L., White, N. G., Brown, A., Thompson, A. L., Kennepohl, P., & Beer, P. D. (2014). Evidence for halogen bond covalency in acyclic and interlocked Halogen-Bonding receptor anion recognition. Journal of the American Chemical Society, 137(1), 499–507.
41. Frontera, A., & Bauzá, A. (2021). On the Importance of σ–Hole Interactions in Crystal Structures. Crystals.
42. Bauzá, A. & Frontera, A. (2022). *Supramolecular Assemblies Based on Electrostatic Interactions.* In Springer eBooks. 203-241
43. Frontera, A. (2020). Tetrel bonding interactions involving carbon at work: Recent advances in crystal engineering and catalysis. C, 6(4), 60.
44. Politzer, P., & Murray, J.S. (2019). An Overview of Strengths and Directionalities of Noncovalent Interactions: σ-Holes and π-Holes. Crystals.
45. Varadwaj, P. R. (2022). Tetrel bonding in anion Recognition: a first principles investigation. Molecules, 27(23), 8449.
46. Alkorta, I., Rozas, I., & Elguero, J. (2001). Molecular Complexes between Silicon Derivatives and Electron-Rich Groups. Journal of Physical Chemistry A, 105, 743-749.

47. Nangia, A.K. (2010). Supramolecular chemistry and crystal engineering. Journal of Chemical Sciences, 122, 295-310.
48. Dunitz, J. D. (1998). A Supramolecular Three-Dimensional Hydrogen-Bonded Network with Potential Application in Crystal Engineering Paradigms. Chemistry - a European Journal, 4(4), 745–746.
49. Yu, G., Jie, K., & Huang, F. (2015). Supramolecular Amphiphiles Based on Host-Guest Molecular Recognition Motifs. Chemical reviews, 115(15), 7240–7303.
50. Lehn, J. (1988). Supramolecular Chemistry—Scope and Perspectives Molecules, Supermolecules, and Molecular Devices (Nobel Lecture). Angewandte Chemie International Edition, 27(1), 89–112.
51. Insua, I., & Montenegro, J. (2020). Synthetic supramolecular systems in life-like materials and protocell models. Chem, 6(7), 1652–1682.
52. Malenov, D.P., Janjić, G.V., Medakovic, V.B., Hall, M.B., & Zarić, S.D. (2017). Noncovalent bonding: Stacking interactions of chelate rings of transition metal complexes. Coordination Chemistry Reviews, 345, 318-341.
53. Soldatov, D.V., Soldatov, D.V., & Terekhova, I.S. (2005). Supramolecular chemistry and crystal engineering. Journal of Structural Chemistry, 46, S1-S8.
54. Bragg, W.H. (1921). The Structure of Organic Crystals. Nature, 110, 115-117.
55. Nesse, William D. Introduction to Mineralogy. Oxford University Press, 2011.
56. Bimal R. (2023). Polymorphism and Isomorphism: Definition and 5 Reliable Differences. Chemistry Notes.
57. Libretexts. (2023). 14.4A: Graphite and Diamond - Structure and Properties. Chemistry LibreTexts.
58. Vologzhanina, A.V. (2019). Intermolecular Interactions in Functional Crystalline Materials: From Data to Knowledge. Crystals.
59. Lovette, M.A., Browning, A.R., Griffin, D.W., Sizemore, J.P., Snyder, R.C., & Doherty, M.F. (2008). Crystal Shape Engineering. Industrial & Engineering Chemistry Research, 47, 9812-9833.

Chapter 2. Theory and experiment: solid-state NMR and X-ray diffraction

a. Nuclear Magnetic Resonance Spectroscopy

Nuclear magnetic resonance spectroscopy (NMR spectroscopy) is a powerful analytical technique used in various fields of science[1]. It helps us understand the complex behaviours of atomic nuclei, specifically those with an odd number of protons or neutrons that possess a non-zero spin quantum number[5]. When exposed to radiofrequency radiation in a strong magnetic field, these nuclei absorb and emit energy at specific frequencies that are highly sensitive to their chemical surroundings.

This method has countless important applications. Scientists rely on NMR spectroscopy to unravel the structures of organic compounds, study reaction kinetics, and identify unknown substances. Its application extends to complex biomolecules such as proteins and nucleic acids, making it an indispensable tool in chemistry, biochemistry, and medicine[2]. What sets NMR apart is its non-destructive nature and its remarkable ability to provide comprehensive insights into chemical environments[5].

One of the most remarkable aspects of NMR is its ability to reveal atomic-level structural information for biological macromolecules dissolved in solution, without the need for the demanding crystallization processes[6]. This feature is especially useful for molecules that cannot form crystals or when the structure determined by X-ray crystallography is in doubt. Furthermore, NMR simplifies the study of protein-ligand interactions in biological contexts, providing a unique glimpse into ligand binding within natural environments[5].

Figure 1 illustrates the core principles of nuclear magnetic resonance spectroscopy, involving the interaction between two distinct states: the ground and excited states. In the presence of an external magnetic field (B_0), radiofrequency photons induce spin transitions between these states, involving alpha and beta spins. The alpha spins, constituting the ground state, align parallel to the magnetic field, while the beta spins, comprising the excited state, align antiparallel to the magnetic field[6].

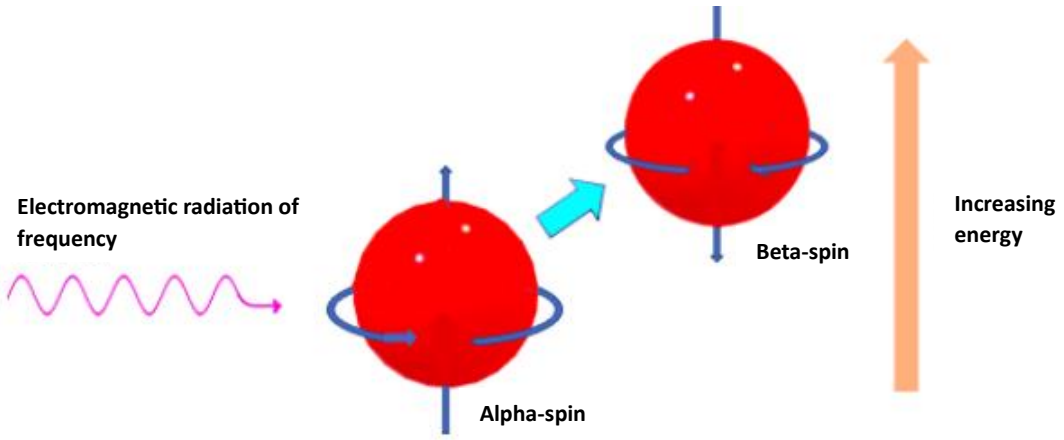

Figure 1. *Fundamentals of Nuclear Magnetic Resonance Spectroscopy*

Also, the concept of T_1 relaxation closely resembles the spontaneous emission process as described by Einstein's law for spontaneous emission, where the system transitions from the higher energy excited state to the lower energy ground state, releasing energy in the form of electromagnetic radiation[4]. The T_1 relaxation time describes the rate of emission or relaxation of this energy. The T_1 relaxation equation, which is frequently expressed as follows:

$$M_z(t) = M_0 \cdot (1 - e^{\left(-\frac{t}{T_1}\right)})$$

Where,

- $M_z(t)$, represents the magnetization (or population) of the excited state at time t.

- M_0, is the initial magnetization or population of the excited state.
- t, the time
- T_1, the longitudinal relaxation time, which characterizes the rate of return to the ground state.

One of the most crucial steps in obtaining and understanding NMR spectra is regulating the relaxation of nuclear magnetization along the z-axis[3]. This is a fundamental procedure that must be carefully considered to accurately interpret the data. Understanding T_1 relaxation times for various nuclei proves indispensable for optimizing experimental parameters and obtaining accurate NMR data.

The generation and interpretation of NMR signals rely on the energy difference between these states, which is determined by the strength of the magnetic field and unique nuclear properties[1]. Through the use of radiofrequency pulses, these spins can be manipulated, causing transitions between the alpha and beta states. Ultimately, NMR spectroscopy is a powerful tool that not only aids in unravelling the complexities of molecular structure, but also offers perceptions into dynamic processes and interactions in the chemical and biological spheres[1].

i. Nuclear spin

In the context of NMR spectroscopy, subatomic particles like neutrons and electrons are conceptualized in a manner that resembles intrinsic spins along their respective axes[7]. Several nuclei, including hydrogen (^{1}H) and carbon (^{13}C), possess nuclei with average spins that are non-zero.[8] The ratio of neutrons to protons within the nucleus is a factor in

the phenomenon of nuclear spin.[7] It is important to remember that the spin of a nucleus is determined by the total number of neutrons and protons it contains[9].

When the sum of neutrons and protons is even, the nucleus has zero spin, indicating a lack of intrinsic angular momentum. However, if the sum is odd, the nucleus develops a half-integer spin, expressed as fractions like 1/2 or -1/2, signifying the presence of non-zero angular momentum. In cases where both the numbers of neutrons and protons are odd, the nucleus acquires an integer spin, resulting in values like 0, 1, -1, 2, -2, and so on[7].

When considering the entire spin of a nucleus, denoted as '*I*,' quantum mechanics predicts that a nucleus with a spin value of '*I*' will have potential orientations or energy levels of 2*I* + 1. For instance, a nucleus with a spin of 1/2 has two possible orientations. These orientations have equal energy in the absence of external forces like a magnetic field.[7] However, when a magnetic field is applied, the energy levels separate or split. Each of these split levels corresponds to a particular magnetic quantum number, represented by the letter "m"[8]. Figure 2 shows the energy level change due to the magnetic field for a nucleus with a spin quantum number of 1/2.

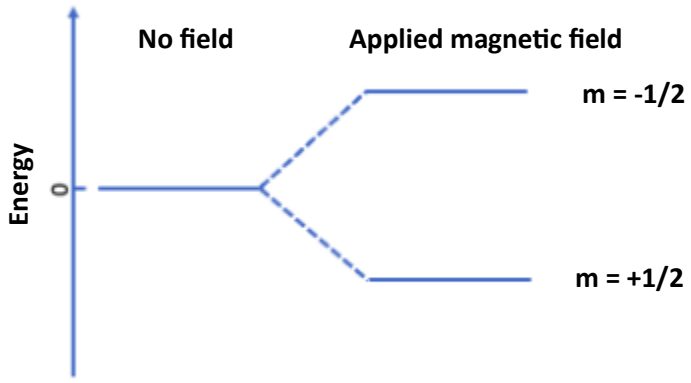

Figure 2. *Splitting of the energy levels for a I = 1/2.*

The initial distributions of energy states are determined by thermodynamics, as seen in the Boltzmann distribution, when a nucleus is exposed to a magnetic field. An important realization is that lower energy levels are more populated than higher ones. To facilitate transitions between these energy states, electromagnetic radiation is employed, with the required photon frequency determined by the energy difference[9].

In summary, understanding the concept of nuclear spin and its relationship to energy levels is essential in the field of NMR spectroscopy. The spin quantum numbers of nuclei, such as 1/2, 1, or 0, play a major role in determining the possible orientations and energy states of these nuclei. When exposed to a magnetic field, these energy levels split, providing useful information for NMR experiments. The Boltzmann distribution emphasizes that lower energy states are more populated, emphasizing the need for electromagnetic radiation to induce transitions between these states. This fundamental knowledge is essential in NMR for interpreting spectra and explaining molecular structures[7-9].

ii. Zeeman interaction

The Zeeman interaction, a fundamental concept in quantum mechanics, describes how an external magnetic field affects the energy levels of a magnetic system[10]. This principle traces its roots back to Pieter Zeeman's late 19th-century observations of spectral line splitting in the presence of a magnetic field[10].

In NMR spectroscopy, the Zeeman interaction assumes paramount importance, offering profound insights into the behaviour of atomic nuclei, particularly those with nuclear spins other than zero, such as hydrogen (^{1}H) and carbon (^{13}C). When these nuclei are exposed

to an external magnetic field (designated as '*B*'), the magnetic moments associated with their nuclear spins align either parallel or antiparallel to this field[11]. The Zeeman interaction can be expressed mathematically as follows:

$$\Delta E = -\mu \cdot B$$

- ΔE represents the energy difference or splitting caused by the Zeeman interaction.
- M (mu) is the magnetic moment of the particle or system.
- B is the external magnetic field.

The Zeeman interaction has implications in NMR spectroscopy. It splits NMR spectral lines into multiple components, commonly referred to as "multiplets" or "split peaks"[12]. In the presence of a magnetic field, each of these split peaks corresponds to a different nuclear spin state. NMR spectra or similar spectra have distinct peaks that are separated in energy, directly correlating with the strength of the applied magnetic field and the magnetic moment of the nucleus under study. A stronger magnetic field affects the magnetic moments of the nuclei, causing them to precess or align at different rates, resulting in a larger gap between the peaks. Simultaneously, the magnetic moment of the nucleus, which is determined by properties such as spin and charge distribution, is essential in determining the energy difference between these states. Fundamentally, the magnetic moment of the nucleus and the strength of the magnetic field are directly proportional to the energy difference between these peaks[11,13].

In conclusion, the fundamental idea of the Zeeman interaction in NMR spectroscopy describes how energy levels split in the presence of an external magnetic field[14]. This

principle enables precise measurement of nuclear spin characteristics and offers profound insights into the structure and behaviour of molecules. Analysing the positions and intensities of these split peaks in an NMR spectrum, one can learn important details about the chemical surroundings and interactions of the nuclei under study. In addition, the understanding of atomic and molecular spectra provided by the Zeeman effect in quantum mechanics provides insights into the composition and characteristics of matter[14].

iii. Larmor frequency

The Larmor frequency, also known as the precessional frequency, plays a crucial role in the field of NMR spectroscopy. As shown in Figure 3, it acts as a fundamental parameter that defines the rate at which a proton's magnetic moment undergoes precession around an axis defined by an external magnetic field (denoted as B_0)[15]. This precessional motion can be metaphorically compared to the rotation of a spinning top around a clearly defined axis.

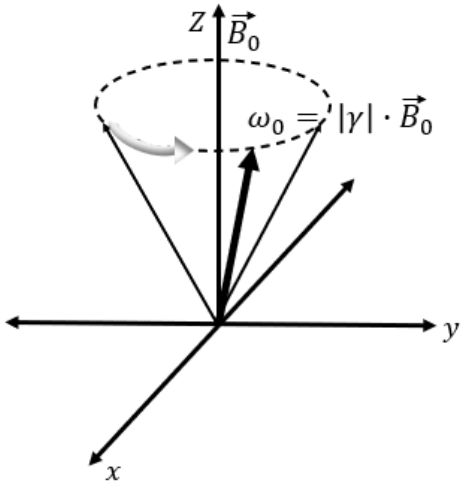

Figure 3. *Larmor frequency. Schematic representation of the precession of the magnetic moment under applied external magnetic field.*

Larmor frequency refers to the precise frequency at which the nuclear magnetic moments within a magnetic field change from their initial orientation—often called "Alpha"—to a particular orientation—often identified as "Beta"[15]. The Larmor frequency shows direct proportionality to the radio frequency required to induce this transition from Alpha to Beta. Consequently, any increase in the Larmor frequency corresponds to an increase in the radio frequency needed to manipulate the nuclear spin as desired[16].

The Larmor frequency can be succinctly stated mathematically as:

$$\boldsymbol{\omega_o = \gamma * B_o}$$

Where:

- ω_0 is the Larmor frequency, typically measure in megahertz (MHz).
- γ is the gyromagnetic ratio, a nuclear-specific constant expressed in megahertz per tesla MHz/T.
- B_0 is the strength of the applied magnetic field, quantified in tesla T.

The fundamental principle of NMR spectroscopy is this relationship between the Larmor frequency and magnetic field strength. This exact relationship enables to selectively probe and reveal the complex properties of atomic nuclei within a wide range of samples. By acting as a beacon of resonance, the Larmor frequency provides precise and in-depth access to a wealth of knowledge regarding molecular structures and dynamic processes[15,16].

b. Solid-state NMR Spectroscopy

The atomic and molecular structure of solid materials can be investigated using solid-state Nuclear Magnetic Resonance (ssNMR) spectroscopy. It is a subset of NMR spectroscopy that is used to study solids. This technique involves applying radiofrequency (RF) pulses and a strong magnetic field to the atom nuclei in a solid sample[18]. The signals that emerge provide information about the interactions and surroundings of these nuclei. As a result, ssNMR, offers an atomic-level approach to determine the molecular structure, 3D configuration, and kinetics of both solid and semi-solid materials[17].

i. Chemical shift and Chemical shift anisotropy

Chemical Shift:

Chemical shift is an important parameter in NMR spectroscopy, representing the resonance frequency of atomic nuclei within solid samples relative to a defined reference standard in a magnetic field[19]. This frequency is highly sensitive to the local chemical environment, making it a vital tool for discerning the structural and chemical characteristics of solids[20].

Solid-state NMR is distinct from solution-state NMR, as it examines materials in their pure, solid form, encompassing a wide range of substances including crystalline solids, nanoparticles, polymers, and inorganic compounds. Chemical shift data in solid-state NMR assists in identifying different chemical environments within the solid lattice, providing insights into atomic arrangements, the presence of specific functional groups, and the level of disorder in crystalline structures[19, 20].

Chemical shift, denoted as δ, is the difference in resonance frequency observed between a nucleus and a reference standard. Tetramethylsilane (TMS) is the typical reference point, set at 0 ppm. This definition is relevant only for ^{1}H and ^{13}C in NMR[21].

The chemical shift (δ) is calculated using the following formula:

$$\delta = \frac{\omega_{obs} - \omega_{ref}}{\omega_{ref}} \cdot 10^{6}$$

Where:

- δ is the chemical shift in ppm.
- ω_{obs} is the observed resonance frequency of the nucleus in the solid sample.
- ω_{ref} is the resonance frequency of the reference standard (TMS) at 0 ppm.

In addition to chemical shift, another significant parameter in NMR spectroscopy is Chemical Shift Anisotropy (CSA). CSA measures variations in the chemical shift due to the orientation of atomic nuclei within a magnetic field, providing insights into molecular orientation in anisotropic environments. This information complements chemical shift data, enhancing our understanding of the structural and chemical properties of solid materials studied via solid-state NMR spectroscopy[22, 23].

ii. Magic angle spinning

Magic Angle Spinning (MAS) is commonly in solid-state NMR spectroscopy for producing high-resolution spectra of solid materials[24]. By adding controlled spinning of the sample (most likely at a frequency of 1 to 130 kHz) at a particular angle known as the "magic angle," denoted as θ_m, MAS effectively addresses the challenges brought on by anisotropic interactions, such as chemical shift anisotropy (CSA) and dipolar coupling[25]. The magic angle, which is set at 54.7 degrees (π/3 radians), ensures that these anisotropic interactions average out to zero over time, resulting in optimized and highly accurate NMR spectra. You can visualize the MAS process in Figure 4, where the sample, shown in blue, rapidly spins inside the main magnetic field (B_0), with the rotation axis inclined at the magic angle θ_m.

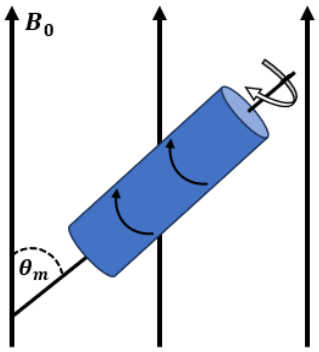

Figure 4. *Magic-angle spinning (MAS) at π/3 radians.*

Furthermore, in solid-state NMR, two primary interactions, CSA and dipolar coupling, often lead to line broadening. These interactions depend on the orientation of the sample and can be partially averaged by MAS.

1. The nuclear dipolar interaction in solid-state NMR spectroscopy is described by the following expression, which depends on the main magnetic field (B_0) and the angle (θ) between the internal nuclear axis and the magnetic field[25]:

$$D(\theta) = \frac{\mu_0}{4\pi} \cdot \gamma^2 \hbar^2 \cdot \frac{3\cos^2(\theta) - 1}{r^3}$$

Where:

- $D(\theta)$ is the dipolar coupling constant as a function of θ
- μ_0 is the permeability of free space.
- γ is the gyromagnetic ratio of the nucleus.
- $\hbar$ is the reduced Planck's constant.
- r is the distance between the interacting nuclei.

Notably, the term $3\cos^2(\theta) - 1$ becomes zero at the magic angle (θ_m), resulting in a significant reduction of the dipolar interaction compared to other angles[26]. The magic angle spinning technique is used to enhance the resolution of solid-state NMR spectra by minimizing the dipolar interaction. However, in cases of imperfect spinning or the presence of additional anisotropic interactions, some residual dipolar coupling may still be observed[26].

2. In solid-state NMR spectroscopy, the chemical shift anisotropy (CSA) quantifies how the chemical shift varies with orientation[26]. Nuclei within a solid sample exhibit orientation-dependent NMR resonances when subjected to an external magnetic field due to the CSA interaction.

This orientation-dependent CSA interaction results in a broad and complex NMR spectrum without Magic Angle Spinning (MAS) due to the distribution of molecular orientations within the sample[27]. However, spinning the sample at the “magic angle” with respect to the magnetic field smears out the powder pattern, averaging the effects of the CSA interaction.

The outcome is a simplified NMR spectrum characterized by a single resonance peak representing the chemical shift of the isotropic state. This peak, in addition to offering a more straightforward and interpretable spectrum, represents the 'center of mass' of the powder pattern[27].

In conclusion, Magic Angle Spinning (MAS) is an essential tool in NMR spectroscopy, particularly when working with solid samples. By precisely rotating the sample at the "magic angle" with respect to the magnetic field, it effectively reduces the negative effects of anisotropic interactions. As a result, high-resolution NMR spectra are obtained, providing valuable insight into the atomic-level motions and structures present in solid materials, ranging from crystalline materials to complex biomolecules[26, 27].

iii. Cross Polarization

NMR spectroscopy employs cross polarization (CP) method, a technique primarily used in solid-state NMR experiments. CP improves the signal-to-noise ratio and facilitates magnetization transfer from abundant nuclei (like protons, ^{1}H) to less abundant nuclei of interest (like ^{13}C, ^{15}N, or ^{31}P), thereby enabling the detection off signals from rare spins[28].

The CP process is governed by the Hartmann-Hahn condition, represented by the equation[29]:

$$\gamma_H B_1(^1\mathrm{H}) = \gamma x\, B_1(X) \pm n\omega_R$$

Where,

- γ_H, The gyromagnetic ratio of hydrogen nuclei (^{1}H).
- $B_1(^1\mathrm{H})$, The RF field strength applied to hydrogen nuclei.
- γ_X, The gyromagnetic ratio of the rare nucleus (X), which can be ^{13}C, ^{15}N, or ^{31}P, for example.
- $B_1(X)$, The RF field strength applied to the rare nucleus (X).
- n, integer value, often representing the rotor frequency in magic angle spinning (MAS) experiments.
- ω_R, The spinning rate (angular frequency) in radians per second.

CP improves the magnetization of the rare nuclei, such as ^{13}C, through two key mechanisms. Firstly, it facilitates the transfer of polarization from abundant nuclei (like ^{1}H spins) to the less abundant nuclei (specifically ^{13}C). As a result, it improves NMR sensitivity, which is directly proportional to the gyromagnetic ratio (γ_{1H}/γ_{13C})[30]. The gyromagnetic ratio is a key factor in determining the resonance frequency at which a nucleus absorbs electromagnetic radiation during nuclear magnetic resonance experiments[30]. Secondly, CP leverages the faster longitudinal spin relaxation (T_1) of ^{1}H nuclei, allowing for shorter recycle delays in NMR experiments and enabling efficient signal averaging[30].

In the CP method, two contact pulses are simultaneously applied to two pools of spins: one is the abundant (^{1}H, referred to “S”) and the other is the less abundant (^{13}C, ^{15}N or ^{31}P, referred to “I”), as shown in Figure 5 below. The process begins with transverse magnetization in the S-spin pool, synchronized with a spinlock pulse. This leads to polarization transfer from the S-spin pool to the I-spin pool. The effectiveness of the transfer depends on the amplitude of the second contact pulse, known as the 'Hartman Hahn pulse,' meeting the Hartman Hahn condition[29]. To initiate transverse magnetization in the I-spin pool, a 90° pulse precedes the I-spin contact pulse, 90° out of phase with the spinlock pulse used for the S-spin pool[28]. This pulse enhances the CP process effectiveness by bringing the I-spin pool's magnetization in phase. The transfer of polarization from the abundant S-spin pool (composed of nuclei like protons, ^{1}H) to the rare nuclei in the I-spin pool (such as, ^{13}C, ^{15}N or ^{31}P) is an important process that significantly enhances the sensitivity of NMR experiments[28]. It allows the observation and analysis of signals from nuclei with lower natural abundance, which would be challenging to detect directly[31].

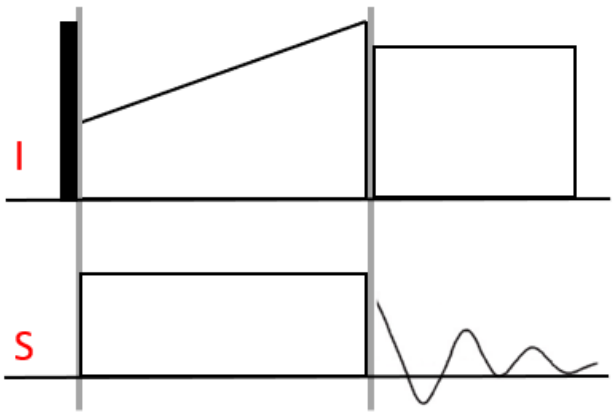

Figure 5. *Display of a basic cross polarization experiment.*

iv. Spin-Spin coupling

In the field of NMR spectroscopy, spin-spin coupling, also known as J-coupling or scalar coupling, is a fundamental phenomenon arising from the magnetic properties of atomic nuclei, specifically their intrinsic angular momentum or spin. Spin-spin coupling plays an important role in determining the structure and connectivity of atoms within molecules, as it results in distinctive spectral patterns in NMR spectroscopy[32]. These patterns reveal important information about the local environment, conformation, and connectivity of atoms in a molecule, making this concept fundamental in modern analytical chemistry and structural biology, aiding in the understanding of complex molecular structures, chemical reactions, and molecular dynamics[32].

Theoretical Foundation:

A basic understanding of quantum mechanics is necessary to understand the essence of spin-spin coupling. Nuclear spins are quantized intrinsic angular momentum, subject to the Pauli exclusion principle, which prohibits multiple fermions (e.g., protons) from occupying the same quantum state at the same time[32].

Spin-spin coupling, typically involving protons in organic molecules, results from the magnetic dipole-to-dipole interactions between nuclei. It is explained by the spin Hamiltonian, which includes the Zeeman effect (which accounts for nuclear energy levels in a magnetic field), the chemical shift (which reflects resonance frequency variations caused by the local electronic environment), and the J-coupling interaction[33]. The J-coupling interaction is characterized by the coupling constant (J) and the angular momentum operators[34], which are written as:

$$\widehat{H}_J = -2\pi J h I_1 \cdot I_2$$

Where,

- $\widehat{H}_J$, is the J-coupling Hamiltonian.
- J, is the coupling constant.
- h, is the reduced Planck constant.
- $I_1 \cdot I_2$, represent nuclear spin operators of the interacting nuclei.

Significantly, the magnitude/strength of *J* determines whether J-coupling appears as first-order or second order coupling[34]. Strong J-coupling produces distinct multiplets, whereas weak coupling produces complicated coupling patterns. Identifying the nature of coupling and the value of *J* is essential for the accurate interpretation of NMR spectra and the determination of molecular structure[34].

Spin-spin coupling in Crystal Engineering:

In crystal engineering, understanding the concept of spin-spin coupling is vital for comprehending the electronic and magnetic properties of crystalline materials. In NMR spectroscopy, spin-spin coupling, results from the interaction of magnetic moments between adjacent nuclei within a crystal lattice[32].

Spin-spin coupling has a variety of applications in the field of crystal engineering[33]. It clarifies the molecular configurations inside crystal lattices, which is essential for creating and managing crystalline materials with specific characteristics. This phenomenon provides valuable information about intermolecular interactions, aids in the identification and differentiation of polymorphs. Such data is particularly important for revealing

information on the non-covalent interactions that bind crystals together and can be used to predict and design crystal structures that are specific to the user's needs[33].

In summary, J-coupling provides valuable information about the connectivity and spatial arrangement of atoms in a crystal, providing a window into the three-dimensional structure of molecules within a solid-state matrix. By measuring the strength and sign of these coupling constants, one can learn about the relative orientations of neighbouring nuclei, assisting in the mapping of the complex network of intermolecular interactions in crystalline materials[33].

c. X-ray Diffraction

Understanding the atomic and molecular structure of crystalline materials is crucially dependent on X-ray diffraction, an important component of crystallography. When interacting with the periodic arrangement of atoms within a crystal lattice, it operates on the theory of X-ray wave interference[35].

Historical development

In the early 20th century, Max von Laue's groundbreaking experiments revealed the wave-like nature of X-rays, marking a turning point in both physics and crystallography[35]. Von Laue's work demonstrated that X-rays exhibit diffraction when they interact with the periodic arrangement of atoms within a crystal lattice. He achieved this by exposing a crystalline substance to X-rays and capturing the resulting diffraction pattern on a photographic plate positioned behind the crystal[35]. The pattern that results looks similar to the ripple pattern produced when stones are thrown into water[35]. This discovery indicated that X-rays were interacting with the atomic lattice of the crystal, leading to

constructive and destructive interference. Hence, Von Laue's discovery of X-rays led to the study of the atomic structure in crystalline materials[35].

Following Max von Laue's work, Lawrence Bragg and his father, William Henry Bragg, made important contributions to X-ray crystallography. The duo established the relationship between the angle of diffraction (θ), the X-ray wavelength (λ), and the interatomic lattice spacing within a crystal (d), which is known as Bragg's Law, equation shown below. This equation made it possible to determine the atomic structure of crystalline materials and provided the mathematical framework for comprehending the diffraction patterns that X-rays cause in crystals[37].

$$2dsin(\theta) = m\lambda$$

Where,

- θ, is the angle at which the X-rays are diffracted.
- λ, is the wavelength of the X-rays.
- d, represents the interatomic spacing.
- m, is an integer representing the order of diffraction.

To understand the diffraction patterns seen in X-ray crystallography, one must understand this equation.

This equation, on the other hand, is applicable not only to single crystalline materials but also to powdered or polycrystalline crystalline materials. The diffraction pattern of such a material reveals information about the crystal structure in terms of interatomic spacings (d-spacings), but not how the atoms are arranged within individual unit cells[35].

Basic Principles

X-ray diffraction relies on the interaction of X-rays with the ordered atomic arrangement in a crystal lattice[35]. This interaction produces the distinctive diffraction pattern. As X-rays pass through the crystal, they come into contact with the electron clouds that surround each atom. X-rays interact with electrons in the crystal, leading to constructive scattering when X-ray waves align in phase, resulting in a stronger signal and better resolution[35]. On the other hand, when X-ray waves are out of phase, they cause destructive scattering, weakening the signal and diminishing resolution[35, 36].

In addition to Bragg's Law, atomic form factors and structure factors both play a major part in determining an X-ray peak's intensity:

Atomic form factors: They are connected to how electrons are distributed among the various atoms. The variation in scattering power among various crystallographic elements is explained by these form factors. A specific element's atomic form factor depends on the scattering angle[37].

Structure factors: Structural factors account for the periodicity of the crystal lattice and contain essential structural information[38]. Mathematically, a diffracted X-ray peak's intensity (*I*) is proportional to the square of the structure factor's magnitude (F(θ)), written as[38]:

$$I(\theta) \propto |F(\theta)|^2$$

This equation is essential for learning more about the electron density distribution, solving the phase problem, determining atomic positions within the crystal, and confirming the accuracy of structural models by comparing calculated and observed diffraction

patterns[35]. X-ray diffraction has many applications in chemistry, biology, materials science, and crystallography for understanding the atomic and molecular world.

Data Interpretation

Information obtained for a single crystal: When X-rays interact with a crystalline lattice, they produce a diffraction pattern, consisting of bright spots on a detector. The positions and intensities of these spots act as a kind of code that reveals the crystal's structure[39]. This information is extracted using Bragg's Law, connecting X-ray wavelength (λ) and interplanar spacing (d) to the diffraction angles (θ)[39]. These spacings allow us to determine the lattice parameters, establishing an outline for the crystal's structure determination. Additionally, each diffraction peak's strength is correlated with the crystal's electron density. This intensity is inversely proportional to the square of the structure factor $|F(hkl)|^2$, which provides crucial information about the distribution of atoms and electrons. We can reveal its crystal's atomic structure by comprehending these components[39].

Data analysis of a single crystal: The first step in data analysis is peak indexing. Each diffraction peak is given a Miller index (hkl), which links them to particular crystallographic planes inside the crystal's unit cell[38]. We can navigate the crystal's internal structure using this method. The dimensions and angles of the unit cell of the crystal are of the utmost importance for understanding the crystal's overall structure. This data includes the lengths (a, b, c) of its edges as well as the angles (α, β, γ) between them[39]. The symmetry of the diffraction spot pattern helps characterize the crystal's space group, which is necessary for determining its overall symmetry. In addition, the observed intensities and existing crystallographic data are used to calculate the structure factors $|F(hkl)|$, which help to

describe the distribution of electrons within the crystal. However, the phase problem must be resolved in order to determine the electron density inside the unit cell. To avoid this problem, techniques such as direct methods, Patterson methods, and Fourier transforms are used to make educated assumptions about these phases, allowing us to figure out the electron distribution in the crystal's unit cell[39, 40]. This information is used to construct an electron density map, guiding the placement of atoms in the crystal. This phase is vital for building a preliminary atomic structure model[38, 39].

Data analysis of a powder sample*:* For a powder compound, deciphering X-ray diffraction (XRD) data requires a methodical approach to reveal the crystal structure and determine the phases present in the sample. The powdered material is first subjected to X-rays to gather XRD data, which produces a diffraction pattern of peaks on the graph. These peaks give us important insights into the sample's structure because they are correlated to crystallographic planes (hkl)[43]. The following steps involve indexing the peaks to determine their Miller indices, which show the presence of phases. To properly understand the dimensions and shape of the crystal, unit cell parameters (a, b, c α, β, γ) are then determined[43]. For complex cases, structural refinement techniques can be used if necessary to solve the atomic structure. Diffraction peak intensities are compared to determine phase proportions. Comparing observed and calculated diffraction patterns is a crucial validation step. This methodical approach ensures accurate insights into the crystal structure and phase composition of powdered materials. Thus, data interpretation in X-ray crystallography is a systematic and essential process that unveils the hidden structures and compositions of crystalline materials[43].

References Chapter 2

1. Abraham, R. J., Fisher, J., & Loftus, P. (1988). Introduction to NMR spectroscopy (Vol. 2). New York: Wiley.
2. Freire, F. (2012). The integrated study by NMR and X-ray Crystallography on the analysis of the molecular interactions in heme-binding proteins.
3. Wong, N. C., Kintzer, E. S., Mlynek, J., DeVoe, R. G., & Brewer, R. G. (1983). Raman heterodyne detection of nuclear magnetic resonance. Physical Review B, 28(9), 4993.
4. Korzhnev, D. M., & Kay, L. E. (2008). Probing invisible, low-populated states of protein molecules by relaxation dispersion NMR spectroscopy: an application to protein folding. Accounts of Chemical Research, 41(3), 442-451.
5. Rashid, M., Singh, S. K., & Singh, C. (2021). Nuclear Magnetic Resonance Spectroscopy: Theory and Applications. In Modern Techniques of Spectroscopy (pp. 469-512).
6. Cavanagh, J., Fairbrother, W. J., Palmer, A. G., & Rance, M. (2007). Protein NMR spectroscopy: principles and practice (2nd ed.). Academic Press.
7. Akitt, J. W., & Mann, B. E. (2017). NMR and Chemistry: An introduction to modern NMR spectroscopy. CRC Press.
8. Levitt, M. H. (2013). Spin dynamics: basics of nuclear magnetic resonance. John Wiley & Sons.
9. Callaghan, P. T. (2011). Translational dynamics and magnetic resonance: principles of pulsed gradient spin echo NMR. Oxford University Press.
10. Bovey, F. A., Mirau, P. A., & Gutowsky, H. S. (1988). Nuclear magnetic resonance spectroscopy. Elsevier.
11. Dybowski, C. (2006). Zeeman Interaction in Nuclear Magnetic Resonance. Encyclopedia of Analytical Chemistry: Applications, Theory, and Instrumentation
12. Kaseman, D. (1994). NMR Interactions. CRC Press.
13. Woelk, K., & Blumen, A. (1994). Nuclear Magnetic Resonance: Concepts and Methods. John Wiley & Sons.
14. Sanders, J. K. M., & Hunter, B. K. (1987). Modern NMR Spectroscopy: A Guide for Chemists. Oxford University Press.

15. Woodman, K. F., Franks, P. W., & Richards, M. D. (1987). The nuclear magnetic resonance gyroscope: a review. The Journal of Navigation, 40(3), 366- 384. (28)
16. De Graaf, R. A. (2019). In vivo NMR spectroscopy: principles and techniques. John Wiley & Sons.
17. Reif, B., Ashbrook, S. E., Emsley, L., & Hong, M. (2021). Solid-state NMR spectroscopy. Nature Reviews Methods Primers, 1(1), 1-23.
18. Andronesi, O. C., Mintzopoulos, D., Struppe, J., Black, P. M., & Tzika, A. A. (2008). Solid-state NMR adiabatic TOBSY sequences provide enhanced sensitivity for multidimensional high-resolution magic-angle-spinning 1H MR spectroscopy. Journal of Magnetic Resonance, 193(2), 251-258.
19. Rangus, M. (2007). NMR spectroscopy in solids: A comparison to NMR spectroscopy in liquids. Physical Methods on Biological Membranes and their Model Systems, Springer.
20. Jacobsen, N. E. (1996). NMR Spectroscopy Explained: Simplified Theory, Applications and Examples for Organic Chemistry and Structural Biology. Wiley.
21. Canet, D., & Merbach, A. E. (2002). Introduction to Magnetic Resonance with Applications to Chemistry and Chemical Physics. Wiley.
22. Stroh, A. N. (1958). Dislocations and cracks in anisotropic elasticity. Philosophical magazine, 3(30), 625-646.
23. Claridge, T. D. W. (2009). High-Resolution NMR Techniques in Organic Chemistry. Elsevier.
24. Zhang, R., Mroue, K. H., & Ramamoorthy, A. (2017). Proton-based ultrafast magic-angle spinning solid-state NMR spectroscopy. Accounts of chemical research, 50(4), 1105-1113.
25. Duer, M. J. (2002). Solid State NMR Spectroscopy: Principles and Applications. Wiley.
26. Parthasarathy, S. (2013). Solid-State Nuclear Magnetic Resonance of Copper-Amyloid Beta, Amylospheroids, Fast Magic Angle Spinning (Doctoral dissertation, the University of Illinois at Chicago).

27. Schanda, P., & Ernst, M. (2016). Studying dynamics by magic-angle spinning solid-state NMR spectroscopy: Principles and applications to biomolecules. Progress in nuclear magnetic resonance spectroscopy, 96, 1-46.
28. Pines, A., & Gibby, M. G. (1973). Waugh, JS. J. Chem. Phys., 1973, 59-569.
29. Hartmann, S. R., & Hahn, E. L. (1962). Nuclear double resonance in the rotating frame. Physical Review, 128(5), 2042-2053.
30. Ernst, R. R., Bodenhausen, G., & Wokaun, A. (1987). Principles of Nuclear Magnetic Resonance in One and Two Dimensions. Springer.
31. Rudakov, T. N. (2017). Magnetic resonance: NQR technique and instruments.
32. Sychrovský, V., Gräfenstein, J., & Cremer, D. (2000). Nuclear magnetic resonance spin–spin coupling constants from coupled perturbed density functional theory. The Journal of Chemical Physics, 113(9), 3530-3547.
33. Freeman, R., & Hill, H. D. W. (1971). High-Resolution Study of NMR Spin Echoes:“J Spectra”. The Journal of Chemical Physics, 54(1), 301-313.
34. Diehl, B. (2008). Principles in NMR spectroscopy. In NMR Spectroscopy in Pharmaceutical Analysis (pp. 1-41). Elsevier.
35. Cullity, B. D., & Stock, S. R. (2001). Elements of X-Ray Diffraction, Third Edition. Prentice Hall.
36. Hyung, N., Kim, J. J., & Lee, J. W. (2000). An NMR Study on Internal Rotation of CH3 Group in 1,1,1-Trichloroethane. Journal of the Korean Magnetic Resonance Society, 4(1), 29-40
37. Taylor, W. C. (1999). X-Ray Diffraction. Dover Science Publications.
38. Sands, D. E. (1993). Introduction to Crystallography. Dover Publications.
39. Ladd, M. F. C., & Palmer, R. A. (2013). Structure determination by X-ray Crystallography. Springer.
40. van Smaalen, S. (2007). Incommensurate Crystallography. OUP Oxford.

Chapter 3. Synthetic experimental

a. Techniques and Instrumentation

This section outlines different instrumentation employed in this research, specifically focusing on ball milling and Resonant Acoustic Mixing (RAM). The explanation of NMR and X-ray instruments was omitted because they had been addressed in the previous chapter.

i. Ball mill

Ball milling is a method frequently used in crystal engineering for the synthesis and modification of crystalline materials. A ball mill is used to efficiently reduce particle size and regulate the crystal structure of materials. It is a type of grinding machine that consists of a rotating cylindrical container that contains grinding media such as stainless balls. This section discusses the importance of ball milling in crystal engineering and the various types of ball milling techniques that are used[1].

Importance of Ball Milling in Crystal Engineering:

Ball milling is essential in crystal engineering because it allows for the manipulation of crystal structures, the induction of polymorphism, and the formation of co-crystals[2]. To achieve the desired crystal properties, milling parameters such as milling time, speed (Hz), and powder ratio must be precisely controlled. This precision is critical for tailoring the properties of crystalline materials to meet specific functional requirements in a wide range of applications[3]. Furthermore, ball milling also enables precise control of particle size, morphology, and surface area, all of which have an impact on the crystallization

process. By reducing the particle size of the starting materials through ball milling, it becomes possible to obtain finer crystals with increased surface area, leading to improved solubility, dissolution rates, and bioavailability. Additionally, ball milling facilitates the formation of metastable phases and amorphous materials, which can serve as precursors for the growth of desired crystalline forms[4].

Mechanochemical Ball Milling:

Mechanochemical ball milling drives chemical reactions between solid-state reactants through mechanical forces and collisions. It promotes the formation of co-crystals, solid solutions, and hybrid materials. This approach proves valuable for crystal engineering as it enables the synthesis of complex materials through green and efficient processes[5].

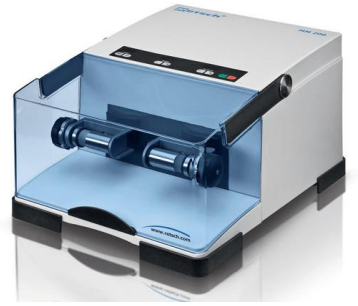

Figure 1.
Mechanochemistry ball mill apparatus[14].

In conclusion, ball milling is important in crystal engineering because of its ability to control crystal structures, promote polymorphism, and facilitate co-crystal formation. It provides a versatile platform for synthesizing and modifying crystalline materials with tailored properties for specific applications in pharmaceuticals, materials science, and chemical engineering[2].

ii. RAM

RAM (Resonant Acoustic Mixing) is a novel technique used in crystal engineering for efficient and homogeneous material mixing. It entails the use of high-frequency acoustic waves to induce resonant motion in a sample, resulting in improved particle mixing and blending. RAM has grown in importance in a variety of fields, including crystal engineering, due to its ability to improve crystal growth quality and uniformity while also optimizing material properties[6]. This section will discuss the significance of RAM in crystal engineering, look at different types of RAM techniques, analyse their applications, and emphasize the importance of RAM in crystal engineering processes.

Importance of RAM in Crystal Engineering:

RAM plays a crucial role in crystal engineering as it enables efficient mixing and homogenization of precursor materials, resulting in improved crystal quality and properties[9]. In crystal growth processes, the even distribution of reactants and precursors is essential for obtaining crystals with desired characteristics such as size, shape, and purity. RAM facilitates the dispersion of particles and promotes their interaction, enhancing the chances of nucleation and the growth of high-quality crystals. The successful implementation of RAM significantly benefits crystal engineering, which involves the design and synthesis of materials with specific crystal structures and properties for various applications, because it enables better control over crystal growth, polymorphism, and crystallographic orientations[7]. By ensuring thorough mixing of components, RAM contributes to the uniformity and reproducibility of crystal structures, ultimately enhancing the ability to tailor materials with desired properties.

Different Types of RAM Techniques:

Several types of RAM techniques are employed in crystal engineering, each offering unique advantages for specific applications. A most common RAM apparatus can be seen on Figure 2 below.

Figure 2. *Resodyn Acoustic Mixer*[15].

However, here are some commonly used types of RAM techniques:

Ultrasonic Resonant Acoustic Mixing:

Ultrasonic RAM uses high-frequency ultrasonic waves to induce resonant motion in the sample. The oscillating waves cause pressure differentials, which cause intense acoustic streaming and promote material mixing. Ultrasonic RAM is useful for dispersing nanoparticles, blending complex formulations, and facilitating the synthesis of uniform crystalline structures[8].

Piezoelectric Resonant Acoustic Mixing:

Piezoelectric RAM utilizes piezoelectric transducers to generate high-frequency vibrations in the sample. The transducers convert electrical energy into mechanical vibrations, resulting in resonant mixing and agitation. This technique is particularly useful for achieving homogeneous mixing of powders, slurries, and viscous materials[6].

Rotary Resonant Acoustic Mixing:

Rotary RAM involves the use of a rotating container or vessel to induce resonant motion in the sample. The combined rotation of the container and the application of acoustic energy led to efficient mixing and blending of materials[7]. This technique is especially well-suited for large-scale mixing applications, such as industrial crystal synthesis and pharmaceutical formulation.

In conclusion, Resonant Acoustic Mixing (RAM) holds significant importance in crystal engineering due to its capability to improve mixing efficiency, uniformity, and control over crystal growth processes. RAM techniques, such as ultrasonic, piezoelectric, and rotary mixing, offer unique advantages for specific applications in crystal engineering[8]. By enabling efficient mixing of precursor materials, RAM contributes to the uniformity and reproducibility of crystal structures, thus facilitating the design and synthesis of materials with tailored properties.

b. Typical Procedures

i. RAM

Resonant Acoustic Mixing (RAM) is a technique used in crystal engineering to promote crystallization and enhance the crystal quality. It involves applying mechanical vibrations to a solution containing the solute to facilitate the nucleation and growth of crystals. The typical procedure of Resonant Acoustic Mixing (RAM) involves the following steps[6]:

1. **Preparation of Sample**: Initiate the process by preparing the starting materials within a vial. Optionally, a tiny amount of solvent can be introduced. Note that while a solvent is not always required, it can aid in the crystallization process.
2. **Placement of Sample**: Place the container or vial containing the mixture of compounds within the RAM apparatus. The RAM apparatus is equipped with a resonant acoustic device capable of generating mechanical vibrations at specific frequencies. Activate the RAM apparatus to produce acoustic resonance inside the mixing vessel. Acoustic streaming, a phenomenon that occurs when high-frequency sound waves interact, is how RAM systems create mixing.
3. **Control of Parameters**: Adjust the frequency and intensity of mechanical vibrations based on the properties of the compound. The objective is to create optimal conditions for crystal growth. The intensity of frequencies can vary from sample to sample and may be categorized as low, medium, or high. It's important to note that the best settings are often determined through trial and error.
4. **Observation and Monitoring**: Visually monitor the crystallization/mixing process or by using techniques such as microscopy, PXRD, SCXRD or melting points analysis. Keep an eye out for the formation and growth of crystals.

5. **Sample Process**: Continue the resonant acoustic mixing process until the desired level of homogeneity is achieved or until crystals are formed.
6. **Isolation of Crystals/Powder**: Isolate the crystals or powder from the container or vial. Wet crystals can be separated using techniques such as filtration or centrifugation, while powder can be carefully removed using a spatula.
7. **Crystals Characterization**: Following isolation, characterize the crystals to ensure they possess the desired properties and meet quality standards. Techniques like PXRD or SCXRD can be used to characterize crystals.

ii. Slow Evaporation

When growing high-quality crystals, slow evaporation and reflux are frequently used techniques. The typical steps for both techniques are listed below[8, 10]:

Slow Evaporation:

Procedure:

1. **Prepare Solvent:** Choose an appropriate solvent for your crystal and consider its compatibility with the compound and its purity. Ensure it dissolves the compound at the desired temperature.
2. **Dissolution (OPTIONAL**): Add the desired compound to the selected solvent. Gently warm the mixture using a hot plate to enhance solubility. Stir to ensure complete dissolution.
3. **Setup:** Select a dry, spotless container for the crystal growth. Glass beakers or vials are common choices. Make sure there are no contaminants in the container.

4. **Placement**: Gradually pour the prepared solution into the chosen container. Cover the container with aluminium foil, leaving a small hole on top to minimize contamination and allow slow evaporation. Place it in a controlled environment with stable temperature conditions to prevent dust and impurities (e.g., fume hood).
5. **Crystal Growth**: Allow the solvent to slowly evaporate over a period of days or weeks. The gradual process facilitates crystal formation. Avoid disturbances during this phase.
6. **Monitor**: Periodically check the crystallization process to ensure the desired crystal growth is occurring.
7. **Harvesting**: Once the crystals are fully formed, carefully remove them from the solution using a glass rod or a clean spatula. To dry, spread the crystals on a piece of weighing paper. However, if no solution remains, proceed to step #9.
8. **Storage**: Transfer the harvested crystals from step #7 to a clean, dry container, cover it with aluminium foil to prevent contamination, and label it with the date and the compound's name.
9. **Storage**: Ensure that the container is sealed with aluminium foil to protect against dust and impurities. Label the container with the date and compound name.
10. **Analysis**: Characterize the crystals using Single-Crystal X-ray Diffraction (SXRD) to confirm their desired characteristics and adherence to quality standards.

iii. Ball Milling

Ball milling is a critical mechanical technique used in crystal engineering for both synthesis and modification of crystalline materials. Below is a typical procedure for ball milling[11]:

Typical Procedure for Ball Milling:

1. **Sample Preparation**: Start by preparing the materials to be used for ball milling. These materials can include crystalline solids, amorphous substances, or a combination of different compounds. Ensure that the sample is accurately weighed and proportionally distributed for the intended experiment.
2. **Loading the Ball Mill**: Add the prepared sample to the open ball mill container, often a ball mill jar or a similar vessel. Include the grinding media, typically stainless-steel beads, to facilitate the milling process. Safely seal and secure the ball mill container to prevent spills during milling.
3. **Mill Operation:** Place the ball mill jar in the apparatus and start the ball mill machine to initiate the grinding process. Adjust the milling time and speed (measured in Hz) based on the material and the desired outcome.
4. **Monitoring the Process**: Continuously monitor the milling procedure by periodically assessing changes in sample particle size or other relevant characteristics. Adjust milling parameters if needed to maintain control over the process.
5. **Post-Milling Treatment (Optional)**: Stop the ball mill and unseal the container once the desired milling time has been achieved. Consider subjecting the milled

material to subsequent treatments, such as annealing, to induce crystallization or facilitate specific reactions, depending on your research objectives.

6. **Sample Collection and Analysis**: Remove the milled sample from the container and conduct comprehensive tests to identify the resulting cocrystal or powder. This may involve research-specific methods, such as microscopy, melting point analysis, and X-ray diffraction (XRD).

iv. Typical NMR Setup

In crystal engineering, NMR spectroscopy is a powerful analytical technique used to study the structure, dynamics, and interactions of molecules in crystalline materials. Below is a typical NMR setup used for crystal engineering studies[12]:

Typical NMR Setup:

1. **NMR Spectrometer:** The central component of the NMR setup is the NMR spectrometer, which generates a strong magnetic field and radiofrequency pulses to manipulate nuclear spins in the sample.
2. **Sample Preparation:** Prepare the finely ground crystalline sample meticulously for NMR analysis, emphasizing the importance of accuracy and reliability in your measurements. Verify that you have an ample quantity of sample available for the NMR tube. Ensure that the rotor is securely sealed with its cap, being mindful not to angle it in such a way that it doesn't close properly. If there's a gap between the rotor and the cap, it may indicate an excess of sample, and some should be removed. Lastly, use a black Sharpie to mark the base of the rotor, allowing the tachometer to accurately monitor its spinning speed.

3. **NMR Probe**: The rotor is introduced into the probe which is a component of the NMR spectrometer that holds the sample tube and enables accurate positioning of the sample within the magnetic field. Additionally, it includes the radiofrequency coil needed to send and receive NMR signals.
4. **Spinning**: Initiate the spinning of the sample, often through an automatic program that allows you to select the spinning speed.
5. **Setting the Spectrometer:** It is crucial to confirm that all the hardware is configured once the sample has started spinning. The first step is to choose the probe you're using. To do this, type "edhead" into the search box. This displays a list of all the available probes. Choose the one into which your sample is already inserted. After choosing this, the screen will display the hardware configuration in use as well as the nucleus you will be probing. If this is incorrect, choose the nucleus that interests you. Additionally, you will be able to determine what frequency this nucleus resonates at.
6. **Tuning Probe:** To probe the transitions, the probe must be tuned to the appropriate frequency range. Furthermore, the RF circuit must match impedance with the spectrometer, which is referred to as matching. When everything is calibrated and set up, you may start the experiment by typing “zg”
7. **Pulse Sequence and Data Acquisition**: Specific pulse sequences are applied to the sample to obtain NMR spectra, and the NMR signals emitted by the nuclei are recorded during data acquisition.

8. **Data Analysis Software**: Specialised software is used to process and analyse the NMR data collected during the experiments, enabling peak assignment and spectral interpretation.

v. Typical X-ray Setup

In crystal engineering, X-ray diffraction (XRD) is an essential technique used to study the atomic and molecular structure of crystalline materials. There are two primary types of X-ray diffraction setups used for crystal engineering: Powder X-ray diffraction (PXRD) and Single-Crystal X-ray diffraction (SCXRD). Below are the typical setups for both techniques[13]:

Typical X-ray Setup for Powder X-ray Diffraction (PXRD):

1. **X-ray Source:** The PXRD setup includes an X-ray source that emits X-ray radiation. Common sources are copper (Cu) or cobalt (Co) anodes, producing X-rays at specific wavelengths.
2. **X-ray Diffractometer**: A goniometer holds the sample, allowing it to rotate while data is collected. Depending on the experiment's requirements, the diffractometer can have a Bragg-Brentano or Debye-Scherrer configuration.
3. **Sample Preparation**: The sample is finely ground to ensure random crystallite orientation and packed into a sample holder, like a zero-background sample holder.
4. **X-ray Detection**: The X-ray beam interacts with the powdered sample, generating diffraction patterns from multiple crystallites with various orientations. A detector, often a solid-state detector, collects the diffracted X-rays.

5. **Data Collection**: The sample is rotated on the goniometer while collecting diffraction data at different angles (2θ). Continuous scan mode is typically used to collect the data.
6. **Data Analysis Software**: Specialized software processes the collected diffraction data, facilitating crystal structure identification through peak indexing and refinement.

Typical X-ray Setup for Single-Crystal X-ray Diffraction (SCXRD):

1. **X-ray Source**: The SCXRD setup features a focused X-ray source, typically using molybdenum (Mo) or copper (Cu) X-ray tubes. These sources produce monochromatic X-rays with specific wavelengths.
2. **X-ray Optics**: X-ray optics, such as monochromators, further focus and filter the X-ray beam, ensuring it's monochromatic and properly collimated. This step enhances the quality of the diffraction pattern.
3. **Sample Preparation**: SCXRD requires a single crystal of high quality, well-shaped, and of an appropriate size for precise diffraction data. The crystal is carefully aligned on a sample holder or goniometer head.
4. **X-ray Detection**: An X-ray detector, often employing area detectors (e.g., CCD or CMOS detectors) or multiwire proportional counters, records the diffraction data as diffracted X-rays interact with it.
5. **Data Collection**: The goniometer rotates and tilts the crystal to collect diffraction data from various crystallographic planes. Step-scan mode ensures precise measurement of individual reflections.

6. **Data Analysis Software**: Specialized software processes the raw diffraction data by indexing diffraction spots, fine-tuning crystal parameters, and solving the crystal structure using mathematical algorithms. Common software includes CRYSTALS, SHELX, or OLEX2.
7. **Structure Visualization and Refinement:** Additional software may be used for further refinement of the crystal structure. Visualization software like PyMOL or Mercury renders and examines the three-dimensional atomic structure.

References Chapter 3.

1. Yadav, T. P., Yadav, R. M., & Singh, D. P. (2012). Mechanical Milling: A Top Down Approach for the Synthesis of Nanomaterials and Nanocomposites. Nanoscience and Nanotechnology, 2(3), 22–48
2. Sopicka-Lizer, M. (2010). High-energy ball milling: mechanochemical processing of nanopowders.
3. Stolle, A., & Ranu, B.C. (2014). Ball Milling Towards Green Synthesis: Applications, Projects, Challenges. Royal Society of Chemistry.
4. Szczęśniak, B., Borysiuk, S., Choma, J., & Jaroniec, M. (2020). Mechanochemical synthesis of highly porous materials. Materials horizons, 7, 1457-1473.
5. Baláž, P. (2008). Mechanochemistry in Nanoscience and Minerals Engineering. Springer.
6. Hope, Karl & Lloyd, Hayleigh & Ward, Daniel & Michalchuk, Adam & Pulham, Colin. (2015). Resonant Acoustic Mixing and its applications to energetic materials.
7. Suryanarayana, C. (2001). Mechanical alloying and milling. Progress in Materials Science, 46(1–2), 1–184.
8. Grover, V., Mandal, B.P., Tyagi, A.K. (2022). Handbook on Synthesis Strategies for Advanced Materials: Volume-II: Processing and Functionalization of Materials. Springer.
9. Zuckerwar, A. J. (2012). Acoustics: sound fields and transducers. In Elsevier eBooks.
10. Pavia, D. L., Kriz, G. S., & Lampman, G. M. (2008). Experimental Techniques in Organic Chemistry.
11. Gilbert, J.C., & Martin, S.F. (2001). Experimental Organic Chemistry: A Miniscale and Microscale Approach. ACS Publications.
12. Günther, H. (2013). NMR Spectroscopy: Basic Principles, Concepts and Applications in Chemistry. Wiley.
13. Sands, D. E. (1993). Introduction to crystallography. Courier Corporation.
14. Mixer Ball Mills MM 200/400. (2023). Retsch.
15. Myroniak, T. (2023). Resodyn Acoustic Mixers. Resodyn Acoustic Mixers.

Chapter 4. Results and Discussion

a. Paper #1

Tuneable tetrel bonds between tin and heavy pnictogens

Liyanage, S., Ovens, J. S., Scheiner, S., & Bryce, D.L. (2023). Chem. Communications, 59, 9001-9004; https://doi.org/10.1039/D3CC02644B

Statement of authenticity: I certify that I have prepared the following article featuring my own work, with guidance from my supervisor Dr. David Bryce. Notably, Jeffrey S. Ovens at the University of Ottawa's X-Ray Core Facility contributed to this work by solving the crystal structure presented in the article. I would like to acknowledge the support and the contribution of Dr. Steve Scheiner from the Department of Chemistry and Biochemistry at the Utah State University, Logan, for carrying out the computational work shown in this article.

Permissions: I declare that I have obtained permission from all authors to include this article in my thesis. The article can be accessed in the *Royal Society of Chemistry* (DOI: https://doi.org/10.1039/D3CC02644B)

Supporting Information: To provide readers with comprehensive insight into our study, all supplementary information relevant to this article is readily available on the RSC website: https://pubs.rsc.org/en/content/articlelanding/2023/CC/D3CC02644B.

Tuneable tetrel bonds between tin and heavy pnictogenss

Sachin Liyanage, [a]Jeffrey S. Ovens, [b]Steve Scheiner and [a]David L. Bryce *

[a]Department of Chemistry and Biomolecular Sciences, University of Ottawa, Ottawa, ON, Canada K1N 6N5

[b]Department of Chemistry and Biochemistry, Utah State University, Logan, Utah 84322-0300, USA

The first example of a binary cocrystal, comprised of $SnPh_3Cl$ and PPh_3, whose components are organized via short and directional tetrel bonds (TtB) between tin and phosphorus, is described. DFT elucidates, for the first time, the factors influencing the strength of TtBs involving heavy pnictogens. A CSD survey reveals that such TtBs are also present and determinative in single component molecular systems, highlighting their significant potential as tuneable structure directing elements.

The design and development of new materials, new catalytic processes, and the myriad of other chemical applications often relies on the control of structural and dynamic features via non-covalent interactions. The most well-known of these include, e.g., hydrogen bonds, but in recent years the concept of so-called secondary bonding interactions,[1] also known as σ-hole-based interactions,[2] has gained popularity. The σ-hole is an area of depleted electron density and elevated electrostatic potential which can act as a Lewis acid and receive electrons from another, electron donating, Lewis base moiety. The halogen bond is the prototypical example of this class of interactions,[3,4] but many analogous element-based interactions have also been identified, the most studied of which include chalcogen bonds,[5] pnictogen bonds,[6] and tetrel bonds.[7] These

interactions are appealing for a variety of chemical applications owing to their tuneability (e.g., substituents can act as electron donating or withdrawing groups) and directionality (i.e., the non-covalent bond tends to align predictably opposite the covalent bonds of the bond donating moiety).

The tetrel bond is one wherein a group 14 (tetrel, T = C, Si, Ge, Sn, Pb, Fl) element acts as an electron acceptor (Fig. 1(a)).Recent crystallographic surveys have highlighted the important role of tin tetrel bonds in controlling crystal packing arrangements.[8,9] For example, recent cocrystal engineering studies with triphenyltin chloride as a prototypical tin tetrel bond (TtB) donor have established its utility as a structure-directing element in cases where relatively light first-row atoms are used as the electron donors (e.g., N, O).[10] Tetrel bonds have also been demonstrated as important in solution, for example in anion binding applications[11] and as model systems for understanding the S_N2 reaction.[12] Tetrel bonds are also established entities in the gas phase.13 Extensive computational work with a focus on nitrogen-based electron donors has established the strength of such interactions *in vacuo*, as well as the role of steric crowding and structural deformations.[14–17]

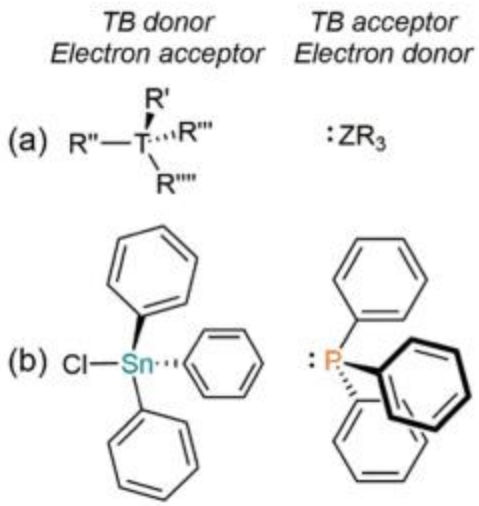

Fig. 1 *Tetrel bond donors (left) and acceptors (right) considered in this work. (a): general formulae of donors and acceptors considered (T = tetrel element; Z = pnictogen element). (b) Molecular structures of compounds used to generate cocrystal 1.*

The strength and utility of tetrel bonds involving a heavier pnictogen as the electron donor is an open question. In the case of halogen bonds, the use of heavier pnictogens such as P, As, and Sb as electron donors remains uncommon and has only recently been explored in a deliberate manner.[18–21] Their rarity may stem from the greater reactivity of compounds containing these heavier pnictogens, relative to lighter amine electron donors. In this context, we sought to establish the viability of the tin-heavy pnictogen tetrel bond as a novel cocrystal engineering tool and structure-directing element in chemistry. Motivated by (i) the established applicability of $SnPh_3Cl$ as a robust TtB donor[10] and (ii) the viability of simple phosphines as 'heavy pnictogen' electron donors in halogen-bonded systems,[18,19] tetrel-bond directed cocrystallization of $SnPh_3Cl$and PPh_3 was pursued as a first step (Fig. 1(b)).

Triphenyltin chloride (95%) and triphenylphosphine (99%) were obtained from ThermoFisher Scientific and Sigma Aldrich, respectively. In a typical procedure, 0.0140 g

PPh_3 and 0.0202 g $SnPh_3Cl$ were dissolved in 6 mL chloroform and the solvent was subsequently allowed to slowly evaporate over a period of a few days. Crystallographic data for cocrystal **1** were collected from a single crystal mounted on a MiTeGen MicroMount using parabar oil. Data were collected on a Bruker Kappa ApexII single crystal diffractometer equipped with a sealed tube Mo Kα source (λ = 0.71073 Å), a TRIUMPH monochromator, and an ApexII CCD detector. The crystal was held at 200 K using a dry compressed air-cooling system. Raw data collection and processing were performed with the Apex3 software package from Bruker.[30] Initial unit cell parameters were determined from 36 data frames from select ω scans. Semi-empirical absorption corrections based on equivalent reflections were applied.[31] Systematic absences in the diffraction data-set and unit-cell parameters were consistent with the assigned space group. The initial structural solutions were determined using ShelxT direct methods,[32] and refined with full-matrix least-squares procedures based on $F2$ using ShelXL and ShelXle.[33] Hydrogen atoms were placed geometrically and refined using a riding model. The structure was deposited with the Cambridge Structural Database, entry 2266467. The triphenyltin chloride triphenylphosphine cocrystal (1) features the two components in a 1:1 ratio.

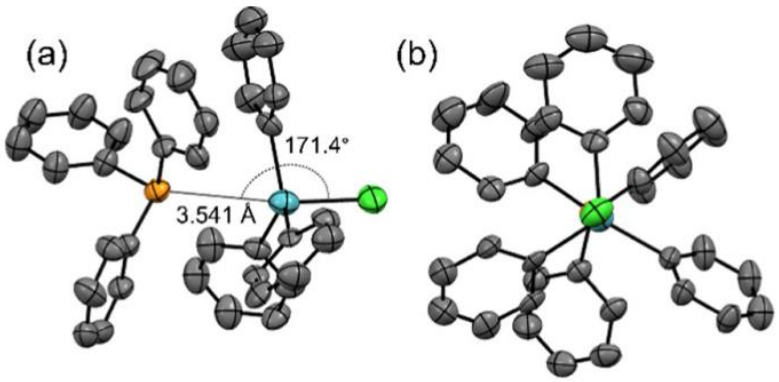

Fig. 2 *ORTEP representations of the triphenyltin chloride–triphenylphosphine cocrystal (1). (a) Side view with TtB metrics; (b) view along the TtB axis. Sn: teal; P: orange; Cl: bright green; C: grey; hydrogen: not shown. CCDC 2266467.*

As presented in Table 1, the structure packs in the P1 space group and features a strong and directional tetrel bond between tin and phosphorus. This TtB is characterized by a distance of 3.541 Å and a nearly linear Cl–Sn···P angle of 171.41° (Fig. 2(a)). An end-on view of the TtB cocrystal, shown in Fig. 2(b), reveals a staggered conformation among the six phenyl groups, possibly to minimize steric contact upon TtB formation. The Sn···P distance is approximately 10% less than what is expected based on non-directional van der Waals (vdW) contact. The normalized distance parameter,[22] N_C, is calculated to be 0.89, where $N_C = d_{Sn\ldots P} / \sum r_{vdw}; d_{Sn\ldots P}$ is the experimental distance, and the denominator is the sum of the vdW radii of Sn and P. The value of this parameter, coupled with the highly directional nature of the contact, are consistent with the formation of a tetrel bond via donation of electron density from the phosphorus lone pair into the σ-hole opposite the Cl–Sn covalent bond on the tin atom. The metrics for **1** may be compared to those for analogous cocrystals of $SnPh_3Cl$ featuring lighter oxygen and nitrogen-based electron donors.[10] In those systems, N_C is closer to 0.60, signifying a shorter stronger

contact, and the Cl–Sn···P angles range from approximately 170 to 180°, consistent with the geometry seen in **1**.

Table 1. *Crystallographic and structural details for 1 (T = 200 K).*

Space group	*P*1
Cell parameters	a = 10.949 (3); b = 11.464 (3); c = 12.442 (3) Å
Cell angles	α = 90.554(7)°; β = 99.184(6)°; γ = 97.708(7)°
Sn···P distance	3.541 Å
Normalized contact, N_C	0.89
$\theta_{Cl\text{-}Sn\cdots P}$	171.4 Å

Density functional theory (DFT) computations approach was used to perform quantum chemical calculations within the framework of the Gaussian 16[34] program, applying the M06-2X functional[35] and the polarized triple-ζ def2-TZVP basis set. Geometries were fully optimized and confirmed as true minima. by the lack of any imaginary vibrational frequencies. The interaction energy E_{int} of each complex was evaluated as the difference between the energy of the full dimer and the sum of the energies of the individual components, each in the geometry they adopt within the dimer, then corrected for basis set superposition error by the counterpoise procedure.[36] Atoms in Molecules (AIM) bond paths and their associated critical points were identified with the aid of the AIMAll program,[36] and measures of charge transfer were assessed within the NBO formalism as contained in the Gaussian set of programs.

A set of calculations using coordinates from the X-ray crystal structure of **1** was carried out to assess the potential role of π-π interactions. The phenyl rings on the Sn are largely perpendicular to those on P, thus mitigating most π-π attractions. There is only

one pair of rings that adopt a nearly parallel orientation. An NBO treatment of this complex finds only a combined second-order perturbation energy E(2) of 0.46 kcal/mol for this pair, far lower than the 11.89 kcal/mol associated with the Sn···P tetrel bond; the density of the critical point along the AIM π···π bond path is only 0.0053 au, as compared to 0.0113 for the Sn···P path. It is reasonable to assert then that the π···π interaction makes only a minor contribution to the total binding between these two triphenyl moieties.

The simple SnH_4 molecule was taken as a prototype Lewis acid with no substituents on the tetravalent Sn. As a first modification, its σ-hole was amplified by replacing one H atom by F. In another variation that makes this model more closely resemble the acid within cocrystal 1, the Sn was surrounded by three methyl groups and a single Cl atom. Three pnictogen Z atoms (N, P, and As) were considered as electron donor atoms in their trivalent configurations. The three R substituents considered on these ZR_3 bases were H, F, and Me. Altogether, there were 24 different acid-base combinations considered here designed to cover a wide range of TtB strength.

The pairing of each Sn-containing Lewis acid with a ZR_3 base resulted in most cases in a clear TtB. The Z lone pair, as defined by the C_3 axis of the base, aligned closely with the extension of the R–Sn covalent bond, which in turn passes through the Sn σ-hole; the Sn···Z distance was shorter than the sum of the individual atomic vdW radii. AIM analysis of each of these complexes confirmed the presence of a Sn···Z bond path as the single path connecting the two units, and NBO analysis revealed the expected charge transfer from the Z lone pair to a σ*(SnR) antibonding orbital. In several of the more weakly bound complexes, however, this alignment was a poor one, and any Sn···Z bond path, if one existed at all, was augmented by weak secondary intermolecular paths,

casting doubt on whether such a complex could legitimately be characterized as tetrel bonded. These questionable TtBs were those whose interaction energies were less than 2 kcal mol^{-1}, as described in more detail below.

The values of these interaction energies for various of these pairs are listed in Table 2 and display certain clear trends. The upper three rows of the table refer to SnH_4 as Lewis acid. Without the benefit of an electron-withdrawing substituent, this acid has only a moderate σ-hole, with V_{max} = 23.5 kcal mol^{-1}, defined as the value of the electrostatic potential on a ρ = 0.001 au isodensity surface. It can form a clear TtB with NH_3, but such a bond is questionable for the heavier PH_3 and AsH_3, as these two base molecules rotate their lone pair away from the Sn···Z axis by more than 301. Nonetheless, this TtB is affirmed by a Sb···Z AIM bond path and by NBO Z lone pair to σ*(SnH) charge transfer. In any case, whether true TtB or not, this interaction is quite weak.

Table 2. *Interaction energies (-Eint, kcal/mol-1) of tetrel-bonded complexes.*

TtB donor	***TtB acceptor***	***Z = N***	**Z = P**	***Z = As***
SnH_4	*ZF_3*	*1.13*	1.31	-
SnH_4	*ZH_3*	*4.76*	1.80	*1.63*
SnH_4	*ZMe_3*	*8.51*	3.67	*3.17*
$SnFH_3$	*ZF_3*	*2.08*	1.85	*0.0*
$SnFH_3$	*ZF_2H*	*4.96*	3.31	*1.65*
$SnFH_3$	*ZFH_2*	*8.38*	4.18	*2.94*
$SnFH_3$	*ZH_3*	*12.27*	4.77	*4.12*
$SnClMe_3$	*ZMe_3*	*14.98*	9.34	*7.37*

Replacing the three H atoms on the base by electron withdrawing F reduces the Z lone pair availability and essentially precludes a TtB of any magnitude with SnH_4, and even the presence of a TtB is itself questionable. For example, the AIM bond path connects the P/As with a H atom of SnH_4, rather than with Sn itself. On the other hand, SnH_4 engages in a robust TtB with all three trimethylated bases. Replacing one of the H atoms of SnH_4 by F doubles its σ-hole depth to 48.8 kcal mol^{-1}. This substituted acid is thus a much more effective electron acceptor, able to form a viable TtB with all bases, save the ZF_3 units. With each successive replacement of an F atom of ZF_3 by a H, this TtB grows progressively stronger, culminating in an interaction energy of 12.3 kcal mol^{-1} for $FH_3Sn\cdots NH_3$. Another clear trend apparent in the data is the weakening of the TtB as the Z atom grows larger: N > P > As. These patterns can be visualized more easily in Fig. 3 which displays the behaviour of the interaction energy for each Z atom as separate curves, where the clear superiority of N as base is readily apparent, as is the smaller decrement on going from P to As.

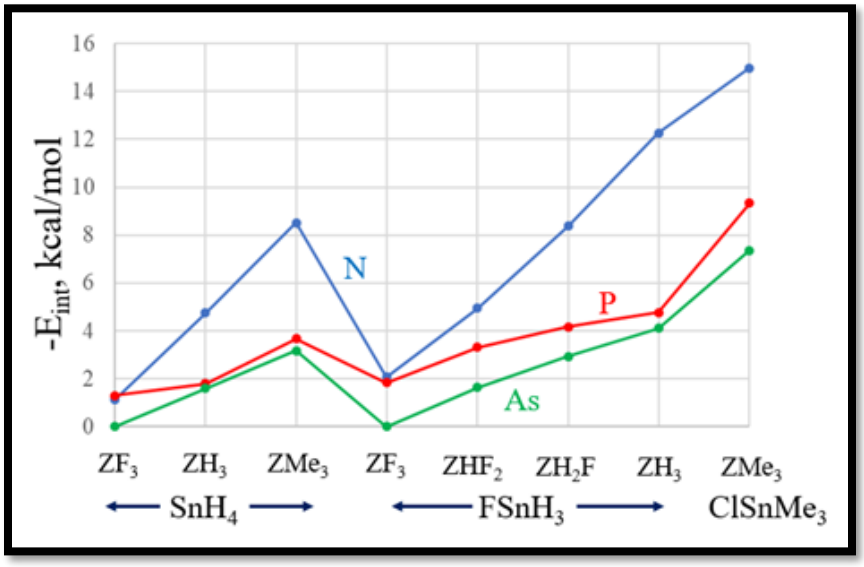

Fig. 3 *Interaction energies of complexes pairing Sn Lewis acid with pnictogen (Z) base.*

The last point on the far right of Fig. 3, and the last row of Table 2, refers to fully methylated acid and base, and with a Cl atom serving to amplify the s-hole on the $ClSnMe_3$ unit. Together, these substitutions lead to a Vmax of 46.1 kcal mol^{-1} for $SnClMe_3$, and to a quite strong TtB, even for Z = As. This system is a particularly faithful model of the novel cocrystal **1** that has been discussed above. For both the acid Sn and base P atoms, the phenyl groups to which they are attached have been simplified to methyl groups. As seen by the bottom entry of Table 2, the TtB in this system can be as strong as 9.3 kcal mol^{-1} if the entire complex is fully optimized. In order to more closely simulate the actual crystal of **1**, all of the non-H atoms in this complex were frozen in their X-ray coordinates, optimizing only the H atom positions. The main perturbation of this atom freezing is to elongate the optimized SnP distance from 3.290 to 3.541 Å. But even with this stretch, the TtB remains strong, decreasing by only 0.5 kcal mol^{-1} to 8.78 kcal mol^{-1}. π···π interactions between phenyl rings in 1 make only a minor contribution to the total binding between PPh_3 and $SnPh_3Cl$.

From a crystallographic perspective, a prime factor in distinguishing a non-covalent bonding attraction is the normalized contact distance N_C. These normalized distances are reported in Table 3 where they are all comfortably less than unity, buttressing the claim of a stabilizing TtB. In some of the stronger bonds, N_C drops below 0.7. These quantities are quite consistent with the interaction energies in Table 2, displaying very similar trends. The distances increase in the N < P < As order, just as the energies diminish, contract as F atoms on the base are swapped out for hydrogens, and also shorten when a F atom is placed on the acid.

Table 3. *Normalized Sn···Z distances (NC).*

TtB donor	TtB acceptor	Z = N	Z = P	Z = As
SnH_4	ZF_3	0.832	0.876	0.920
SnH_4	ZH_3	0.754	0.875	0.903
SnH_4	ZMe_3	0.696	0.843	0.872
$SnFH_3$	ZF_3	0.760	0.825	0.875
$SnFH_3$	ZF_2H	0.719	0.804	0.855
$SnFH_3$	ZFH_2	0.685	0.798	0.841
$SnFH_3$	ZH_3	0.661	0.800	0.833
$SnClMe_3$	ZMe_3	0.680	0.762	0.816

The leading crystallographic reviews of tetrel bonds in solids[8,9] both focus largely on N, O, and halide electron donors and only mention phosphorus in passing.[9] Although cocrystal **1**, reported above, appears to be the first cocrystal to be purposely engineered on the basis of a tin-phosphorus tetrel bond, the generality of this motif may be further assessed via a survey of the Cambridge Structural Database (CSD) (Figure A7; Appendix) The database was searched via Conquest software for all structures featuring tin-phosphorus distances between 2.50 and 4.00 Å. Note that the sum of the covalent radii of Sn and P is 2.46 Å and the sum of their vdW radii is 3.97 Å. The survey revealed 46 hits, 15 of which do not show characteristics of TtBs (e.g., distances close to the sum of the covalent radii; no directionality along the extension of the covalent bond opposite Sn). Of the remaining 31 hits, none are cocrystals wherein distinct chemical entities have been brought together in the crystallization process as a result of a TtB to form a novel product. Instead, these hits show pure one-component molecular systems with probable intramolecular Sn···P tetrel bonds, as assessed by TtB distance, angle, and directionality.

Published examples tend to discuss ‘intermolecular coordination’ of Sn and P in general terms, not in terms of tetrel bonds, if these interactions are discussed at all. In these 31 systems, the Sn···P distances range from 2.988 Å (NC = 0.75) in an organometallic sandwich complex (refcode USUFOG25) to 3.917 Å (NC = 0.99) in diphenyl{2-[(triphenylstannyl)methyl]phenyl}phosphane (FOWCOM[26]).

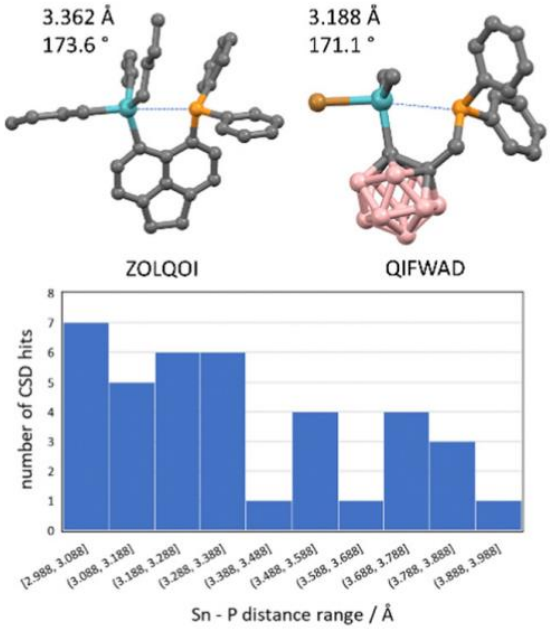

Fig. 4 *Top: two examples of intramolecularly Sn. . .P tetrel bonded structures with distances and TtB angles shown. Colours as in Fig. 2; B: pink; Br: brown. Bottom: Histogram of Sn···P distances for likely TtBs (see text).*

It is instructive to highlight a few intramolecular examples which mirror the structural characteristics seen in **1**. For example, as shown in Fig. 4, entry ZOLQOI[27] contains a short intramolecular Sn···P tetrel bond with a distance of 3.362 Å and a nearly linear C–Sn···P angle of 173.6°. While the preorganization of the tin and phosphorus moieties arises from their proximate 1,3-substitution on the substituted naphthalene core, the highly directional nature of the Sn···P tetrel bond provides some indication that such interactions are present and determinative even in the absence of strong electron

withdrawing groups. Entry QIFWAD[28] (Fig. 4) provides another interesting example of the ability of a Sn···P tetrel bond to organize and lock the conformation of substituents on a carborane core. Beyond molecular crystals, the role of Sn–P and Ge–P interactions in two-dimensional optoelectronic materials, SnP_3 and GeP_3, with possible photoconversion applications, has recently been demonstrated.[29]

In summary, we have described a first example of an expressly engineered cocrystal whose structure is governed by a strong and directional tin-phosphorus tetrel bond. DFT computations have established for the first time that while TtBs involving the heavier pnictogens (P, As) as electron donors tend to be weaker than those involving nitrogen atoms, a judicious tuning of electron-withdrawing substituents on the tetrel bond donor moiety can create the conditions for tin-heavy pnictogen tetrel bonds with interaction energies on the order of 10 kcal mol^{-1}. A survey of available X-ray diffraction structures has further confirmed for the first time the generality of the Sn···P tetrel bond and its determinative role in directing molecular conformation (thereby also indirectly affecting crystal packing) in the solid state. These conclusions suggest the applicability of tin-heavy pnictogen tetrel bonds as novel structure-directing elements in an array of areas in solid-state chemistry (e.g., crystal engineering and materials design) and in solution (e.g., homogeneous catalysis).

Paper #1 References:

1. N. W. Alcock, Adv. Inorg. Chem. Radiochem., 1972, 15, 1.
2. P. Politzer, J. S. Murray, T. Clark and G. Resnati, Phys. Chem. Chem. Phys., 2017, 19, 32166.
3. G. R. Desiraju, P. S. Ho, L. Kloo, A. C. Legon, R. Marquardt, P. Metrangolo, P. Politzer, G. Resnati and K. Rissanen, Pure Appl. Chem., 2013, 85, 1711.
4. G. Cavallo, P. Metrangolo, R. Milani, T. Pilati, A. Priimagi, G. Resnati and G. Terraneo, Chem. Rev., 2016, 116, 2478.
5. C. B. Aakeroy, D. L. Bryce, G. R. Desiraju, A. Frontera, A. C. Legon, F. Nicotra, K. Rissanen, S. Scheiner, G. Terraneo, P. Metrangolo and G. Resnati, Pure Appl. Chem., 2019, 91, 1889.
6. G. Resnati, et al. 2023. https://iupac.org/recommendation/definitionof-the-pnictogen-bond/Copyright r 2023 IUPAC. Accessed May 2023.
7. A. Bauzá, T. J. Mooibroek and A. Frontera, Angew. Chem., Int. Ed., 2013, 52, 12317.
8. A. Bauzá, S. K. Seth and A. Frontera, Coord. Chem. Rev., 2019, 384, 107.
9. P. Scilabra, V. Kumar, M. Ursini and G. Resnati, J. Mol. Model., 2018, 24, 37. 10
10. V. Kumar, C. Rodrigue and D. L. Bryce, Cryst. Growth Des., 2020, 20, 2027.
11. M. S. Taylor, Coord. Chem. Rev., 2020, 413, 213270.
12. A. Karim, N. Schulz, H. Andersson, B. Nekoueishahraki, A.-C. C. Carlsson, D. Sarabi, A. Valkonen, K. Rissanen, J. Gräfenstein, S. Keller and M. Erdélyi, J. Am. Chem. Soc., 2018, 140, 17571.
13. A. C. Legon, Phys. Chem. Chem. Phys., 2017, 19, 14884.
14. S. Scheiner, J. Phys. Chem. A, 2017, 121, 5561.
15. W. Zierkiewicz, M. Michalczyk and S. Scheiner, Phys. Chem. Chem. Phys., 2018, 20, 8832.
16. M. Michalczyk, W. Zierkiewicz, R. Wysokiński and S. Scheiner, Chem. Phys. Chem., 2019, 20, 959.
17. R. Wysokiński, M. Michalczyk, W. Zierkiewicz and S. Scheiner, Phys. Chem. Chem. Phys., 2019, 21, 10336.
18. Y. Xu, J. Huang, B. Gabidullin and D. L. Bryce, Chem. Commun., 2018, 54, 11041.

19. D. N. Zheng, P. M. J. Szell, S. Khiri, J. S. Ovens and D. L. Bryce, Acta Cryst., 2022, B78, 557.
20. Lisac, K., Topić, F., Arhangelskis, M., Cepić, S., Julien, P. A., Nickels, C. W., Morris, A. J., Friščić, T., & Cinčić, Nat. Commun., 2019, 10, 61.
21. A. M. Siegfried, H. D. Arman, K. Kobra, K. Liu, A. J. Peloquin, C. D. McMillen, T. Hanks and W. T. Pennington, Cryst. Growth Des., 2020, 20, 7460.
22. S. A. Alvarez, Dalton Trans., 2013, 42, 8617.
23. Y. Zhao and D. G. Truhlar, Theor. Chem. Acc., 2008, 120, 215.
24. M. J. Frisch, G. W. Trucks, H. B. Schlegel, G. E. Scuseria, M. A. Robb, J. R. Cheeseman, G. Scalmani, V. Barone, G. A. Petersson and H. Nakatsuji, et al., Gaussian 16 Rev. C.01, Wallingford, CT, 2016.
25. C. Müller, J. Warken, V. Huch, B. Morgenstern, I.-A. Bischoff, M. Zimmer and A. Schäfer, Chem. – Eur. J., 2021, 27, 6500.
26. J. J. Salazar-Díaz, M. A. Muñoz-Hernández, E. Rufino Felipe, M. Flores-Alamo, A. Ramírez-Solís and V. Montiel-Palma, Dalton Trans., 2019, 48, 15896.
27. E. Hupf, E. Lork, S. Mebs and J. Beckmann, Organometallics, 2014, 33, 2409.
28. T. Lee, S. W. Lee, H. G. Jang, S. O. Kang and J. Ko, Organometallics, 2001, 20, 741.
29. A. Slassi, S. M. Gali, A. Pershin, A. Gali, J. Comil and D. Beljonne, J. Phys. Chem. Lett., 2020, 11, 4503.
30. APEX Software Suite v 2010 Bruker AXS Inc. Madison Wisconsin USA, 2010.
31. R. H. Blessing, Acta Crystallogr. Sect. A 1995, 51, 33.
32. G. M. Sheldrick, Acta Crystallogr. A, 2008, 64, 112.
33. C. B. Hübschle, G. M. Sheldrick,
and B. Dittrich, J. Appl. Crystallogr., 2011, 44, 1281.
34. M. J. Frisch, G. W. Trucks, H. B. Schlegel, G. E. Scuseria, M. A. Robb, J. R. Che eseman, G. Scalmani, V. Barone, G. A. Petersson, H. Nakatsuji, et al. Gaussian 16 Rev. C.01, Wallingford, CT, 2016.
35. Y. Zhao and D. G. Truhlar, Theor. Chem. Acc., 2008, 120, 215.
36. S. F. Boy and F. Bernardi, Mol. Phys. 1970, 19, 553.
37. T. A. Keith, AIMAll, TK Gristmill Software: Overland Park KS, 2013

b. Paper #2

Tetrel bond in the triphenyltin(IV) chloride–cyclohexyldiphenyl-phosphane oxide (1/1) cocrystal

Liyanage, S., Ovens, J. S., & Bryce, D.L. (2023). IUCrData, 8(8);

https://doi.org/10.1107/s2414314623006375

Statement of authenticity: I certify that I have prepared the following article featuring my own work, with guidance from my supervisor Dr. David Bryce. Notably, Jeffrey S. Ovens at the University of Ottawa's X-Ray Core Facility contributed to this work by solving the crystal structure presented in the article.

Permissions: I would like to confirm that I have diligently obtained the necessary permissions from all co-authors to include this article within my thesis. The article is publicly accessible through the IUCrData (CCDC: 2267964).

Supporting Information: To provide readers with comprehensive insight into our study, all supplementary information relevant to this article is readily available on the IUCrData website: https://iucrdata.iucr.org/x/issues/2023/08/00/bv4048/

Tetrel bond in the triphenyltin(IV) chloride–cyclohexyldiphenyl-phosphane oxide (1/1) cocrystal

Sachin Liyanage, Jeffrey S. Ovens, and David L. Bryce *

Department of Chemistry and Biomolecular Sciences, University of Ottawa, Ottawa, ON, Canada K1N 6N5

Edited by R. J. Butcher, Howard University, USA (Received 14 June 2023; accepted 21 July 2023; online 1 August 2023)

The single-crystal X-ray diffraction structure of the title compound, [SnCl(C_6H_5)$_3$]·$C_{18}H_{21}$OP, is reported. The 1:1 cocrystal features a short and directional tetrel bond between tin and oxygen. The tin–oxygen distance is 2.346 (4) Å, representing 62% of the sum of the van der Waals radii of Sn and O. The Cl—Sn···O angle is 174.0 (1)° and this nearly linear arrangement is consistent with a tetrel bond formed via a σ-hole opposite the tin–chlorine covalent bond. Some weak C—H···Cl interactions are noted between adjacent molecules.

Structure description

The tetrel bond (TB), a moderately strong and directional non-covalent interaction, has received renewed interest in recent years as a useful structure-directing element and crystal engineering tool.[1] TBs form between a region of depleted electron density and elevated electrostatic potential (σ-hole) on a Group 14 (tetrel) element and an electron-donor moiety. Scilabra et al. (2018)[8] have reviewed the literature and summarized the available information on TBs involving tin and germanium. The title compound features a

short and highly linear TB between the Sn^{IV} atom of triphenyl-tin(IV) chloride and the O atom of cyclohexyldiphenylphosphane oxide. The asymmetric unit consists of one complete molecule of each type. The tin–oxygen distance is 2.346 (4) Å and the Cl—Sn···O TB angle is 174.0 (1)° (Fig. 1).

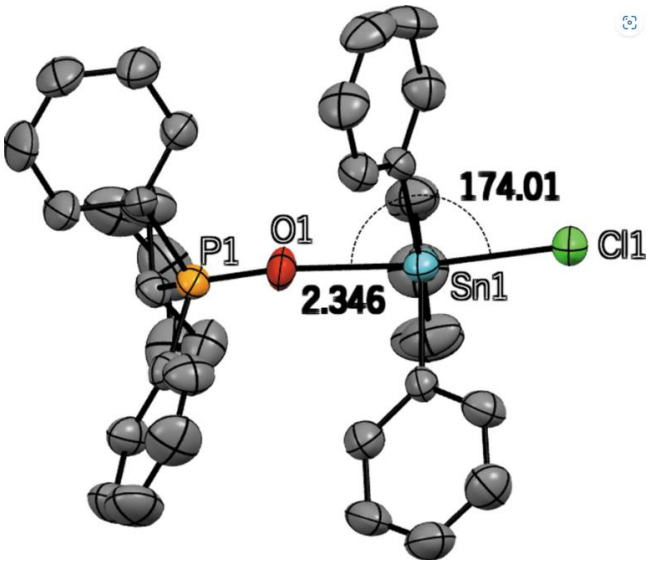

Fig. 1 *The molecular structure of the title compound. The tin–oxygen tetrel bond distance and chlorine–tin–oxygen angle are shown. H atoms are not shown. H atoms have been omitted for clarity.*

This distance represents approximately 62% of the sum of the van der Waals radii of Sn and O. The nearly linear arrangement is consistent with a TB inter-action via a σ-hole opposite the tin–chlorine covalent bond. These metrics may be compared to those for an analogous system comprised of trimethyl tin chloride and triphenylphosphine oxide, where the tin–oxygen TB distance is 2.375 (2) Å and the Cl—Sn···O TB angle is 177.57 (7)°.[3] Similar metrics are reported for the tin–oxygen TBs in [chloridobis(*p*-chlorophenyl)(*p*-tolyl)tin]-μ-1,2-bis-(diphenylphosphoryl)ethane-κ^2O:O′-[bromidobis(*p*-chlorophenyl)(*p*-tolyl)tin] (Lo & Ng, 2004), $(Ph_2ClSnCH_2)_2{\cdot}(Me_2N)_2PO$ (Jurkschat et al., 1990) and bromidotri(*p*-tolyl)tin–hexamethylphosphoramide[7] and for a series of

cocrystals of $SnPPh_3Cl$ formed with pyridine N-oxides, dimethylurea, and diphenyl sulfoxide[5] The packing of the title compound (Fig. 2) does not feature any other strong non-covalent inter-actions; the only other weak interactions of note are between the Cl atom and the H atoms of the phenyl rings of adjacent molecules (Table 1)

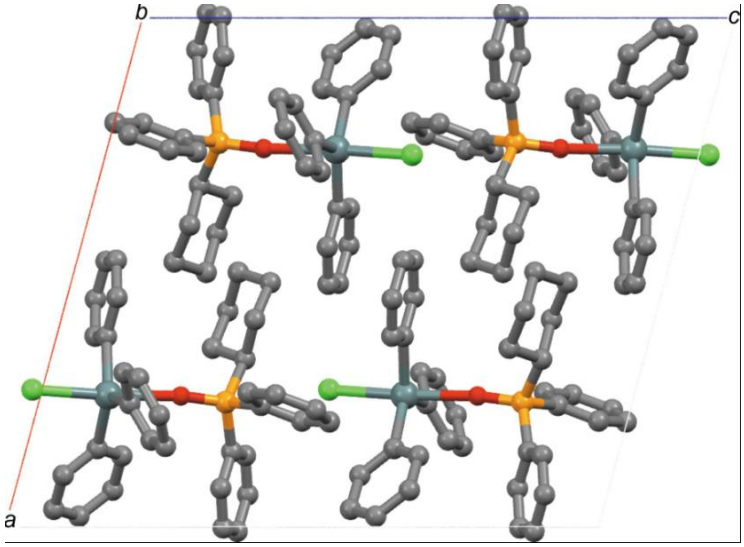

Fig. 2 *Packing diagram of the title compound, viewed along the b axis. H atoms have been omitted for clarity.*

Table 1. *Hydrogen-bond geometry (Å, °).*

D*—H···*A	***D*—H**	**H···*A***	***D*···*A***	***D*—H···*A***
C1—H1···Cl1^{i}	0.98	2.87	3.803 (6)	159
C18—H18···Cl1^{i}	0.93	2.88	3.637 (7)	139
Symmetry code: $(i)\ x, -y+\frac{1}{2}, z+\frac{1}{2}$				

Synthesis and Crystallization

In a typical procedure, triphenyltin(IV) chloride (0.0614 g) and cyclohexyldiphenylphosphane (0.0894 g) were added to hexane (60 ml) in a beaker. The mixture was heated and stirred until the solids were completely dissolved. Cocrystals grew via slow evaporation of the solvent in a fume hood over a period of 5 d. Evidently, during the synthesis, the phosphane was oxidized to give the phosphane oxide, as the process was not carried out under an inert atmosphere.

Refinement

The crystal data, data collection and structure refinement details are summarized in Table 2. H atoms were placed geometrically and refined using a riding model.

Table 2. *Experimental details/Structural data.*

Crystal data	
[SnCl(C6H5)3]·C18H21OP	*F*(000) = 1368
Mr = 669.76	Dx = 1.388 Mg m−3
Monoclinic, $P2_1/c$	Mo Kα radiation, λ = 0.71073 Å
a = 16.548 (2) Å	Cell parameters from 4222 reflections
b = 10.7496 (15) Å	θ = 2.3–21.9°
c = 18.665 (3) Å	μ = 0.96 mm−1
β = 105.110 (4)°	T = 273 K
V = 3205.4 (8) Å3	Plate, colourless
Z = 4	0.31 × 0.17 × 0.08 mm
Data collection	
Bruker APEXII CCD diffractometer	2948 reflections with I > 2σ(I)
Graphite monochromator	R_{int} = 0.090
ω and πhi scans	θ_{max} = 25.1°, θ_{min} = 1.3°
Absorption correction: multi-scan SADAB[9]	h = −19→13
Tmin = 0.621, Tmax = 0.745	k = −12→12
19012 measured reflections	l = −22→21
5547 independent reflections	
Refinement	

Refinement on F^2	Primary atom site location: structure-invariant direct methods
Least-squares matrix: full	Hydrogen site location: inferred from neighbouring sites
R[$F^2 > 2\sigma(F^2)$] = 0.052	H-atom parameters constrained
wR(F^2) = 0.116	$w = 1/[\sigma2(F_o^2) + (0.0456P)^2]$ where $P = (F_o^2 + 2F_c^2)/3$
S = 0.95	$(\Delta/\sigma)_{max} = 0.001$
5547 reflections	$\Delta\rho_{max} = 1.08$ e Å^{-3}
361 parameters	$\Delta\rho_{min} = -0.62$ e Å^{-3}
0 restraints	

Computer programs: *APEX3*[2], *SAINT*[2], *SHELXT2014*[10] and *SHELXL2018*[11]

Paper #2 References:

1. Bauzá, A., Mooibroek, T. J. & Frontera, A. (2016). Chem. Rec. 16, 473–487.
2. Bruker (2012). APEX3 and SAINT. Bruker AXS Inc., Madison, Wisconsin, USA.
3. Davis, M. F., Levason, W., Ratnani, R., Reid, G., Rose, T. & Webster, M. (2007). Eur. J. Inorg. Chem. 2007, 306–313.
4. Jurkschat, K., Hesselbarth, F., Dargatz, M., Lehmann, J., Kleinpeter, E., Tzschach, A. & Meunier-Piret, J. (1990). J. Organomet. Chem. 388, 259–271.
5. Kumar, V., Rodrigue, C. & Bryce, D. L. (2020). Cryst. Growth Des. 20, 2027–2034.
6. Lo, K. M., Ibrahim, A. R., Chantrapromma, S., Fun, H.-K. & Ng, S. W. (2001). Main Group Met. Chem. 24, 301–302.
7. Lo, K. M. & Ng, S. W. (2004). Acta Cryst. E60, m717–m719.
8. Scilabra, P., Kumar, V., Ursini, M. & Resnati, G. (2018). J. Mol. Model. 24, 37.
9. Sheldrick, G. M. (1996). SADABS. University of Göttingen, Germany.
10. Sheldrick, G. M. (2015a). Acta Cryst. A71, 3–8.
11. Sheldrick, G. M. (2015b). Acta Cryst. C71, 3–8.

c. Synthesis and Results

In this section, we will provide a comprehensive discussion on the methodology employed to create the two novel cocrystals described in papers #1 and #2.

These cocrystals were carefully crystallized using three different techniques: the slow evaporation process (cocrystal 1 and 2), as detailed in section C.1a and C.1b, respectively, the innovative processes of RAM, as described in section C.2 and ball milling, as described in section C.3.

C.1a Slow evaporation, cocrystal 1

In this experiment, as illustrated in Figure 1 below, we introduce an equimolar amount of two solid substances: triphenyltin chloride and triphenylphosphine, into a vial. A precise and minimal volume of the chosen solvent, chloroform, was carefully added to the vial to aid in the dissolution of the compounds. Following that, the vial was vortexed to ensure that all compounds are completely dissolved. Aluminium foil is then placed over the vial, leaving a small hole. This permits the solvent to gradually evaporate, which we carry out in a fume hood at room temperature to prevent any disruptions. Depending on the type of solvent used, the entire process typically takes 6 to 7 days.

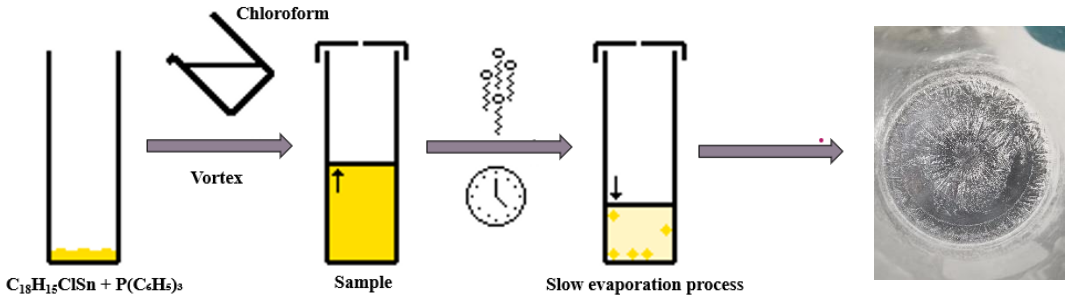

Figure 1. *Slow evaporation process and the product (cocrystals).*

Several experiments were conducted for cocrystals 1, as evident in the data presented in Table 1 below. Highlighted in green is the successful formation of the crystalline structure between triphenyltin chloride and triphenylphosphine. A total of 0.0342 g of the cocrystal was obtained; however, this quantity proved insufficient for conducting PXRD analysis. Consequently, it became necessary to scale up the sample, a step elaborated in Table 2 below. Once more, the green highlight signifies the successful formation of the crystalline structure resulting from the interaction between triphenyltin chloride and triphenylphosphine.

Table 1. *Starting materials and details of the cocrystal 1.*

Beaker #	Triphenylphosphine (g)	Triphenyltin chloride (g)	Total mass (g)	Solvent (ml)	Slow evap. duration	SCXRD (yes or no)	Successful?
#36	0.0141	0.0198	0.0339	Diethyl Ether 6.5 mL	June 7th to June 9th	Yes	No
#37	0.0135	0.0213	0.0348	Diethyl Ether 7.0 mL	June 7th to June 9th	Yes	No
#38	0.0140	0.0202	0.0342	Chloroform 6 mL	June 7th to June 9th	Yes	Yes
#39	0.0138	0.0197	0.0335	Chloroform 6 mL	June 7th to June 9th	Yes	No
#40	0.0143	0.0202	0.0345	Acetonitrile 10 mL	X	No	No

Table 2. *Provides an overview of the starting materials and essential details concerning the scaling of the cocrystal 1.*

Beaker #	Triphenylphosphine (g)	Triphenyltin chloride (g)	Total mass (g)	Solvent (ml)	Slow evap. duration?	SCXRD (yes or no)	Successful?
#57	0.1017	0.1493	0.2510	Chloroform 20 mL	July 18th to July 21st	Yes	Yes
#58	0.1015	0.1482	0.2497	Diethyl Ether 30 mL	July 18th to July 21st	Yes	No

C.1b Slow evaporation, cocrystal 2

The procedure in this experiment was very similar to the one described in the previous section, *C.1b*. To begin, we put an equimolar amount of two solid substances, triphenyltin chloride and cyclohexyldiphenylphosphine, into a vial. To dissolve these compounds, we precisely add a minimal amount of the chosen solvent, hexane. Following that, thorough vortexing ensures that all components are completely dissolved. However, not everything was completely dissolved in this case, so the vial was gently heated on a hot plate while being stirred until the sample was completely dissolved. Following that, the vial was allowed to come to room temperature, which was done under the fume hood. We cover the vial with aluminium foil, leaving a small opening, to start the solvent evaporation. To avoid disruptions, this reaction was carried out in a fume hood at room temperature. The entire procedure generally takes roughly 4 to 5 days.

Multiple experiments were conducted for cocrystal 2, and the results are shown in Table 3. Green highlights the successful formation of the crystalline structure between triphenyltin chloride and cyclohexyldiphenylphosphine. The combined yield was 0.1508 g of cocrystal 2.

Table 3. *Starting materials and details of the cocrystal 2.*

Beaker #	Cyclohexyldiph-enylphosphine (g)	Triphenyltin chloride (g)	Total mass (g)	Solvent (ml)	Slow evap. duration?	SCXRD (yes or no)	Successful?
#65	0.0635	0.0865	0.150	DCM 30 mL	August 17th to August 21st	Yes	No
#66	0.0632	0.0865	0.1497	DCM 30 mL	August 17th to August 21st	Yes	No
#67	0.0619	0.0889	0.1508	DCM 30 mL	August 17th to August 21st	Yes	No
#68	0.0610	0.0882	0.1492	DCM 30 mL	August 17th to August 21st	Yes	No
#69	0.0614	0.0894	0.1508	Hexane 60 mL	August 17th to August 21st	Yes	Yes
#70	0.0611	0.0880	0.1491	Hexane 60 mL	August 17th to August 21st	Yes	No

C.2 RAM

In this part of the synthesis, RAM was used to create a homogeneous powder by breaking down larger crystalline structures of triphenyltin chloride and triphenylphosphine into smaller particles. Table 4 below shows the results of several attempts with varying parameters. This was done to ensure the acquisition of the necessary outcome for a PXRD pattern that matches the simulated PXRD between triphenyltin chloride and triphenylphosphine.

Table 4. *Starting materials and parameters.*

Beaker #	Triphenylph-osphine (g)	Triphenyltin chloride (g)	Total mass (g)	Solvent (uL)	Frequency	Duration (min)	PXRD	Successful?
#108	0.1213	0.1782	0.2995	Dry	High	10	Yes	No
#109	0.1216	0.1787	0.3003	Dry	High	15	Yes	No
#110	0.1213	0.1781	0.2994	Methanol (50 uL)	High	10	Yes	No
#111	0.1215	0.1792	0.3007	Methanol (50 uL)	High	15	Yes	No
#112	0.1214	0.1781	0.2995	Ethanol (50 uL)	High	10	Yes	No
#113	0.1219	0.1785	0.3004	Ethanol (50 uL)	High	15	Yes	No
#114	0.1216	0.1785	0.3001	Chloroform (50 uL)	High	20	No	No
#115	0.1218	0.1787	0.3005	Chloroform (50 uL)	High	20	No	No
#116	0.1613	0.2386	0.3999	Dry	High	45	No	No
#117	0.1618	0.2385	0.4003	Dry	High	45	No	No

C.3 Ball milling

The final synthesis method used was ball milling, which involved placing the starting materials, triphenyltin chloride and triphenylphosphine, within a metal cylinder alongside stainless steel balls. The process begins with the ball milling apparatus crushing these crystalline samples inside the cylinder, resulting in distinct powder forms. Table 5 shows the results of multiple attempts with different parameters. This approach was chosen to ensure the achievement of the essential outcome required for achieving a PXRD pattern

that corresponds to the simulated PXRD between triphenyltin chloride and triphenylphosphine.

Table 5. *Starting materials and parameters.*

Beaker #	Triphenylph-osphine (g)	Triphenyltin chloride (g)	Total mass (g)	Solvent (uL)	Frequency (Hz)	Duration (min)	PXRD
#A1	0.1619	0.2387	0.4006	Dry	30	20	White powder
#A2	0.1620	0.2389	0.4009	Chloroform (50 uL)	30	20	Liquefy powder
#A3	0.1611	0.2389	0.4000	Dry	30	15	White smooth powder
#A4	0.1605	0.2390	0.3995	Dry	30	15	White smooth powder
#A5	0.1620	0.2386	0.4006	Dry	35	15	Fine white powder
#A6	0.1622	0.2386	0.4008	Dry	35	15	Fine white powder
#A7	0.1617	0.2385	0.4002	Dry	40	20	White powder
#A8	0.1619	0.2381	0.4000	Dry	40	20	White powder

i. Characterization of Products, Melting Points

After successfully synthesizing the samples and identifying promising compounds, we carefully approached the characterization process to optimize both time and cost. It is critical to ensure the purity of the samples in order to obtain reliable results. We used a variety of precise characterization techniques in this study, including melting point analysis, solid-state Nuclear Magnetic Resonance (ssNMR), Powder X-ray Diffraction (PXRD), and Single-Crystal X-ray Diffraction (SCXRD).

Melting Points

The melting point is a fundamental property of solid crystalline substances, indicating the precise temperature at which the solid-to-liquid phase transition occurs. When heat is applied to a substance, it undergoes a transformation in which all the energy introduced is absorbed as heat of fusion. The temperature most likely remains constant throughout this phase change. This technique is critical in characterizing both organic and inorganic crystalline compounds, particularly in confirming purity.

When pure substances are examined, they have a distinct and well-defined melting point that is confined within a relatively narrow temperature range. Impure or contaminated compounds, on the other hand, typically have a broader temperature range over which melting occurs. The use of melting point analysis is extremely beneficial, particularly in the field of cocrystal development. It enables us to confidently determine whether the formation of new cocrystals has occurred.

Table 6-8 presents data on the melting points of cocrystals 1 and 2, the powder product resulting from Ball milling and RAM, and the starting materials. This data provides a key

indicator of whether a chemical transformation has occurred during the cocrystal formation process. If the melting point of the cocrystal differs from that of the starting materials, it indicates that a new solid-state structure distinct from the initial components has successfully emerged. This distinction in melting points confirms the creation of a purified and distinct cocrystals.

Table 6. *Melting points of novel cocrystals and starting materials.*

Compounds	Melting points (°C)
Triphenyltin chloride	108
Triphenylphosphine	80
Cocrystal #1 (Beaker #38)	56 – 65
Cocrystal #1 (Beaker #57)	55 – 64
Cocrystal #2 (Beaker #69)	51-61

Table 7. *Melting points of powder products from ball milling.*

Compounds	Melting points (°C)
Triphenyltin chloride	108
Triphenylphosphine	80
A#1	62 – 71
A#2	N/A
A#3	60 – 72
A#4	61 – 73
A#5	62 – 72
A#6	62 – 71
A#7	61 – 70
A#8	61 – 69

Table 8. *Melting points of powder products from RAM.*

Compounds	Melting points (°C)
Triphenyltin chloride	108
Triphenylphosphine	80
#108	61-81
#109	61-81
#110	61-90
#111	60-91
#112	62-92
#113	61-90

#114	N/A
#115	N/A
#116	59 – 82
#117	60 – 81

ii. ssNMR Results

We used CP/MAS ssNMR studies to investigate the electronic environment of the tetrel atoms in cocrystal 1. Specifically, we conducted ^{31}P CP/MAS NMR for the starting material, triphenylphosphine (Figure A1; Appendix), and the ^{13}C CP/MAS NMR for another the starting material, triphenyltin chloride (Figure A3; Appendix). The corresponding Figures can be found in the appendix at the end of the thesis.

In addition to these, we also performed ^{31}P CP/MAS NMR for cocrystal 1 and the results are presented in Figure 2, followed by the spectral analysis. Note that that all these experiments were conducted using the Bruker Avance 200 NMR instrument using a 7mm MAS probe.

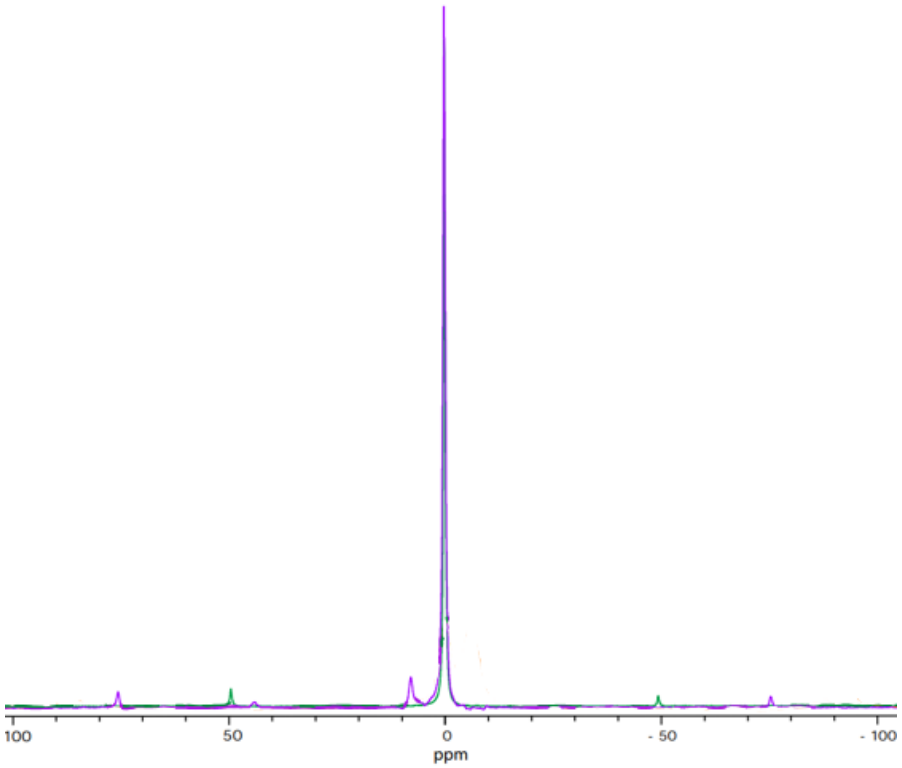

Figure 2. *Shows an overlay of ssNMR spectra. It includes the ^{31}P spectrum of our novel cocrystal #1 (purple) and triphenylphosphine (green).*

To get the necessary information of our ssNMR data, we overlaid the CP/MAS ssNMR of the starting material (shown in green) with the experimental CP/MAS of the new cocrystal (shown in purple), as shown in the Figures in the Appendices. However, it is important to note that obtaining significant data from the novel cocrystal 1 presented some challenges due to its limited quantity. To address this, we introduced the sample in a 7mm probe with a layer of Teflon tape at the bottom of the rotor. The sample, in its powdered form, was then placed atop this layer, with additional Teflon tape on top, effectively creating a sandwich-like sample arrangement where the cocrystal sat in the middle.

In our case, while examining the ssNMR spectrum of my novel cocrystal, an intriguing observation emerged. While one peak corresponded to the expected ^{31}P spectrum, the appearance of two unexpected shorter peaks raised concerns (8ppm and 45ppm). Typically, each peak in this type of spectrum (except for the sidebands at roughly 75 ppm and -75 ppm) represents a unique chemical environment for phosphorus within the cocrystal, reflecting the different molecular interactions and bonding environments in the sample. Additionally, the number of peaks reveals information about the different types of phosphorus atoms that are present, while their relative intensities indicate the abundance of each species. The occurrence of additional peaks in the spectrum here indicates unwanted impurities. Such complexities in the tetrel atoms' electronic environment complicate the interpretation of data and highlight the need for a thorough investigation to fully understand the NMR results and the cocrystal's underlying properties.

No further NMR spectrum experiments on cocrystal 1 were performed until we obtained a significantly purer and sufficient quantity of the sample to proceed. We temporarily set aside the NMR experiments and shifted our focus to an alternative identification method,

PXRD. This approach will serve to confirm the purity of our obtained cocrystal 1 by comparing it with a simulated PXRD pattern of the cocrystal 1. Additionally, it is important to note that cocrystal 2 was not analysed through NMR as the project's priority was directed toward investigating cocrystal 1.

iii. PXRD Results

In this section, we will be discussing the Powder X-ray Diffraction diffractogram results of our cocrystal 1 obtained through the slow evaporation synthesis method. Aso, we will be discussing some of our Powder X-ray Diffraction results obtained through our second synthesis method, RAM (Resonant Acoustic Mixing).

Powder X-ray diffraction was utilized to characterize and compare the pure starting material with the cocrystal of interest to confirm that the samples were not mere combination of the starting materials. When certain peaks in the PXRD pattern of the cocrystal align with peaks from the starting materials, it suggests a structural connection between the two. This alignment can indicate a variety of scenarios. For example, it could imply that the cocrystal is a physical mixture of the starting materials rather than a distinct compound. Second, it is possible that the cocrystal formation process is incomplete, with both the cocrystal and the starting materials coexisting. Furthermore, the cocrystal and starting materials may share some structural features or motifs, resulting in peak correspondence.

Moreover, in the context of this research project, when we find a visible difference between the cocrystal and the starting materials in the PXRD data, it leads to two divergent but equally important interpretations. A possible interpretation of this divergence

in PXRD patterns is that it indicates a high probability of tetrel bonding within the cocrystal, which is a positive outcome. This scenario is consistent with the main goals of our research and implies that the cocrystal is a novel material with unique chemical interactions. On the other hand, this divergence can simply be viewed as a potential error in the crystal structure, necessitating further investigation and refinement.

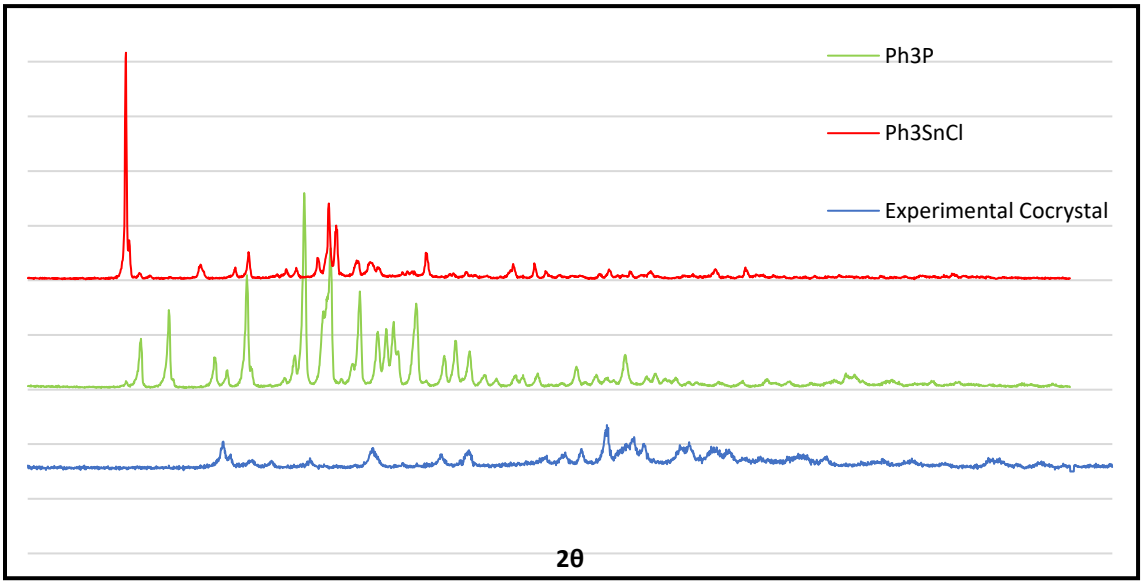

Figure 3. *Experimental X-ray Diffraction patterns of experimental cocrystal (blue) compared with starting materials, triphenyltin chloride (red) and triphenylphosphine (green).*

In this research, we speculate the formation of a novel cocrystal held together by tetrel bonding, as evidenced by Figure 3. A significant difference in the diffractogram peaks between the starting materials and the experimental cocrystal patterns supports this conclusion. This discovery marks an important milestone in the progression of our research, encouraging us to investigate deeper into the properties of our sample. However, further analysis is needed to confirm this hypothesis. Here, we compared our

experimental cocrystal to the simulated diffractogram pattern to ensure the purity and accuracy of the novel cocrystal powder product (Figure 4).

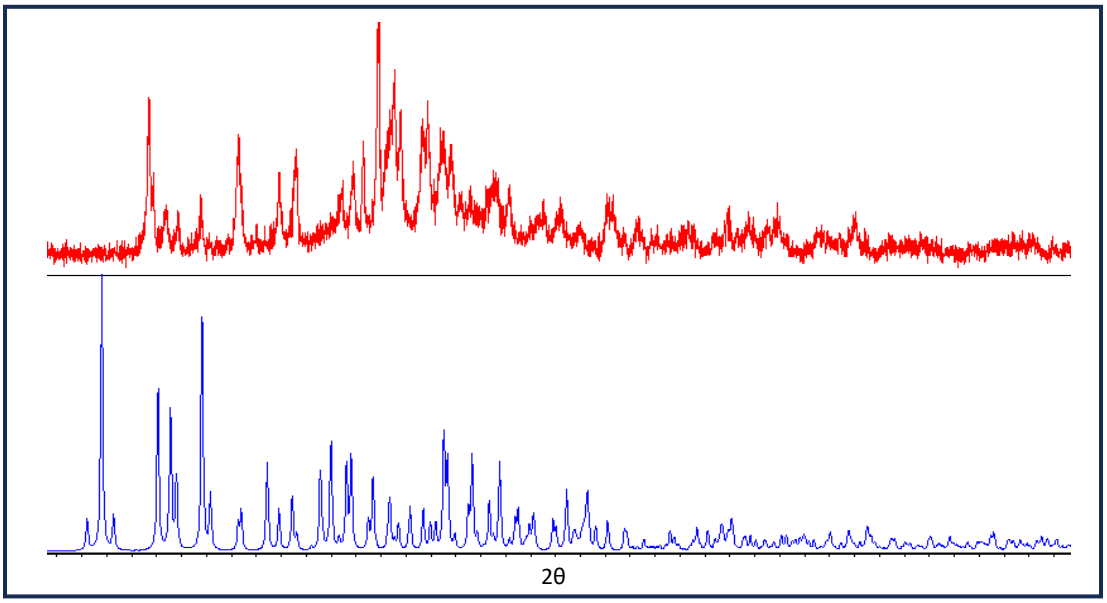

Figure 4. *Simulated (blue) vs Experimental cocrystal 1 (red), owder X-ray Diffraction diffractogram patterns.*

When looking at Figure 4, it becomes evident that our “novel cocrystal 1” was not completely pure and it did not algin perfectly with the simulated diffractogram data (Blue). As we already know, an X-ray diffraction pattern is like a unique fingerprint for a material, and it should closely match the simulated pattern if the sample is pure. When it does not align, it indicates that the cocrystal sample we tested was not entirely composed of the desired cocrystal material. Instead, impurities or other substances were most likely mixed in, causing variations in the X-ray pattern compared to what we expected based on the experiment.

Another reason why the data did not match was the grinding process. The process of grinding sample compounds with a mortar and pestle is widely used in chemistry and materials science. It is frequently used to prepare samples for analysing. However, this mechanical action can have an impact on the sample's integrity. When compounds are crushed, the mechanical forces applied can be substantial, causing stress on the molecular structure. In some cases, this stress can cause chemical bonds within the sample to break or decompose. Thus, while some peaks may algin, the overall pattern differed significantly, suggesting a potential polymorph or mixture of materials.

Furthermore, RAM (Resonant Acoustic Mixing) was used as an alternative method to replicate our cocrystal 1. In this approach, we conducted ten different experiments in an effort to successfully create our desired tetrel-bonded compound. We used the resulting product and compared it to the obtained simulated X-ray diffractogram. Only the PXRD patterns from Beakers 109, 110 and 112 are shown below, each accompanied by their respective starting materials and experimental parameters. (For the other RAM diffractograms, consult the Appendix Figures A4-A6).

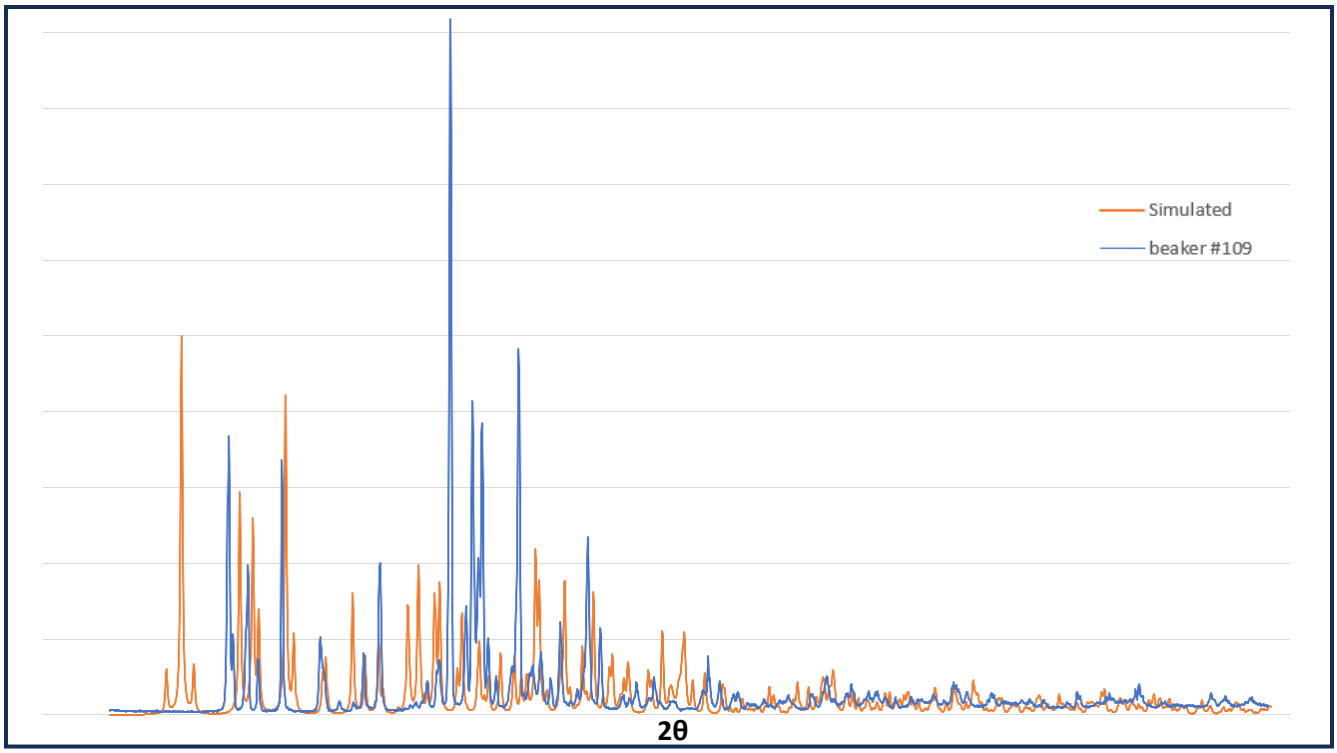

Figure 5. *Simulated (orange) vs Beaker #109 (blue), PXRD patterns.*

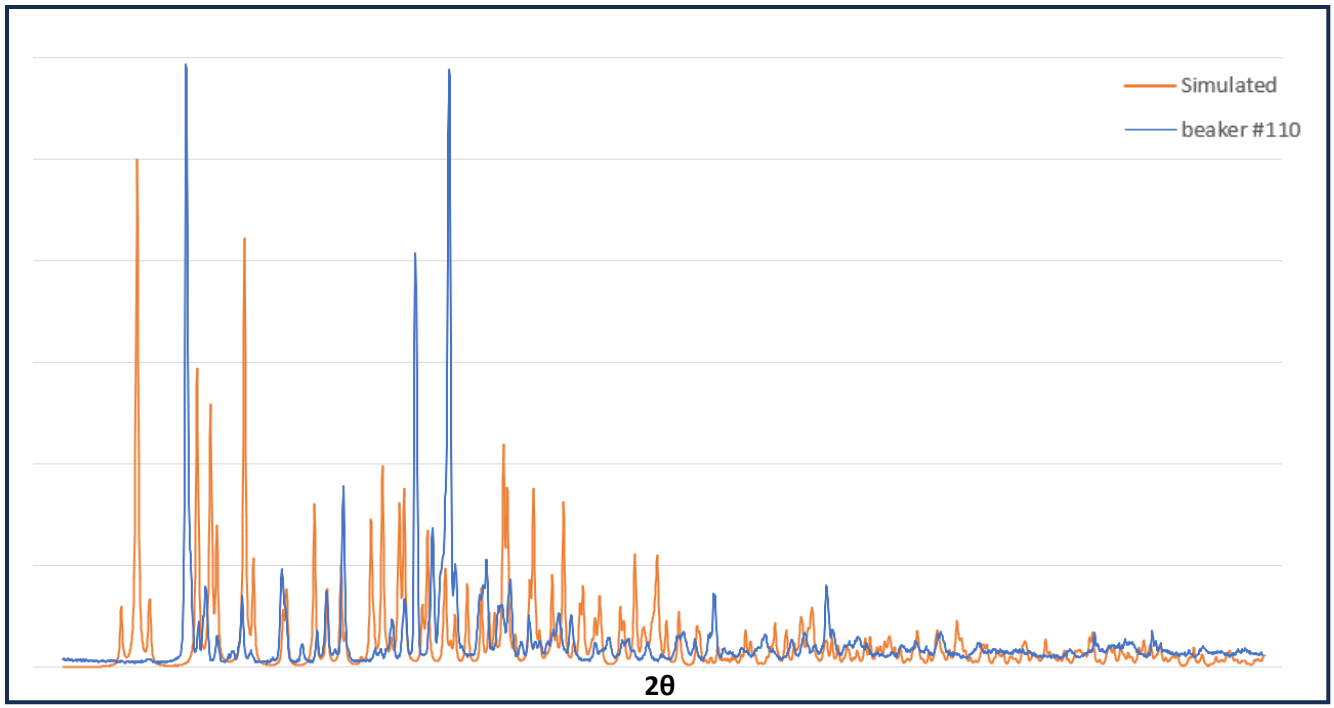

Figure 6. *Simulated (orange) vs Beaker #110 (blue), PXRD patterns.*

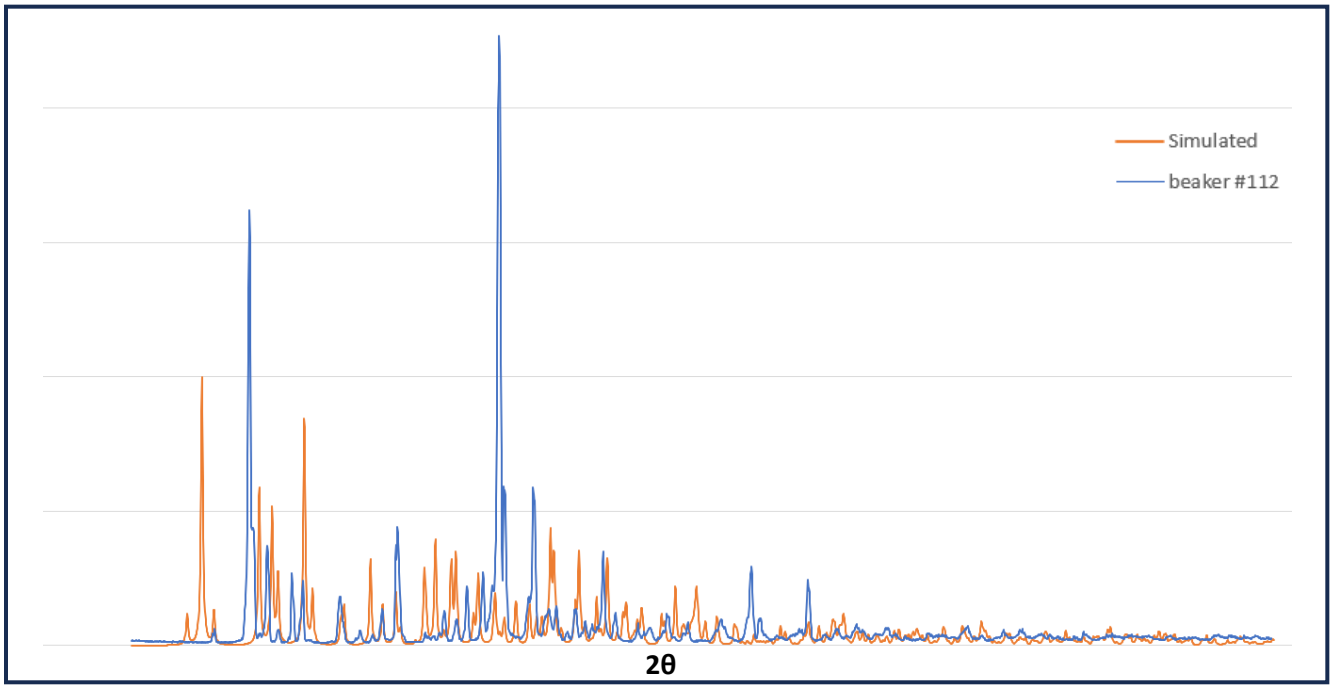

Figure 7. *Simulated (orange) vs Beaker #112 (blue), PXRD patterns.*

The RAM (Resonant Acoustic Mixing) products did not match the simulated cocrystal, revealing a significant difference. When such situations arise, as seen in Beakers 109, 110, and 112, where the simulated X-ray diffractogram data do not match the experimental data, several potential explanations must be considered.

Firstly, these differences might indicate the presence of contaminants in the experimental samples. These impurities, which alter the overall composition and crystal structure, may come from the reaction's byproducts or starting materials, resulting in the discrepancy of the observed data. Additionally, there's a chance that the procedure—in this example, the RAM synthesis—was not carried out entirely, meaning it was incomplete. Partially formed products, unreacted starting materials, or the presence of intermediate compounds are all possible outcomes of incomplete reactions, and they can all explain the observed differences between the simulated data and the experiment results.

Chapter 5. Conclusions and Future Work

i. Conclusions

In the course of this research, we have focussed on crystal engineering using tetrel bonds and heavy pnictogens, as a novel avenue for exploring tetrel bonds. Our primary objective in this study was to successfully synthesize a cocrystal featuring tetrel bonding. This cocrystal is formed through the interaction of triphenyltin chloride, acting as the electrophilic bond donor, with triphenylphosphine serving as the TtB acceptors. Following the successful synthesis and structural confirmation of this cocrystal, we used quantum chemical calculations, specifically density functional theory (DFT), to precisely determine and validate the strength of these tetrel bonds.

We initiated our research by synthesizing two novel cocrystals were. In experiment C.1a, an equimolar mixture of triphenyltin chloride and triphenylphosphine was dissolved in chloroform and was let to slow evaporate under the fume hood at room temperature for 6 to 7 days, which gave the result to cocrystal 1. However, the initial 0.0342 g of cocrystal obtained proved insufficient for PXRD analysis, necessitating a scale-up as detailed in Table 2 (Chp. 4 section C.1a). On the other hand, C.1b, which follows a similar procedure, the combination of triphenyltin chloride and cyclohexyldiphenylphosphine was dissolved in hexane, heated, and then subjected to slow evaporation. This method took approximately 4 to 5 days in a fume hood at room temperature, which gave the result to cocrystal 2. Table 3 (Chp. 4 section C.1b) shows the results for cocrystal 2, which shows successful crystalline structure formation and yield of 0.1508g. Alternative methods, namely RAM and ball milling, were used in attempts to synthesize the two novel

cocrystals. However, it is important to note that these methods did not yield the desired results and were thus unsuccessful in this case.

Additionally, we investigated the melting points of cocrystals 1 and 2, as well as the starting materials, in our study. The melting point is the temperature at which a solid turn into a liquid, and it remains constant during this phase transition. Pure substances have a well-defined and narrow melting point range, whereas impurities result in broader melting temperature intervals. This analysis is especially useful in the field of cocrystal development because it provides a reliable method of determining the formation of new compounds.

Knowing this, Table 6 (Chp. 4 section melting point) displays the melting points of our cocrystals and starting materials. Notably, when the melting point of a cocrystal differs from that of the starting materials, it is a sign of a chemical transformation occurring during cocrystal formation. In our case, the melting points of cocrystal 1 (56°C to 65°C) and cocrystal 2 (51°C to 61°C) differ from those of the starting materials, triphenyltin chloride (108°C) and triphenylphosphine (80°C). This disparity emphasizes the independent formation of a purified and unique cocrystal entity distinct from its components. Moreover, when the melting points of cocrystal 1 are compared to the powder products obtained from Ball Milling (Table 7; Chp. 4 section melting point) and RAM (Table 8; Chp. 4 section melting point), it is clear that they are not the same. The melting point of cocrystal 1 ranges from 55°C to 65°C, whereas the powder products of ball milling and RAM have a wider temperature range. The powder products' varied melting points (ranging from 59°C to 92°C) raise concerns about the accuracy of the results, as they lack the well-defined and narrow melting point characteristic of pure substances.

In addition, we investigated the electronic environment of tetrel atoms in cocrystal 1 using CP/MAS ssNMR. We performed ^{31}P CP/MAS NMR on triphenylphosphine and ^{13}C CP/MAS NMR on triphenyltin chloride, and the results are shown in the appendix. An overlay of ssNMR spectra (Figure 2; Chp. 4 Results/Discussion section ssNMR results) included the ^{31}P spectrum of cocrystal 1, triphenylphosphine, and the ^{13}C spectrum of triphenyltin chloride. Notably, during the ssNMR analysis, two shorter peaks at 8 ppm and 45 ppm appeared alongside the expected ^{31}P spectrum. As stated earlier, each peak in this type of spectrum represents a distinct chemical environment for phosphorus within the cocrystal, reflecting the sample's various molecular interactions and bonding environments. These unexpected peaks indicate a possible deviation from the expected pattern, which could be caused by structural variations, impurities, or unique magnetic interactions within the cocrystal lattice. Subsequent experiments were put on hold until a purer and larger sample could be obtained. Meanwhile, we used PXRD to confirm the purity of cocrystal 1 by comparing it to a simulated PXRD pattern. Notably, cocrystal 2 was not subjected to NMR analysis because cocrystal 1 was our primary focus.

Afterwards, we looked at the Powder X-ray Diffraction (PXRD) results of cocrystal 1, obtained through slow evaporation synthesis and an alternative approach, RAM. The PXRD technique was critical in determining whether the cocrystal was pure or just a mixture of the starting materials. A significant difference in the PXRD patterns of cocrystal 1 and its starting materials in our study indicated the presence of tetrel bonding, which was consistent with our research objectives. However, the incomplete match between the experimental cocrystal 1 and the simulated diffractogram suggested that impurities or other substances in the sample were affecting the X-ray pattern. Furthermore, RAM

experiments did not match the simulated cocrystal, raising the prospect of impurities or incomplete reactions. Also, the data discrepancy can be explained by the grinding process, which is a standard sample preparation method in materials science and chemistry. Although using a mortar and pestle for grinding is common, the sample's integrity may be compromised by the strong mechanical forces used. Grinding can cause stress on the molecular structure due to the crushing action, which could cause chemical bonds in the sample to break down or decompose. These findings highlight the importance of further research into the differences between expected and observed X-ray diffraction patterns.

One of the most important parts in this research, was the structural analysis through Single-Crystal-X-ray Diffraction (SCXRD) data of cocrystal 1 and 2. A prominent feature of the cocrystal 1 was the strong and directional TtB between tin (Sn) and phosphorus (P), with a specific distance of 3.541 Å and an angle of approximately 171.41 degrees between the chlorine atom (Cl) and the Sn···P direction. The staggered arrangement of the six phenyl groups allowed for less steric contact during TtB formation, emphasizing the importance of this structural feature. Remarkably, the Sn···P distance was about 10% shorter than that which would be expected from non-directional van der Waals (vdW) interaction, highlighting the tetrel bond's specificity and directionality. For further details, the structural characteristics of cocrystal 1 are summarized in Table 9 (Chp. 4 section SCXRD) and in Paper #1, which offers a clear and thorough summary of the information gathered. On the other hand, cocrystal 2 structural analysis also revealed the presence of a tetrel bond between the tin atom of Triphenyltin chloride and the oxygen atom of cyclohexyldiphenylphosphane oxide. The structure and properties of the cocrystal are

influenced by this TtB. The structural details revealed a tin-oxygen distance of 2.346 Å, indicating the proximity of these two atoms within the crystal lattice. Furthermore, the Cl—Sn···O TB angle is approximately 174.0°, indicating a nearly linear alignment, a critical feature in characterizing the TB interaction. For further details, Table 10 (Chp. 4 section SCXRD) and Paper #2 in Chapter 4 provides an in-depth overview of the structural characteristics of cocrystal 2.

Lastly, we collaborated with Dr. Steve Scheiner from the Department of Chemistry and Biochemistry at the Utah State University, who conducted insightful DFT computations. These computations uncovered intriguing aspects of tetrel bonding. We notice that TtBs with heavier pnictogens as electron donors, such as phosphorus (P) and arsenic (As), tended to be weaker than those involving nitrogen. By carefully introducing electron-withdrawing substituents, we were able to create robust tin-heavy pnictogen TtBs with interaction energies of around 10 $kcalmol^{-1}$. Further, reviewing the data from the X-ray diffraction structures has newly established the generality of the Sn···P tetrel bond, and its determinative role in directing molecular conformation in the solid state, further details in Paper #1, Chapter 4.

In conclusion, this research opens doors to the potential use of tin-heavy pnictogen tetrel bonds as novel structural determinants in various domains of solid-state chemistry, including crystal engineering, materials design, and solution chemistry.

ii. Future Work

The first step is improving the quality of cocrystal 1 which is essential for increasing the reliability of my research. To achieve this, I will consider employing purification techniques like recrystallization to eliminate impurities and obtain higher quality cocrystals. During the scale-up process, meticulous measurements, precise temperature control, and extended reaction times should be applied to maximize cocrystal yield. Experiment with different solvents and synthesis conditions to find the best combination for producing high-quality cocrystals. Addressing these problems will aid in gaining better results for our cocrystal 1. Once high-quality cocrystals are synthesized, running solid-state nuclear magnetic resonance (ssNMR) experiments on the novel cocrystal will provide a crucial step to identify and confirm the formation of the tetrel bond.

Cocrystal 2 offers a promising avenue for further investigation. To refine my study, I will conduct a thorough PXRD analysis, experimenting with various measurement conditions and sample preparations to match the experimental data and the simulated diffraction patterns more closely. I will also experiment with ^{31}P CP/MAS ssNMR and ^{13}C CP/MAS ssNMR to investigate the electronic environment of tetrel atoms and confirm the presence of tetrel bonding. Collaborating with computational chemists, such as Dr. Steve Scheiner, to perform DFT calculations that can reveal structural properties and bonding interactions/energies. Lastly, investigate potential applications of cocrystal 2 in fields such as materials science, catalysis, or crystal engineering, ultimately contributing to cocrystal chemistry advancement.

Finally, extending my research to investigate novel cocrystals involving other heavy pnictogens like antimony (Sb) and bismuth (Bi) opens new possibilities for future

research. With the right experimental design and dedication, the creation of diverse cocrystals is well within reach. Antimony (Sb) and bismuth (Bi) have distinct electron-donating properties, which can lead to interesting interactions within cocrystals. I should begin my exploration by identifying suitable tin-based electron donors (Triphenyltin chloride or others) along with suitable acceptors (N, As, etc.). Subsequently, I will experiment with various synthesis techniques and conduct thorough screenings to identify potential cocrystal candidates with intriguing properties and applications.

Appendix

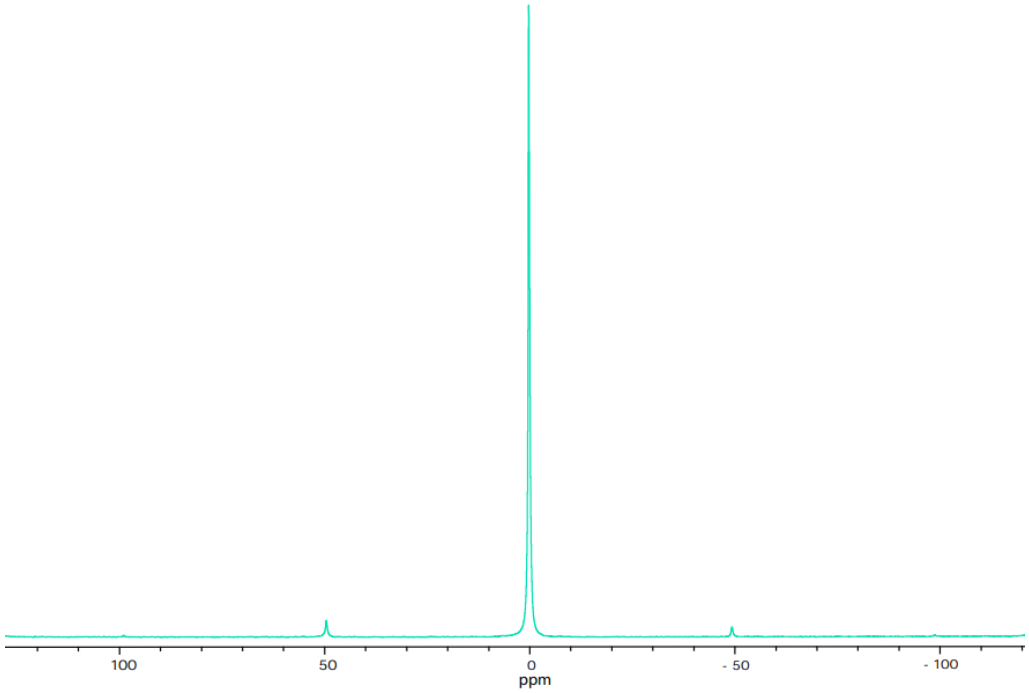

Figure A1. *ssNMR spectra of ^{31}P CP/MAS of triphenylphosphine at a spinning rate of 4.5 kHz.*

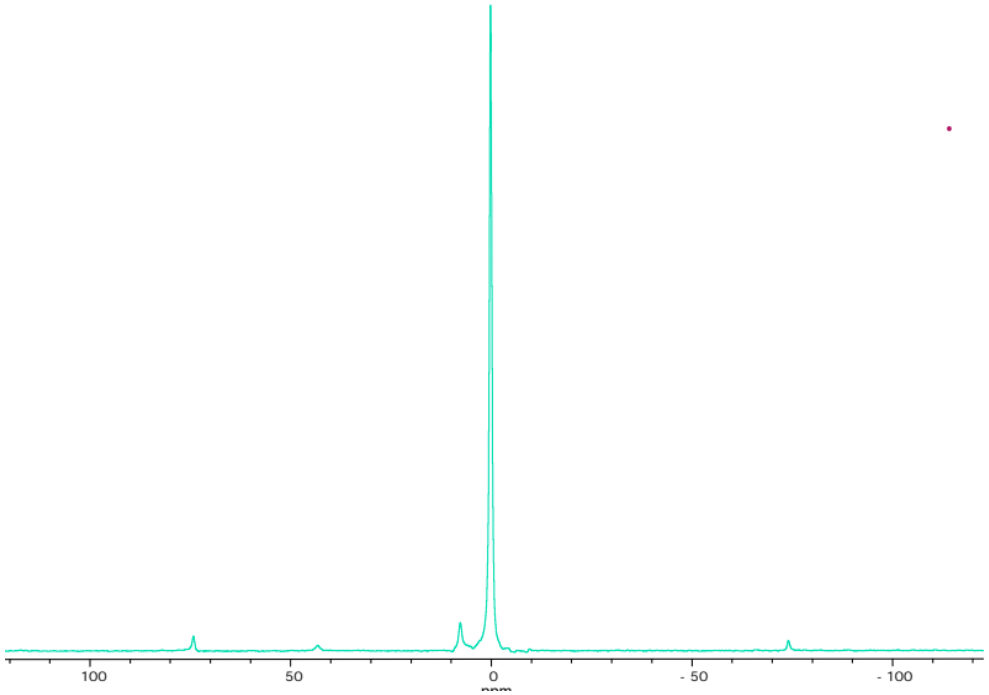

Figure A2*. ssNMR spectra of ^{31}P CP/MAS of novel cocrystal 1 at a spinning rate of 4.5 kHz*

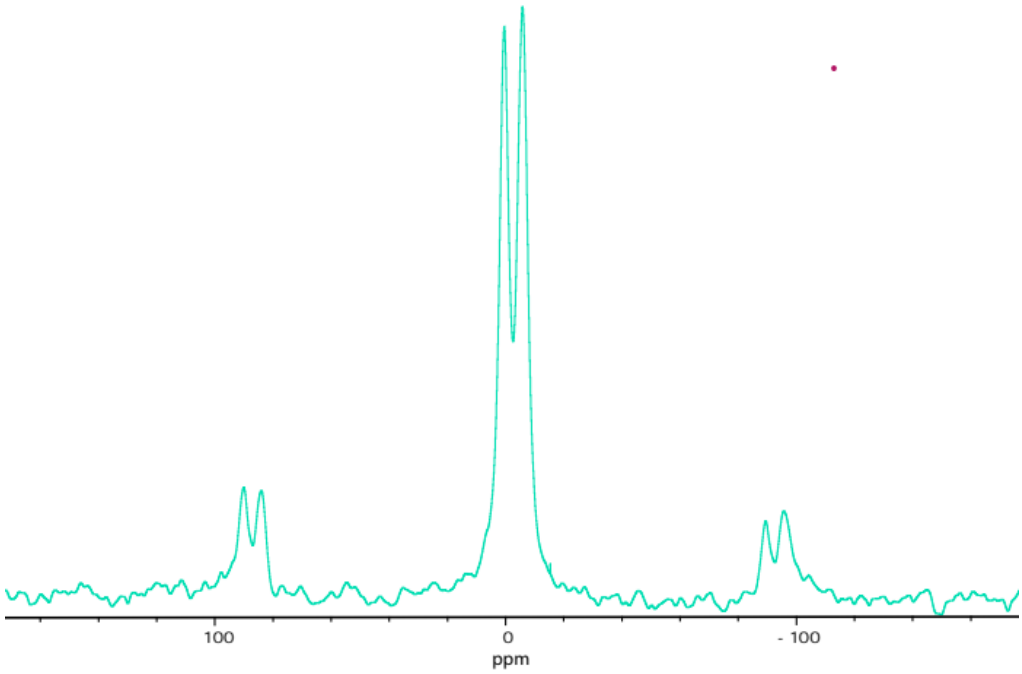

Figure A3. *ssNMR spectra of ^{13}C CP/MAS of triphenyltin chloride at a spinning rate of 4.5 kHz.*

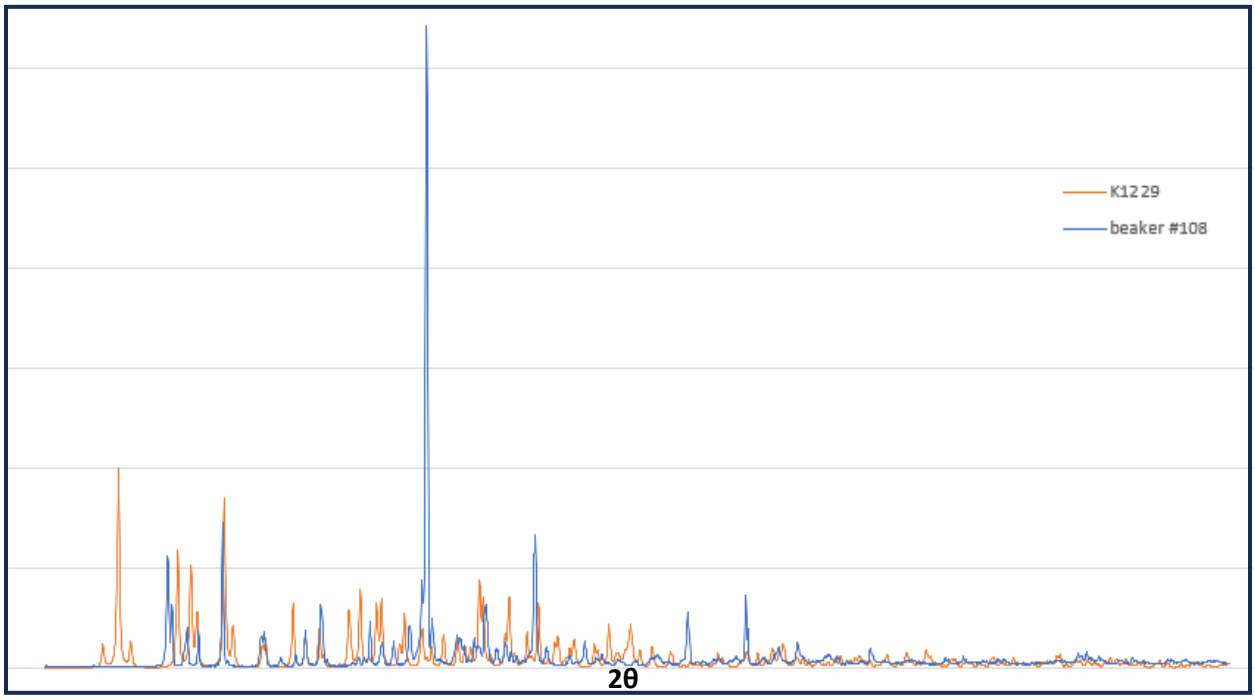

Figure A4. *Simulated (orange) vs Beaker #108 (blue), PXRD patterns.*

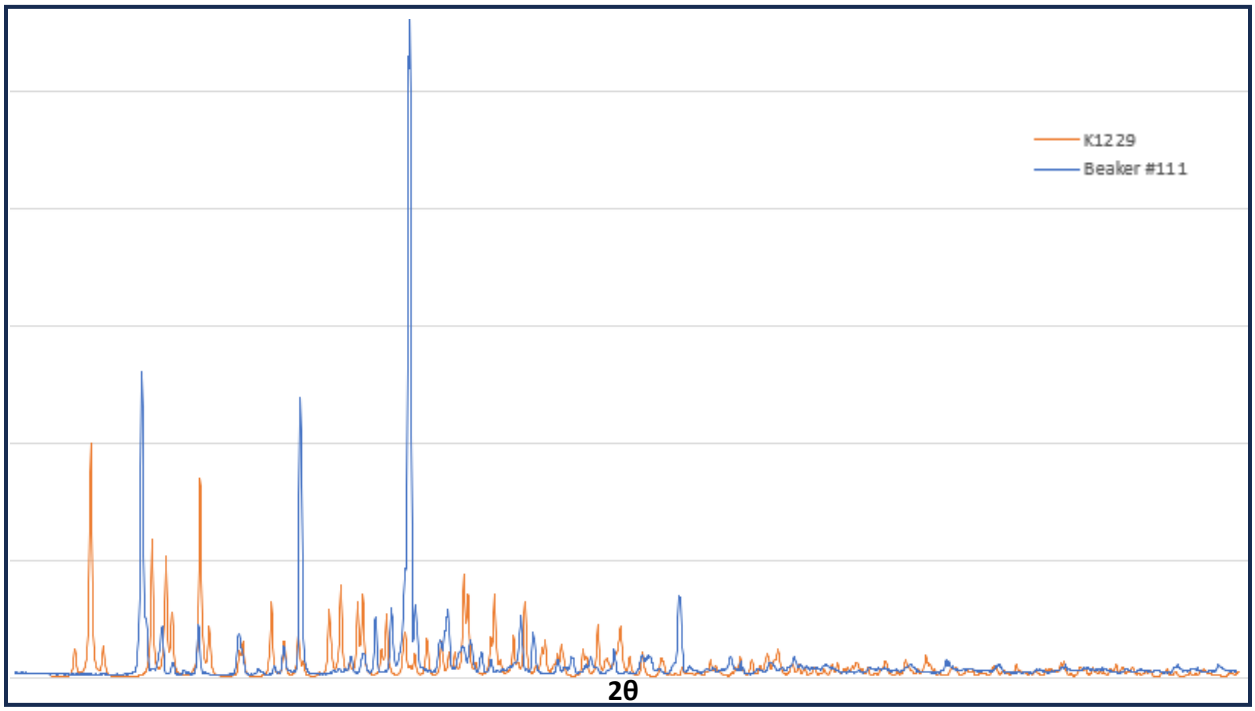

Figure A5. *Simulated (orange) vs Beaker #111 (blue), PXRD patterns.*

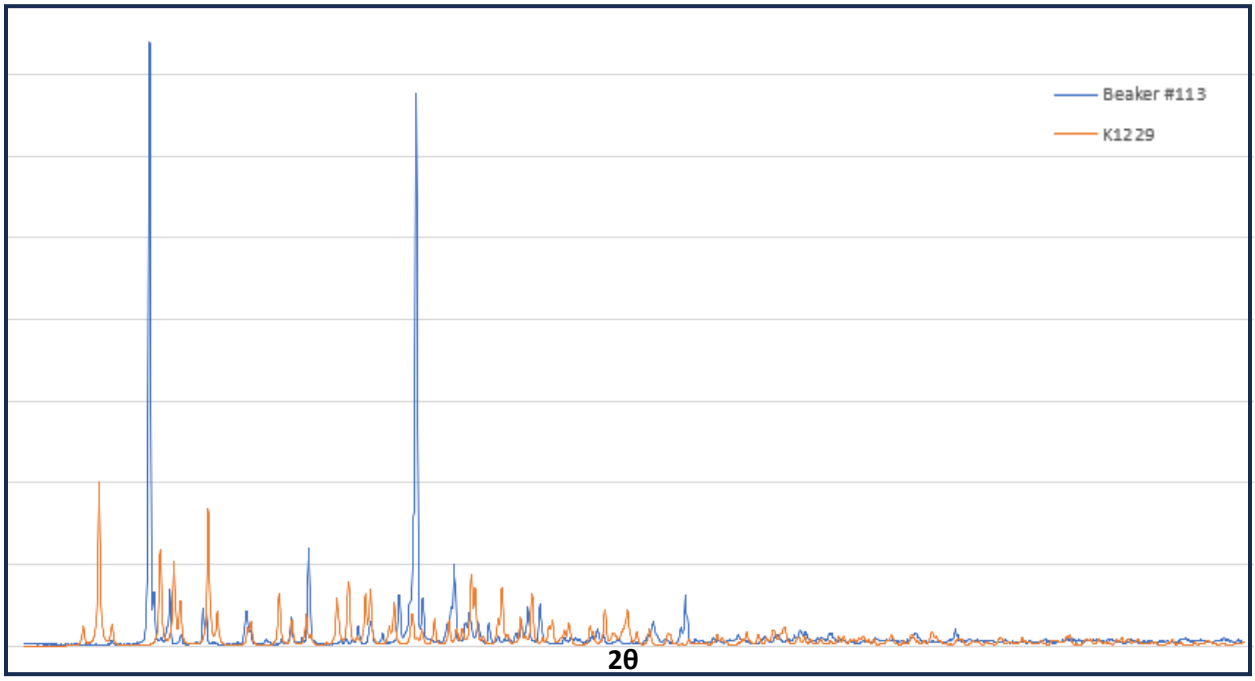

Figure A6. *Simulated (orange) vs Beaker #113 (blue), PXRD patterns.*

CCDC refcode	CIF number	Sn-P distance / Å	type
USUFOG	2038373	2.988	organometallic sandwich; possible TB
		2.992	molecule; possible intramolecular TB
PUYVAJ	1975272	3.001	molecule; possible intramolecular TB
XARHUT	127416	3.020	molecule; possible intramolecular TB; two P with one Sn
UMEGUR	2025725	3.058	molecule; possible intramolecular TB
XAPCEW	143976	3.064	molecule; possible intramolecular TB
MOVJAI	170812	3.086	molecule; possible intramolecular TB; two P with one Sn
		3.091	molecule; possible intramolecular TB
NUVGET	1995876	3.136	molecule; possible intramolecular TB
LEHKIS	1204971	3.139	molecule; possible intramolecular TB
ZOLBAF	992228	3.141	molecule; possible intramolecular TB
QIFWAD	161249	3.188	cluster with pendant arms; possible intramolecular TB
		3.191	molecule; possible intramolecular TB
YERBUT	623248	3.228	molecule; possible intramolecular TB
ZOLFUD	985249	3.247	molecule; possible intramolecular TB
XANMEI	2041511	3.249	molecule; possible intramolecular TB
ZOKZEG	992224	3.251	molecule; possible intramolecular TB
YICNOP	928769	3.285	molecule; possible intramolecular TB
TIZFAM	1856313	3.308	molecule; possible intramolecular TB
ILEDIM	207947	3.310	molecule; possible intramolecular TB
TILNOR	1270939	3.348	organometallic sandwich; possible TB
		3.353	molecule; possible intramolecular TB; two P with one Sn
ZOLQOI	985248	3.362	molecule; possible intramolecular TB
TOCHUO	1272982	3.369	molecule; possible intramolecular TB
PEHFOB	2152292	3.487	molecule; possible intramolecular TB
FOWDAZ	1909930	3.533	molecule; possible intramolecular TB; two P with one Sn
		3.536	molecule; possible intramolecular TB
RAQHAW	2097501	3.555	molecule; possible intramolecular TB
USUFAS	2038370	3.566	organometallic sandwich; possible TB
PUCQIP	1022565	3.608	molecule; possible intramolecular TB
FOWCUS	1909929	3.692	molecule; possible intramolecular TB
TIDVAD	1270841	3.760	molecule; possible intramolecular TB
RAQHEA	2097502	3.763	molecule; possible intramolecular TB
KOJMII	1896344	3.785	molecule; possible intramolecular TB
		3.843	molecule; possible intramolecular TB
		3.867	molecule; possible intramolecular TB; two P with one Sn
GUXTUP01	1057381	3.875	molecule; possible intramolecular TB
FOWCOM	1909928	3.917	molecule; possible intramolecular TB
MOVJEM	170813	2.605	molecule; unlikely to be TB
		4.041	molecule; unlikely to be TB
MOVJUC	170816	2.930	molecule; example with TB geometry but very short
MOVKAJ	170817	3.415	molecule; Sn-O-P over two bonds
XOWSEI	680524	3.290	molecule; Sn-N-P over two bonds
		3.247	molecule; Sn-N-P over two bonds
MOVJIQ	170814	2.686	molecule; example with TB geometry but very short
QIWTAT	947192	3.553	molecule; unlikely to be TB
ROBKUP	694941	3.748	molecule; unlikely to be TB
		3.767	molecule; unlikely to be TB
		4.089	molecule; unlikely to be TB
		4.126	molecule; unlikely to be TB
NUVFUI	1995874	3.476	molecule; unlikely to be TB
HAPLUF	1172232	3.912	molecule; Sn-O-P over two bonds
MOVKIR	170819	3.438	molecule; Sn-O-P over two bonds
QIWSUM	947191	2.727	molecule; covalent bond?
BUXWEW	1117734	3.885	molecule; Sn-O-P over two bonds
		3.642	molecule; Sn-O-P over two bonds
FACHAT	1151284	3.516	molecule; Sn-O-P over two bonds
		3.386	molecule; Sn-O-P over two bonds
FOJVUV	1158717	3.824	molecule; Sn-O-P over two bonds
		3.611	molecule; Sn-O-P over two bonds
ACAWAC	171551	3.453	framework; Sn-O-P over two bonds
		3.416	framework; Sn-O-P over two bonds
		3.830	framework; Sn-O-P over two bonds
		3.620	framework; Sn-O-P over two bonds

Figure A7. *CDS Survey. (CSD search results for Sn···P contacts between 2.50 and 4.00 Å.)*